NUMERICAL AND EXPERIMENTAL STUDIES ON NANOFLUID BASED NATURAL CIRCULATION LOOP

A Thesis submitted in the partial fulfillment of the requirements for the award of the degree of

DOCTOR OF PHILOSOPHY

by

RAMESH BABU BEJJAM
(ROLL NO: 701344)

DEPARTMENT OF MECHANICAL ENGINEERING

NATIONAL INSTITUTE OF TECHNOLOGY

WARANGAL (T.S) INDIA 506 004

September - 2018

NUMERICAL AND EXPERIMENTAL STUDIES ON NANOFLUID BASED NATURAL CIRCULATION LOOP

A Thesis submitted in the partial fulfillment of the requirements for the award of the degree of

DOCTOR OF PHILOSOPHY

by

RAMESH BABU BEJJAM
(ROLL NO: 701344)

Under the supervision of

Dr. K. KIRAN KUMAR

DEPARTMENT OF MECHANICAL ENGINEERING

NATIONAL INSTITUTE OF TECHNOLOGY

WARANGAL (T.S) INDIA 506 004

September – 2018

THESIS APPROVAL FOR Ph.D.

This thesis entitled **"Numerical and Experimental Studies on Nanofluid based Natural Circulation Loop"** by **Mr. Ramesh Babu Bejjam** is approved for the degree of Doctor of Philosophy.

Examiners

_____

_____

_____

_____

Supervisor

Dr. K Kiran Kumar

Associate Professor, Mechanical Engineering Department, NIT Warangal

Chairman

Prof. P Bangaru Babu

Head, Mechanical Engineering Department, NIT Warangal

Dedicated

to

- **My beloved Parents & Family**
- **All my Teachers and Professors who taught and encouraged me with positive thoughts**

NATIONAL INSTITUTE OF TECHNOLOGY
WARANGAL (T.S) INDIA 506 004

DECLARATION

I, hereby declare that the matter embodied in this thesis titled **"Numerical and experimental studies on nanofluid based natural circulation loop"** is the result of research carried out by me under the supervision of **Dr. K Kiran Kumar,** Department of Mechanical Engineering, National Institute of Technology, Warangal, Telangana. This work or any part of this work has not been submitted to any other University or Institute for the award of any other degree or diploma.

Date:
Place: Warangal

(Ramesh Babu Bejjam)
Research Scholar,
Roll No.701344

NATIONAL INSTITUTE OF TECHNOLOGY
WARANGAL (T.S) INDIA 506 004

CERTIFICATE

This is to certify that the thesis entitled **"Numerical and experimental studies on nanofluid based natural circulation loop"**, that is being submitted by **Mr. Ramesh Babu Bejjam (701344)** in partial fulfillment for the award of Doctor of Philosophy (**Ph.D.)** in the Department of Mechanical Engineering, National Institute of Technology Warangal, is a record of bonafide work carried out by him under my guidance and supervision. The results embodied in this thesis have not been submitted to any other Universities or Institutes for the award of any degree or diploma.

Place: Warangal.
Date:

Dr. K. Kiran Kumar
Associate Professor
Department of Mechanical Engineering
NIT Warangal- India.

ACKNOWLEDGEMENTS

I would like to express my sincere gratitude and it gives me an immense pleasure to acknowledge the people who were the part of this research work in plenty ways. It would not have been possible without close association with many people. I take this opportunity to extend my sincere gratitude and appreciation to all those who made this research work possible. First and foremost, I would like to express my sincere gratitude to my research supervisor Dr. K. Kiran Kumar for introducing me to this exciting field of natural circulation systems and for his dedicated help, advice, inspiration, encouragement and continuous support, throughout my research work. His enthusiasm, integral view on research and mission for providing high-quality work, has made a deep impression on me. I am indebted to him for his persistence in moulding me as a researcher with his methodical supervision that enabled me to complete the research work in the present form. I will never forget his association and encouragement and whole hearted support during my entire tenure of research. During our course of interaction, I have learnt many things, like how to explore new possibilities and how to approach a problem by systematic thinking. I owe him lots of gratitude for showing me this way of research.

I would like to express special words of thanks to my DSC members Prof. S Srinivasa Rao, Dr. K. V. Gobi, Dr. G. Nagasrinivasulu for their continuous support, encouragement and valuable suggestions towards my research.

I would like to acknowledge with gratitude to Prof. P Bangaru Babu, Head, Department of Mechanical Engineering for providing the necessary facilities to carry out the research.

I am always grateful to my institute NITW, where I learn many things along with the research. I express my heart-felt gratitude to some of the faculty members of the institute during the stay. They are very kind enough to extend their help at various phases of this research, whenever I approached them, and I do hereby acknowledge all of them. Prof. R.V Chalam, Prof. K Madhu Murthy, Prof. L Krishnanand, Prof. C.S.P Rao, Prof. A. Neelakanteswara Rao, Prof. C. Guru Raja Rao, Prof. A Venu Gopal, Prof. N Selvaraj, Prof. K V Sai Srinadh, Prof. Ravi Kumar Puli, Prof. G. Amba Prasada Rao, Dr. V. Hari Kumar, Dr. V. Vasu, Dr. P V Suresh Babu, Dr. Karthik Balasubramanian, Dr. Syed Ismail, and other faculty members of the department for their timely suggestions and cooperation during the entire period of research. I would like to express heartful thanks to Dr. M. R. Vishwanathan faculty member of the H&SS department for his timely suggestions during my thesis preparation.

My heartfelt thanks to fellow-scholars for their consistent help, moral support and encouragement. My special thanks to Dr. J. A. Ranga Babu, S. Venkata Sai Sudheer, V. Venkateswarlu, G. Prabhakar Rao, Brundaban Patro, V. Ranjith Kumar, P. Mahesh and many others for always standing by my side and sharing a great relationship as compassionate friends. I will always cherish the warmth shown by them. My special thanks to Dr. G. Suresh and P. Sampath Kumar for their financial support to manage my family during my research period.

In this auspicious moment, I owe my deepest regards to my family members for their eternal support and understanding of my goals and aspirations. My heartfelt regards go to my parents, Sri B. Bhaskara Rao, and Smt. B. Prabhavati. My wife Parveen Bhanu, share a perpetual role with her infallible affection, love and support, it has always been my strength. Her patience and sacrifice will remain my inspiration throughout my life. Without her support, I would not have been able to complete what I have done and become who I am. My kids Sanjana and Sanjay miss many cherishable moments in their life due to being busy with my research. My special regards to my brother Mr. B. Vijay Kumar, sister Smt. D. Usha Rani and brother-in-law Sri D. Jaya Krishna and many other friends for their patience and understanding during the entire period of the research work. I also must thank all my hostel mates and neighbors near my quarter for making my stay at NIT Warangal become more memorable.

As always it is impossible to mention everybody who had an impact to this work, however, there are those whose spiritual support is even more important. I feel a deep sense of gratitude to each and every one who directly or indirectly extended their support to fulfill my research.

Finally, I am thankful to library staff and administrative staff of NITW for their cooperation.

NIT Warangal (**Ramesh Babu Bejjam**)

September 2018

ABSTRACT

Natural circulation loops (NCLs) offer a very efficient option of heat transport from source to sink without any prime mover. In the NCL, buoyancy is the driving force to circulate the working fluid in the entire loop. The buoyancy force is developed due to a temperature gradient between source and sink which causes the fluid to circulate and hence no pump is required. Due to the absence of a pump, NCLs offer advantages such as high reliability, safety and low maintenance cost. Thereby, it offers some unique and distinctive applications such as nuclear reactor core cooling, geothermal heat extraction, solar water heaters, refrigeration systems, electronic cooling systems etc.

The present scenario of high thermal loading coupled with high flux levels demands exploration of new heat transfer augmentation techniques. In this context, '*Nanofluid*' emerged as alternative heat transfer fluid. The term 'Nanofluid' is used to indicate a special class of heat transfer fluids that contain nanoparticles ($\leq$ 100 nm) of metallic/non-metallic substances uniformly and stably suspended in a conventional fluid. This opens the possibility of enhancing the thermo-physical properties of the base fluid in a desired manner. The idea of suspending some solid phase material in conventional liquids is to enhance its heat transfer properties. With this background, the present dissertation focuses to study the thermal performance of natural circulation loop working with nanofluids.

The main objective of this research was to carry out theoretical and experimental studies on nanofluid based single phase natural circulation loops (NCL). For this research work, three water based nanofluids such as SiO_2-water, Al_2O_3-water and CuO-water at different particle concentrations were used. Initially a comparative study was made between water and nanofluids that can be used in natural circulation loops for various heat transfer applications. At the same operating conditions, the enhanced thermophysical properties of the nanofluid facilitate to reduce the size of NCL compared to that of water. Analytical studies were conducted at laminar and turbulent flow conditions, the results show that in both flow conditions the improved thermo-physical properties of the nanofluid brings compactness to the NCL. Experimentally, the effect of temperature on viscosity and thermal conductivity of nanofluids was also studied.

Further, a one-dimensional (1-D) numerical modelling was carried out to analyse rectangular NCL with end heat exchangers operating at steady-state conditions. This study predicts the balanced mass flow rates of NCL for different design and operating conditions.

From the results, it was concluded that, for given input conditions, there exist an optimum value of heat exchanger length and loop pipe diameter. The noteworthy conclusion drawn from the result was, the external fluid (water) flow rate does not influence the loop performance. However, the external fluids temperatures affect the loop performance strongly.

In extended work, a three-dimensional (3-D) numerical modelling was carried out for single phase natural circulation loop with heater as heat source. For this study, a 3-D NCL model was developed and simulated using Ansys-Fluent 14.0. The effect of power input, particle concentration, loop inclination angle and multiple channels (double riser and double downcomer-DRDD) on thermal performance of the NCL were studied. The results show that as particle volume concentration increases the temperature difference at the heater decreases hence, the steady-state mass flow rate increases. Another notable outcome from the analysis was, as the particle concentration increase from 0% to 5%, the mass flow rate in the NCL increases, but further increment in particle concentration reduces the mass flow rate due to viscous forces that dominate the buoyancy forces. Therefore, for this NCL geometry, 5% particle concentration was considered as an optimum value. Effectiveness of the nanofluid based NCL is more than the water based NCL. The effectiveness increases with the loop inclination angle. One more important conclusion from this analysis was lower inclination angles up to 15° will be preferable without much effect on Rayleigh number and average heat transfer coefficient. The performance of the NCL with multiple channels (DRDD) was enhanced by 2.5% when compared with single channel NCL (SRSD) in terms of the mass flow rate.

Based on the numerical studies, two perfectly instrumented rectangular NCLs were fabricated with heater as heat source and heat exchanger as heat source, separately. Experiments were conducted on both the test rigs with nanofluids as loop fluid and results were compared with water. The experimental results were validated with the numerical results as well as with the published data. The experimental results show that NCL operated with nanofluid quickly reaches a steady-state condition compared with that of water. Stability of NCL was studied by the sudden perturbation of power input to heater. Within the scope of this study, oscillatory or reversed flow in NCL was not found. Finally based on the theoretical and experimental work, several conclusions were drawn and recommendations were made for future studies.

CONTENTS

List of tables

List of figures

Nomenclature

Symbol	*Name*	*Unit*
A	Area	m^2
C_p	Specific heat	J kg^{-1} K^{-1}
d	Diameter	m
F	Body force	N
f	Friction factor	
g	Acceleration due to gravity	ms^{-2}
Gr_m	Modified Grashof number	
H	Height of the loop	m
h	Specific enthalpy	J kg^{-1} K^{-1}
h_{avg}	Average heat transfer coefficient	$Wm^{-2}K^{-1}$
I	Current	amps
k	Thermal conductivity	W m^{-1} K^{-1}
L	Length of the pipe	m
L_c	Characteristic length	m
$\dot{m}$	Mass flow rate	kg s^{-1}
nm	Nanometer	
N_G	Effective loss coefficient	
Nu	Nusselt number	
Pe	Peclet number	
Pr	Prandtl number	
Q	Power input	W
Re	Reynolds number	
q''	Heat flux	Wm^{-2}
St	Stokes number	
T	Temperature	K
τ_p	Particle response time	s
t_s	System response time	s
u	Fluid velocity	m/s
U	Overall heat loss coefficient	$Wm^{-2}K^{-1}$
V	Voltage	volts
V	Volumetric flow rate	m^3/s
V_s	Characteristic velocity of the fluid	m/s
Y	Overall resistance parameter	

Subscripts

avg	average
bf	base fluid
c	cold fluid
cs	cross section
eff	effective
h	hot fluid
hy	hydraulic
in	in
lf	loop fluid
nf	nanofluid
np	nanoparticle
out	out
p	particle
sa	Surface area
ss	steady state
w	water

Greek symbols

β	Thermal expansion coefficient	K^{-1}
ρ	Density	kg m^{-3}
∅	Volume concentration	
μ	Viscosity	N-S m^{-2}
θ	Angle	degree

Chapter 1

Introduction

1.1 Background of natural circulation system

From an engineering perspective, the term *circulation* defined as the flow of fluid through a closed circuit. One common example would be blood circulation in the human body (fig. 1.1a) and oceanic current circulations in nature (fig. 1.1b). However, there is a fundamental difference between the two types. In fig. 1.1a, the central component which is the human pumps blood and imparts enough driving force for circulation to the body and this kind of phenomena is termed as assisted or forced circulation. In fig. 1.1b, circulation takes place solely due to the density gradient in different parts of the medium (air or water) caused by thermal imbalance and this kind of circulation is termed '*natural circulation*'. Gebhart [1] addressed the flows arising in a body of fluid enclosed in a cavity or totally surrounded by surfaces using the term 'internal natural convection'. The specific features of natural circulation systems are mainly susceptible to unstable operation and high sensitivity to operating conditions due to the completely coupled nature of flow and temperature fields. In natural circulation systems, flow rates are very low compared to forced circulation (flow imposed by prime movers like pumps or fans). As a result, equivalent orders of viscous and momentum effects playing a vital role in natural circulation systems.

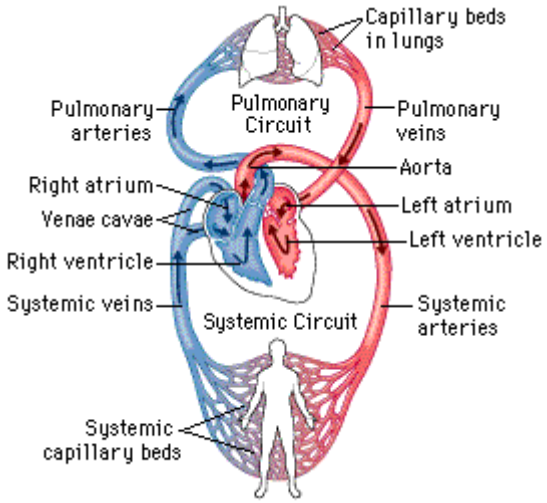

(a) Blood circulation in human body forced by the heart [2]

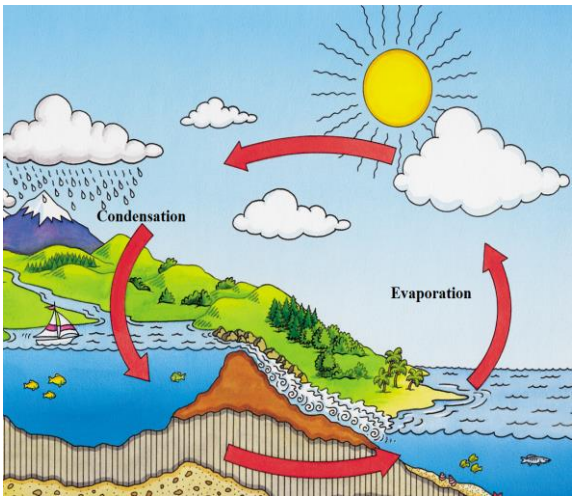

(b) Water evaporation from oceans and rainfall completes a natural cycle [3]

Fig. 1.1 Examples of forced and natural circulation in everyday world

1.1.1 Working principle of the natural circulation loop

The concept of fluid motion (Natural circulation) arose due to bottom heating at the bottom and top cooling at the top, as was investigated by Lord Rayleigh [4]. Before going further, it would be sensible to look at the working principle of simple Natural Circulation Loop (NCL) which consists of two horizontal pipes (heat source and heat sink) and two adiabatic vertical pipes (riser and down comer) as shown in fig. 1.2. The fluid flowing through the loop is called a loop fluid or working fluid. The loop fluid flows in anti-clockwise direction as shown by arrows in fig. 1.2. When the system reaches a steady - state condition, the fluid circulates in one direction unless external input parameters changed. So, we considered flow takes place in the clockwise direction. The entire analysis is considered to be steady state. This tendency is most likely caused by geometrical imperfections in the tubes that make the loop asymmetric and drive the fluid motion in a preferred direction. The loop fluid absorbs heat in the heat source, and becomes warm and lighter as it flows through the heat source. The resulting buoyancy force drives the fluid through the riser up to the heat sink. In heat sink, the loop fluid becomes colder and denser due to heat rejection. The colder and denser loop fluid flows back to the heat source through the downcomer due to gravity to complete the cycle. In NCLs, simultaneous heating and cooling cause the density gradient which results in buoyancy, that drives the fluid. Usually the heat source is located under the heat sink to promote natural circulation. If the heat source and heat sink are maintained at constant temperature, a steady-state condition is predictable

when the heat absorbed by the loop fluid at heat source is equal to the heat rejected by the loop fluid at the heat sink. It is apparent that the flow in the loop is enhanced by the density difference between the riser and downcomer.

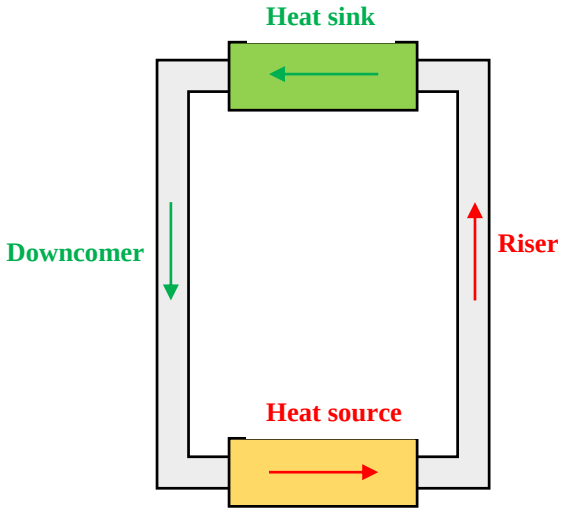

Fig. 1.2 Simple construction of natural circulation loop

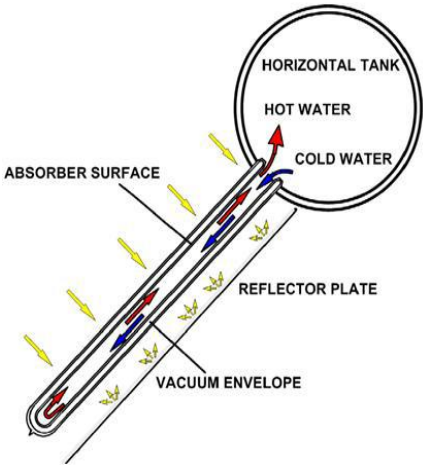

Fig. 1.3 An example of thermosyphon is evacuated tube solar water heater [5]

The NCLs are sometimes called thermosyphons or natural convection loops. Japikse [6] summarised the difference between "thermosyphon" loop where the flow is upward along the wall of the tube with an associated downward return flow in the core, and 'natural circulation loops', where the flow is generally in one direction around the loop. Figure 1.3 shows an example of a thermosyphon.

1.1.2 Classification of natural circulation loops

NCLs are categorized based on several aspects [7]:

a) Based on the shape of the loop
   - Toroidal
   - Rectangular

b) Based on the state of the working fluid
   - Single-phase NCL
   - Two-phase NCL
   - Supercritical NCL

c) Based on the interaction with surroundings
   - Closed loop

- Open loop

d) Based on the number of heated channels for nuclear and solar applications
    - Single-channel
    - Multi-channel

e) Based on the body force field
    - Centrifugal force
    - Gravitational force

f) Based on invention of the system for steam generators
    - Single-phase
    - Two-phase

1.1.3 Advantages of natural circulation loops

- **Simple in construction**

Simplicity is the main advantage and a key feature of NCL. NCLs have greatly simplified maintenance, operation and construction by eliminating pumps and other power supply units. In addition, all safety issues related to the failure of the circulating pumps are removed due to the elimination of pumps.

- **Safety characteristics**

Since natural circulation loops work on a natural physical law, they are not expected to fail like the fluid moving machinery such as pumps. This aspect of NCL has enabled its application in many systems where safety is of highest importance. Apart from this, NCLs have relatively low power densities and large volumes when compared with forced circulation loops under the same power conditions. As a result, NCL has a slow thermal response, giving operators ample time to respond to plant aspects: giving operators enough time to reply to plant elements.

- **Better flow distribution**

The flow distribution in parallel channel cores of NCLs is more uniform.

- **Flow characteristics**

As there is no prime mover, the two phase region of the loop should not be restricted within a specified zone. In principle two phase flow may occur throughout the entire length of the loop [8].

1.1.4 Disadvantages of natural circulation loops

- **Low driving head**

The main drawback of NCL is that the driving head is low. To increase the loop fluid mass flow rate at a given power would require either a decrease in the loop resistance or a increase in loop height either of which may increase the cost of the plant.

- **Low mass flow rate and instability effects**

In common, the mass flow rate in NCL is low. Consequently, the allowable maximum power is less prominent for a larger core volume compared to a forced circulation system of the same rating. In addition, large volumes can result in stability of the system and enable one to avoid zonal control problems. This is attributable to the nonlinear nature of the natural circulation phenomenon, where any change in the driving force affects the flow, which may lead to oscillatory behaviour.

- **Low critical heat flux**

The critical heat flux of the system is also influenced by the low mass flow rate. Since flow in natural circulation reactors is low, they tend to use the maximum allowable exit quality to minimize their size. In the process, their critical heat flux value tends to be significantly lower than that of forced circulation systems.

In summary table 1.1 presents the highlights of advantages and disadvantages.

Table 1.1 Advantages and disadvantages of natural circulation loop

Advantages	Disadvantages
Better two phase characteristics	Specific start-up procedures required
Simplicity and low cost	Critical heat flux is less
More thermal inertia	Driving head is less
No pumps required	Maximum power per passage is less
Uniform flow distribution	Potential instabilities

1.1.5 Applications of natural circulation loops

NCLs have been employed very successfully in a wide variety of engineering and industrial:

- Closed loop pulsating heat pipe (Khandekar et al. [9], Khandekar et al. [10]; Tong et al. [11]).

- Turbine blade cooling (Cohen and Bayley [12]),
- Solar heaters (Close, [13]; Mertol et al. [14]; Ong [15]; Shitzer et al. [16]; Zvirin et al. [17], Koca et al. [18]),
- Thermosyphon reboilers (McKee [19]; Sarma et al. [20]),
- Geothermal energy extraction processes (Kreitlow et al. [21]),
- Electronic chip cooling (Tuma et al. [22]),
- Chemical process industries (Joshi, [23]),
- Nuclear power generation (Choi et al. [24]) and plenty more.

Other novel ideas for application of NCLs are:

- Models of thermal springs of Virginia (Torrance [25]),
- Heat dissipation employing the so-called 'liquid fins' (Madejski et al. [26]), in the study of deterministic chaos (Wang et al. [27])
- Refrigeration (Kiran et al. [28])
- Recently in the field of liquid fuels, Gumus et al. [29] proposed a model to improve combustion performance as well.

1.2 About nanofluids

A new approach to improve the thermo-physical properties of the working fluid is the suspension of high thermal conductive solid particles in inherently poor conductive conventional working fluid. However, suspension of solid particles in base fluid is not a new idea, it is traced back to the 19^{th} century. Maxwell [30] is the pioneer in the area of dispersing solid particles in a liquid medium to enhance the effective thermal conductivity of the working fluid. He proposed an appropriate theoretical basis, to estimate effective thermal conductivity of particle suspended in fluids. In continuation of this, Hamilton and Crosser [31] carried out an outstanding research on particles suspended in fluids and modified the Maxwell correlation [30] to estimate effective thermal conductivity of working fluid more precisely. But both [30], [31] dispersed micro sized solid particles in base fluids, and so their studies are limited by some flaws like the rapid settlement of the solid particles, necessity of more pumping power, wall erosion and clogging of flow passage in flow field. However, advancement in material technology facilitates to produce the availability of nanosized solid particles gives scope to introduce an innovative and novel heat transfer fluid. For the first time, Wang et al. [32] addressed the phenomenon of suspending nanosized solid particles in a base fluid and this particle suspended fluids are nanofluids. Homogeneous suspension of solid nanoparticles in

conventional base fluids recasts the thermo-physical properties of base fluid and increases the heat transfer rate. These enhanced thermophysical properties of nanofluids provide huge incentive for many researchers to employ nanofluids as new generation heat transfer fluids in various engineering applications. These nanofluids exhibit superior characteristics such as high specific surface energy, higher thermal conductive capabilities and enhanced thermophysical properties, which are favourable characteristics to use nanofluids in NCLs [33], [34], [35] and [18].

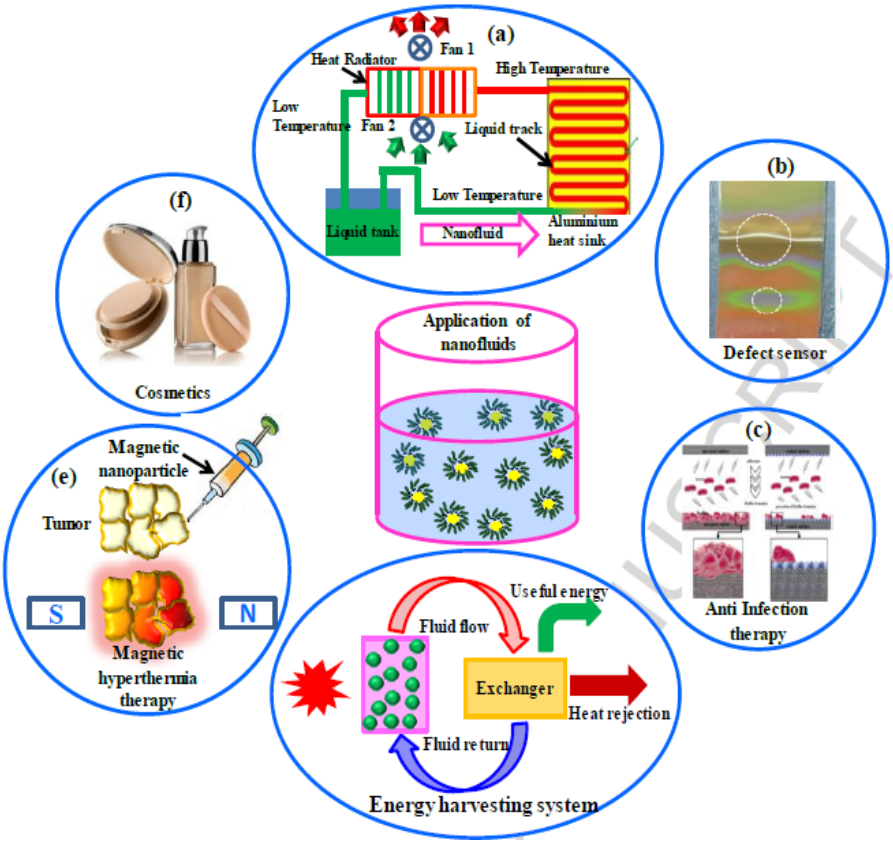

Fig. 1.4. A schematic representation of some applications of nanofluids [36]

In recent years, several researchers have analysed the synthesis, preparation and characterization of various nanofluids for different heat transfer applications [37], [38], [39] [40], [41] and [42]. Many numerical and experimental results have been reported on various combinations of nanoparticles and base fluids. Among these many kinds of nanoparticles, some commonly used nanoparticles are Al, Ag, Au, Cu, Fe (metals), Al_2O_3, CuO (metal oxides), SiC, TiC (carbide ceramics), AlN, SiN (nitride ceramics), SiO_2, TiO_2 (semiconductors), carbon in various forms (like nano-diamond, graphite), carbon nanotubes with single wall, double wall and multi walls, fullerene and shell composites. Conventional base fluids are water, polymer solutions, transformer oil, and ethylene glycol.

Many of the earlier researches reported how elevated thermophysical properties were exhibited by nanofluids. Some notable works on the enhancement of heat transfer characteristics are presented here and detailed information regarding nanofluid characteristics and their use in various heat transfer applications are discussed in the subsequent literature review chapter. Pak and Choi [43] examined the heat transfer behaviour of water based Al_2O_3 and TiO_2 nanofluids at different Reynolds and Prandtl numbers. They found that the convective heat transfer coefficient linearly increased with particle volume concentration. Sharma et al. [44] attained 23.7 % heat transfer improvement at 0.1 vol. % with Al_2O_3/water nanofluid. Sajadi et al. [45] obtained 22% enhancement in heat transfer coefficient with TiO_2/water nanofluid at 0.25 vol. % . Zhu et al. [46] observed 38 % improvement in heat transfer with Fe_2O_3/water nanofluid at 4 % volume concentration. S. W. Lee et al. [47] reported 102 % enrichment in heat transfer with SiC-DI water nanofluid at 3 vol. %. Ding et al. [48] considered CNT/water nanofluid and reported 350 % enhancement in heat transfer at Reynolds number of 800 with 0.5 % wt. %. The reliable refinement and uniqueness in heat transfer and fluid transport properties make nanofluids versatile for various engineering applications like heat exchangers [40] and [49] car radiator [50], electronic cooling [51], [52] and solar energy [53], [54] and [55], etc. A schematic representation of some applications of nanofluids is shown in fig. 1.4.

1.3 Structure of the thesis

- Chapter 1 presents a brief introduction to natural circulation loops and nanofluids.
- A comprehensive review of important literature related to present research work is presented in chapter 2. This is accompanied by the research gaps identified and conclusions drawn from the literature review are furnished. All the major objectives and the scope of the research work are also included.
- Chapter 3 deals with the suitability of the nanofluids as working fluids in NCLs. A comparison is made both for laminar and turbulent flows. It also presents the various synthesis methods available and discusses in detail earlier research for producing nanofluids. Along with that various methods to prepare stable nanofluid are explored. The method adapted for nanofluid preparation in the current research is provided. This chapter also summarizes the estimation of various thermo-physical properties of nanofluids from the correlations available in open literature. It also compares the experimentally measured properties with empirical correlations. A considerable deviation is observed between the measured results and the empirical solutions.

- To optimize geometrical dimensions of the loop, one-dimensional (1-D) steady state analysis is carried out on single phase nanofluid based natural circulation loops with end heat exchangers and this is presented in chapter 4.
- In chapter 5, the influence of the loop inclination angle, multiple channel and heater power input on thermal performance of the nanofluid based NCL is studied using three-dimensional (3-D) numerical modelling.
- Detailed experimental studies are presented in chapter 6. Two test rigs have been designed based on the numerical results. Tests have been conducted to study the system performance by varying the operating parameters. The chapter concludes with the validation of numerical results presented in chapter 4 with the experimental results.
- Chapter 7 presents the general conclusions and scope for future work.

1.4 Closure

The present chapter elaborates the background and motivation governing the research problem taken up for investigation in the present thesis. It also documents various relevant features of all the chapters of the thesis to provide a clear idea to the reader.

Chapter 2

Literature review

In the present chapter a literature review on various aspects of natural circulation loops, such as theoretical and experimental studies on single phase Natural Circulation Loop (NCL) is presented. In addition to this, detailed studies on the properties of nanofluids, applications, and nanofluid based heat exchange systems etc. are also presented.

2.1 Natural circulation loops

Single-phase natural circulation loops are very efficient, yet simple in terms of system construction and operation. Hence, they find widespread applications in a number of important technical fields, particularly in cases where heat removal from a body at high temperature is the primary objective and possible utilization of that thermal energy at the low - temperature end is secondary. Utilization of natural circulation for nuclear reactor core cooling, turbine blade cooling, electronic chip cooling, refrigeration, chemical processes etc., come under such category. Other applications such as use in solar water heaters, PWRs, geothermal power generation focus more on the effective exploitation of secondary-side energy. Details of different possible applications of single-phase NCL were presented by Japikse [6], Zvirin [56] and Greif [57].

NCL systems are always subjected to oscillatory flow and possible flow reversals due to the strong dependence of the flow field on operating conditions. Strong interaction between

frictional and buoyancy forces dominate the events. Various modes of flow instabilities have been observed for almost all kinds of configuration. Along with periodic flow reversals, flow bifurcation and chaotic behaviour can also appear. That poses a real challenge to the researchers and over the years, a large number of researchers have worked on natural circulation and related effects. Both theoretical and experimental findings have been reported. It is truly an arduous job to have an elaborate discussion on each of the available studies in a few pages. Hence, in the present section, efforts have been made mention some of the most significant contributions from the literature and to generate some idea about the gradual development of concept regarding natural circulation loops, associated configurations and detailed review on nanofluids.

2.1.1 Theoretical studies on single-phase natural circulation loops

There are several types of problems related to natural circulation loops in which researchers have been interested for many decades. Natural circulation loops with different geometric configurations, steady state, transient and stability behaviour; single phase and two phase loops are some of the areas of interest. Due to the coupled nature of momentum and energy equations, a theoretical analysis of the natural circulation loop is relatively complex. So many studies available in the literature deal with simple cases like rectangular and toroidal loops, loops with point heat source and sink, etc. Most of the studies tend to be idealized that consider either a known heat flux condition, or as convective heat transfer with known coefficient of heat transfer and wall temperature. Though, many studies have been carried out on two-dimensional (2-D) and three-dimensional (3-D) variation of flow parameters along the loop a majority of the studies are one dimensional. The study of stability is important in the field of nuclear engineering where the flow reversal or flow oscillations and flow stagnation may cause severe damage have been as a result of undesirable increase in local temperature at a particular point. Hence, many studies have been carried out on the stability aspects of natural circulation loops.

Comprehensive reviews on natural circulation systems have been presented by McKee [19], Ostrach [58], Japikse [6], Zvirin [56], Norton and Probert [59], Greif [57] and Sarkar [60]. Their articles give an insight into the categorization of loops and basic understanding of the phenomena.

Keller [61] developed a one dimensional model to study the stability of a rectangular NCL with point heat source and heat sink. He showed that oscillations can occur in the absence of inertial effects, merely requiring an interplay between friction and buoyancy forces.

Welander [62] discussed the cause of instabilities in rectangular loops. According to Welander, the unstable motions were related with thermal irregularities in the fluid that were advected materially around the loop. The irregularities increase through the correlated variations in flow rate. A warm pocket of fluid creates a maximum flow rate through the upper part and a minimum flow rate going through the lower part of the loop. Both Keller and Wallander showed analytically that loop flow instabilities were predicted by the dynamics of the system independent of fluid properties.

Damerell and Schoenhals [63] used the same geometry used by Creveling et al. [64] but with various tilt angles (θ) of the heated section. They reported that the maximum flow rate was achieved with vertical configuration i.e. 0°, for a fixed heat flux and a constant wall temperature cooled section. As the tilt angle (θ) was increased, with the other parameters kept constant, the flow rate diminished towards zero. For $\theta > 60°$, the agreement between the one dimensional (1-D) model and experimental observations seemed to be good. For small tilt angles ($\theta < 60°$), their model predictions overestimated the experimentally observed flow rates.

Grief et al. [65] studied the transient and stability behaviour of the toroidal loop. For the first time they solved numerically the governing equations using a finite difference method to calculate the spatial and temporal variation of the temperature and velocity field. Results from these calculations were in good agreement with a linear stability analysis.

Mertol et al. [66] carried out a two-dimensional (2-D) analysis of a natural circulation loop. Their model allowed radial and axial variations of temperature and radial velocity variations. When the governing equations were non-dimensionalized, Graetz number emerged as a parameter. The friction factor (f) and the Nusselt number (Nu) were not needed as input data; instead they were now the outputs of the solution. It was shown that both f (friction factor) and Nu (Nusselt number) reach their fully developed values when Graetz number was small. They compared the flow rates, obtained in the two dimensional numerical simulations, with the experimental results of Creveling et al. [64] and reported good agreement.

Zvirin and Greif [67] presented a numerical model to evaluate the transient behaviour of a rectangular NCL with point heat sink and heat source. To estimate the mass flow rate and temperatures with time the integral forms of the momentum and energy equations were solved.

He noted that instability depends strongly on the shape of the temperature distribution. Zvirin [68] in another paper theoretically evaluated the effect of dissipation in rectangular and toroidal loops. He found that for a laminar flow in a rectangular NCL, dissipation affects only the temperature distribution, but not stability characteristics or the steady state flow rate. He also found that, the steady-state flow rates were enhanced by dissipation for laminar and turbulent flows in a toroidal loop.

Chen [69] studied the stability of the flow in a rectangular NCL. He presented both numerical and analytical solutions for different loop aspect ratios for both laminar and turbulent flows. He defined a dimensionless parameter. The flow was stable when this dimensionless number was less than a critical value; and flow was unstable when its number was above the critical value. The calculated neutral stability condition showed that flow was least stable for a square loop. Chen [70] presented another theoretical study on the optimum configuration of a rectangular loop for maximum heat transfer rate. He derived a dimensionless parameter which was used as a criterion for maximum heat transfer. But in both the papers he had given the analytical solution by considering the constant temperature boundary conditions. Of course, in practice, the temperature is never constant at the heat source and heat sink.

Vijayan et al. [71] reported a comparison between forced and natural circulation data in a figure of eight loops. They found that the pressure loss coefficient of NCL exceeded 30% compared to forced flow conditions. A generalized correlation of pressure loss coefficient was then derived in terms of a modified Grashof number.

Ambrosini et al. [72], reported the influence of truncation error on stability phenomena. For this study, they considered three different NCL configurations under a single-phase mode and different boundary conditions. The methodology adopted for investigating the impact of various finite-difference discretization techniques can be considered as the numerical analogue of the usual techniques adopted for partial differential equation (PDE) stability analysis.

Rao et al. [8] presented the effects of geometric parameters of NCL with heat exchangers at both ends. An analysis was made based on some assumptions, and it was concluded that heat capacities of hot and cold streams should be large and the number of transfer units (NTU) of both end heat exchangers should be equal to get maximum flow rate. Rao et al. [73] had shown the pressure variation of loop fluid along the loop for NCL with end heat exchangers. No general conclusion was drawn from this study, but the observations can be useful to understand the temperature field in an implicit manner.

Vijayan et al. [74] investigated the heater and cooler orientations on the stability behaviour of the single-phase NCL. They briefly explained the nature of oscillatory flow behaviour in NCL. Vijayan [75] numerically studied the steady state behaviour of uniform and non-uniform diameter NCLs and he developed new correlations in terms of Reynolds number and modified Grashof number for fully laminar and fully turbulent flows in loop. Testing of the laminar flow correlation showed very good agreement with data from both uniform and non-uniform diameter loops. The turbulent flow correlation showed excellent agreement with data from non-uniform diameter loops. However, the turbulent uniform diameter loop data showed a significant deviation from the turbulent flow correlation. The deviation can be mainly attributed to the neglect of the local pressure losses while plotting the data.

Seyed et al. [76] made a detailed analysis of transient and stability characteristics of a single phase natural circulation loop. He made a comparison between the results obtained using a finite difference method (FDM), experimental observations and RELAP5 code. Also, he analysed data by changing the position of the heater from horizontal to vertical leg and proposed that this analysis can also be applicable to this change of orientation of the cooler. All the techniques were found to be in good agreement with each other.

Dipankar et al. [77] investigated the influence of the ambient temperature on loop performance and reached general conclusions like increase in ambient temperature results in higher coolant outlet temperature, etc. In continuation, Dipankar et al. [78] studied the effects of geometric parameters of rectangular NCL and came to conclude that a loop with smaller diameter and shorter height produced higher effectiveness, i.e., carry large amounts of energy to the sink, but retaining lower flow rate caused by reduced buoyancy.

Dipankar et al. [79] also numerically compared the dynamic performance of toroidal and rectangular NCLs with identical dimensions. They reported that rectangular NCL exhibits higher mass flow rates at the same operating conditions. However, the toroidal loop was integrally more stable which can be attributed to the prevalence weaker buoyancy force. Dipankar et al. [80] have proposed an analytical solution for four different loop configurations under steady-state with identical boundary and operating conditions. They concluded that the rectangular NCL model has higher flow rates.

Pilkhwal et al. [81] analyzed the unstable behaviour of the single-phase NCL with system codes like RELAP5, in-house non-linear tools for 1D and FLUENT commercial code for 3D. They

changed the orientation of the heater and cooler and found the effects on stability of the loop fluid in the loop.

Lin et al. [82] investigated the effects of the wall thermal conductivity and the wall thickness on the heat transfer rate of NCL. The presence of axial conduction through thick and highly conductive loop walls tends to strengthen markedly the buoyancy-induced circulating flow in the loop at lower Rayleigh number. However, this study was for a specified range and not for general applicability.

The impact of geometrical parameters on the stability of NCL under steady state condition was numerically studied by Dipankar et al. [83]. They concluded that stabilities can be suppressed by increasing the loop height because of stronger buoyancy effects. They also found that NCL with a smaller pipe diameter has more stability due to enhancement in friction. An NCL with wider loop and a longer heat source section has greater stability. They also reported that a small loop inclination angle (10° – 15° range) was adequate to reduce instabilities in the loop even at high powers.

Kiran Kumar et al. [84] numerically evaluated a 1-D rectangular NCL under steady state for low temperature applications with hot and cold heat exchangers at the source and the sink respectively, and they developed a new relation for determining suitability of various fluids in NCL in terms of pipe diameters and temperature rise/drop.

Chen et al. [85] numerically and experimentally studied the effect of loop tilt angle on the performance of a supercritical carbon dioxide based natural circulation loop. For their numerical study 2-D numerical NCL model was developed and simulated. They also conducted experiments on the same geometrical NCL to validate the numerical results. They reported that at high heat flux, the effect of tilt angle on average Nusselt number was minimal. At low heat flux, however, this effect was considerable.

Wang et. al [86] numerically investigated the heat and flow characteristics in an NCL with water as the working fluid. In their study the effect of two different loop inclination angles (30° and 75°) was studied. Their simulation results matched well with the published experimental data.

Yadav et. al [87] carried out a numerical study on CO_2 based NCLs and they developed new correlations for heat transfer and friction. In their extended work [88], transient analysis of CO_2 based NCLs was numerically studied. In their study the effect of loop inclination angle on NCLs was discussed. They reported that NCL reaches a steady state in the shortest time at 45°

tilt angle. Steady state mass flow rate and heat transfer rates were reduced with an increase of tilt angle. This was due to the reduced loop height which causes a decrease in buoyancy force.

D. Lu et. al [89] numerically studied the stability analysis of single-phase rectangular NCLs by considering liquid metal as a working fluid. The effects of the geometrical parameters and the types of working fluids on the stability of NCLs were estimated. They found that sodium–potassium alloy (NaK) loop and liquid sodium (Na) loop would be more stable than lead bismuth eutectics (LBE) loop. The NCL with a lower aspect ratio (ratio of vertical center distance between the cooling and heating section to the width of loop) was supposed to be more stable.

Goudarzi et. al [90] carried out a non-linear stability analysis and the entropy generation for a uniform and non-uniform diameter loop under single-phase natural circulation. In this investigation, a constant heat flux boundary condition at the heater and constant wall temperature boundary condition at cooler were considered. The effect of geometrical dimensions of the loop and power input to heater on stability and entropy generation in the loop was investigated. They reported that a large aspect ratio (Lt/D) causes more entropy generation within the loop. It was found that larger heater length led to more entropy generation within the loop. Also decreasing the heater diameter caused more entropy generation within the loop. The stability of the system was strongly influenced by the diameter of the cooler. A larger cooler diameter rather than the average loop diameter decreased the unstable region and rendered the system more stable.

Srivastava et al. [91] carried out a transient study on molten salt based NCL. For this study a one-dimensional in-house code (LeBENC) was developed and the results were validated with experimental results of molten salt based NCL (MSNCL). Jayaraj et al. [92] developed a three-dimensional CFD model and simulated it to study the transient characteristics of MSNCLs.

Karadeniz et al. [33] carried out a 3-D numerical study to investigate the effect of loop inclination on the performance of mini-NCL for low heat transfer applications with Al_2O_3/water nanofluids at different particle volume concentrations (1%, 2% and 3%). In this study power input to the heater and loop inclination angle were varied between 10-50W and 0-50° respectively and the heat sink temperature was assumed as 20 °C. They concluded that the loop fluid temperature difference in the heater and maximum temperature of the loop fluid increases with power input, particle concentration and loop inclination angle. They also reported the effectiveness of the loop increases with particle concentration and inclination angle.

Luzzi et al. [93] evaluated and developed analytical and numerical models on experimental data to study the natural circulation dynamics in vertical loops. They concluded that the thermal inertia of piping wall materials influences NCL behaviour. Also they reported that the SST *k*-ω model could be a better option for CFD turbulent flow in NCL.

Krishnani et al. [94] studied the influence of the loop inclination on the stability of single-phase rectangular NCL. They concluded that, unstable oscillations were observed in the loop with an increase in power input and cooler temperature. However, the loop that operated with 15° was found to be very stable for all the cases.

Goudarzi et al. [95] employed a non-linear stability method used to investigate the stability of NCL and an entransy dissipation (heat flow direction) method used to estimate thermodynamic performance of the NCL. In this work, various geometrical and operating parameters and orientation of the heater and cooler were investigated. They concluded that under steady state conditions, the horizontal orientation of the heater and cooler leads to higher mass flow rates than other orientations. In horizontal orientation of the heater and cooler, more stable was observed by enhancing the heater diameter.

2.1.2. Experimental studies on single-phase natural circulation loops

Creveling et al. [64] experimentally studied the instabilities of a toroidal loop. Their study confirmed the observations of Keller and Wallander by observing flow instabilities even at atmospheric pressure and moderate temperatures. They developed a theoretical model for turbulent region as well.

Misale et al. [96] experimentally studied the effect of pressure drop on the stability of the loop. For this study, they made a provision for introducing localized pressure drops by using orifices with different diameters. A small diameter orifice stabilized the loop faster than larger diameter orifices.

Vijayan [75] developed a correlation based on experimental results for flow rate in terms of Reynolds number, Grashof number and a dimensionless loop parameter. Testing these correlations with experimental data showed reasonable agreement. The developed correlation suggests that the simulation of the steady-state flow in single-phase NCL's can be attained by simulating the non-dimensional parameter (Gr_m/N_G).

Misale [97] experimentally investigated the effect of orientation angle of a rectangular natural circulation loop and found that the deviation of the quiescent state (steady temperature

difference across the heat sinks) increases when power decreases while the loop inclination increases.

Vijayan et al. [98] demonstrated the effect of the heater and cooler orientations on single-phase natural circulation loop and concluded that a loop operated with horizontal orientation of heater and cooler achieved the maximum flow rate. However, this orientation was found to be the least stable and the orientation with both heater and cooler vertical was found to be the most stable.

Nayak et al. [99] studied the circulation behaviour in a rectangular loop with water and Al_2O_3-water nanofluids. From this study it was demonstrated that, not only the flow instabilities were suppressed, but also the natural circulation flow rates were enhanced by using nanofluids. The enhancement in the natural circulation flow rate and suppression of instabilities were found to be dependent on the concentration of nanoparticles in water.

Garibaldi et al. [100] experimentally studied the influence of geometrical parameters and fluid properties on the thermal performances of rectangular single phase natural circulation mini loops, which could be used for cooling electronic devices. Water and FC43 (a commercial secondary fluid) were chosen for comparison. Results show that at the same power, the velocity of FC43 was almost twice that of water, but the thermal performance was worse because FC43 was characterized by low specific heat. Misale et al. [101] studied the effect of heat sink temperatures on the stability of the loop. They reported that, by tuning the heat sink temperature the loop was switched from unstable to stable flow condition without varying power input. The stability behaviour of the water based NCL was better than FC43 based NCL.

Misale et al. [102] conducted experiments on natural circulation mini loop operated with water and Al_2O_3-water nanofluid at different loop inclinations. The result showed that nanofluid based mini loop at 75^o inclination exhibits enhanced thermal performance when compared with water based mini loop.

Doganay et al. [35] experimentally studied the effect of loop inclination angle on effectiveness of Al_2O_3-water nanofluid based single phase rectangular natural circulation mini loop. They concluded that the time required to reach steady state conditions increases with loop inclination angle. The steady state mass flow rates of any loop fluid decrease with loop inclination angle. It happens due to decreasing gravitational acceleration. But the effectiveness of the NCL was enhanced proportionally with loop inclination angle and particle concentration.

The effect of power steps on thermal and hydraulic behaviour of NCL was experimentally studied by Misale [103]. The experiments were carried out at constant power input and variable

power inputs. The amplitude of steps was ±20% or ±50% of the power input, whereas the period of the oscillations varied between 50 s and 7200 s. All test results showed unstable behaviour, i.e., temperature oscillations across the heated sections occur in the fluid, at both variable power and constant power input conditions. Furthermore, the frequency and the amplitude of the oscillations increase with power input. The thermal inertia of the loop plays a vital role in oscillatory flow in case of smaller time steps.

Koca et al. [18] experimentally analysed the thermal performance of natural circulation mini-loop using Ag/water nanofluid as working fluid for solar applications. They reported that the effectiveness of NCL was enhanced by 11 % at 1 % particle volume concentration compared to pure water. Furthermore, the effectiveness was enhanced with the loop inclination angle and particle concentration at a fixed power input.

Sadhu et al. [104] experimentally studied an air cooled NCL using supercritical CO_2 as working fluid under steady-state operation. The effectiveness of the NCL was found to be in the range of 63–91% of the operating range of parameters considered. The effectiveness was significantly influenced by the inlet temperature of the heat sink. There was a stable operation observed for the entire range of operation. For a particular heater power level, an optimum charge was found at which the thermal conductance of the heat sink was maximized.

2.2 Nanofluids and its applications

Advancements in nanotechnology opens a gateway to a new generation of fluids for heat transfer applications. Suspending the nanoparticles in the working fluid at low concentrations significantly alters the thermal conductivity and consequently heat transfer properties. In the past several years, nanofluids have found widespread applications in various industrial and commercial applications such as in refrigerators, cooling electronic devices, solar collectors, different heat exchangers, nuclear reactor core cooling, liquid fuels and lubricants.

Nanofluids are a relatively new class of heat transfer fluids spread over all fields of technology and engineering due to their prevalent properties. Higher thermal conductivity of nanofluids attracts and encourages researchers to use them in many technological applications. The other pivotal thermophysical property is viscosity, which defines the hydrodynamic behaviour of a fluid. Both thermal conductivity and viscosity increase with that particle concentration. Along with particle concentration, another considerable parameters that influence the thermophysical properties of nanofluid are temperature, size of particle, properties

of base fluid etc. Suspension of solid particles in fluids to promote their thermal properties is not a new idea. Maxwell et al. [30] dispersed solid particles in liquid medium to enhance the thermal conductivity of the working fluid and developed a correlation to estimate the thermal conductivity of particle suspended fluid. Hamilton et al. [31] extended the Maxwell research and modified Maxwell thermal conductivity correlation for more precise prediction. But both researchers [30], [31] suspended micro-size particles in flowing fluids.

The capability to produce nano sized solid particle with the advanced material technology create a new platform for a new class of innovative heat transfer fluids. For the first time Choi et al. [105] addressed the phenomenon of suspending nano sized solid particles in a base fluid to augment its thermal and flow properties and labelled such fluid as nanofluids.

Wen and Ding [106] conducted experiments with Al_2O_3-water nanofluid in a test tube and reported 47 % increase in the heat transfer coefficient at 1.6 vol. %. In their extended work, Ding et al. [48] used CNT/water nanofluid as working fluid in a horizontal tube and reported 350 % enhancement in heat transfer coefficient at Reynolds number of 800 with 0.5 wt.%.

John Philip et al. [36] reviewed and summarized the research progress on nanofluids preparation, stability, thermal and rheological characteristics of alumina (Al_2O_3) nanofluids. While Fotukian et al. [107] reported a 25 % heat transfer enhancement at 0.24 vol. % of CuO/water nanofluid with a 20 % penalty of pressure drop.

Kao et al. [108] examined the characteristics of Al_2O_3 brake nanofluids produced by plasma charging system. They reported that the boiling point temperature was increased by 8 °C when compared with conventional brake fluid. Also, viscosity and thermal conductivity of the nanofluid based brake fluid was higher than conventional brake fluid. Kao et al. [109] analysed the performance of CuO brake nanofluids produced by arc-submerged synthesis system. From their results, it was observed that the boiling point, viscosity and thermal conductivity of CuO brake nanofluid were higher than conventional brake fluid.

Ahammed et al. [110] experimentally examined the viscosity and surface tension of graphene-water nanofluid at different concentrations and temperatures. They reported that the viscosity of the nanofluid following the incremental trend with the particle concentration and following the inverse trend with the temperature, while surface tension was decreasing with both particle concentration and temperature as well. At 1.5 % particle concentration and 50 °C the viscosity of nanofluid was augmented by 47.12 %, while the surface tension reduced by 18.7% for the same concentration and temperature.

Strong Van Der Waals interactions between nanoparticles suggest a technical challenge for preparing a stable homogeneous suspension. Ghadimi et al. [111] proposed and tested chemical method by adding surfactant to modify the surface of particles and physical methods, applying powerful forces on the clustered nanoparticles to produce stable nanofluids. Xuan and Li [112] also recommended the addition of surfactants and ultrasonication to improve the stability of nanofluids.

Ramanujam Lenin et al. [113] conducted experiments to study the influence of base fluid properties on enhancement of thermal conductivity of nanofluid. For their study, they considered toluene, xylene, mesitylene, and kerosene as base fluids and magnetic nanoparticle coated with oleic acid as suspended particles. They observed that the base fluid having a lower thermal conductivity exhibits the maximum thermal conductivity enhancement. They also noticed that, below a certain limit of particle concentration, there was no considerable improvement in thermal properties and that concentration was termed as the critical concentration. The critical concentration was different for different base fluids and among all the considered working fluids, kerosene exhibits the lowest critical concentration and highest thermal conductivity enhancement than other working fluids. They mentioned that the base fluid and nanoparticle interactions at the interface was a critical parameter which will directly influence the stability and thermophysical properties of a nanofluid. If the particle concentration was above the critical concentration, nanoclusters may form due to Van der Waals interactions, leading to the enhancement of thermal conductivity.

Ghasemi et al. [51] experimentally evaluated the performance of a circular heat sink with Al_2O_3/water nanofluid at different flow rates and particle concentrations. They reported that Nusselt number and heat transfer coefficients were also increasing with volume flow rate at the heat sink, while the pumping power was also proportionally increasing with flow rate, whereas the friction factor was decreasing with the flow rate.

Ilyas et al. [114] experimentally investigated the stability and thermophysical properties of Multi Wall Carbon Nano Tubes (MWCNT)/thermal-oil nanofluid of up to 1.0 % concentration. To conduct the experiments, MWCNTS were neither functionally treated nor was the surfactant used to prepare the stable nanofluid. At 1.0 % particle concentration, viscosity and thermal conductivities increased by 76 % and 33.6 % respectively than that of thermal oil. Since, there was a considerable variation between the empirical and experimental results, they proposed a new correlation for both thermal conductivity and viscosity of nanofluids.

Ueki et al. [115] experimentally studied the thermal conductivity and specific heat of water based nanofluids. They conducted experiments on two water based nanofluids, which were prepared from soot Carbon Black (CB) and Carbon Nano Powder (CNP). In their work, CB particles were synthesized by the combustion process, while CNP was purchased from a vendor. It was clear from their experimental results that the nanoparticle shape and nanofluid temperatures had great influence on the enhancement of thermal conductivity. The effective thermal conductivity of CB and CNP was augmented by 7 % and 19 % at a particle concentration of 1.5 %. They concluded that the fine soot CB particles can be produced either by thermal decomposition or by incomplete combustion of hydrocarbons at commercial scale at relatively low cost, which was the prime motto of their experimental work.

Singh et al. [116] studied the use of nanofluids in a Proton-exchange membrane fuel cells (PEMFC) cooling system (for vehicle applications) and they concluded that the radiator frontal area can be minimised by 10%. From the studies of Wong and De Leon [116] it was concluded that aerodynamic drag decreased with smaller radiator frontal area leading to reduced fuel consumption.

Kim et al. [117], [118] carried out a study to evaluate the performance of water-cooled systems with nanofluids in nuclear applications. The plasma divertors, accelerator targets, primary coolant, pressurized water reactor (PWR), standby safety systems were possible applications [119].

Tzeng et al. [120] examined the heat transfer performance of Al_2O_3 and CuO nanofluid based engine transmission oil of the rotary coupling 4-wheel vehicle. They reported that the lowest transmission temperatures were observed for both nanofluids at low and high rotating speeds. Thus, from the thermal performance viewpoint, the use of nanofluid in the transmission has a clear advantage.

Lin et al. [121] analysed the silver nanofluid based heat pipes and found heat transfer characteristics were improved with silver nanofluid. Nguyen et al. [52] examined thermal performance of Al_2O_3-water nanofluid based cooling system (closed loop) designed for electronic devices. Their results reveal that in the use of nanofluid in the cooling system, the convective heat transfer coefficient significantly increased. The heat transfer coefficient increased as much as 40% compared to the base fluid of water at 6.8% particle concentration. Smaller nanoparticles showed higher convective heat transfer coefficients than larger ones.

To develop the difference of transient temperature response between conventional cryosurgery and nano-cryosurgery, Yan and Liu [122] performed simulations on the combined phase change bio-heat transfer problems in a single cell level and its surrounding tissues.

2.3 Research gap observed from the literature review

- Though numerical and experimental studies on water based NCLs were carried out, studies on nanofluid based NCLs are relatively few.

2.4 Objective and scope of the present research work

The objectives of the present work are as follows:

- To study the suitability of nanofluids in NCL.
- To optimize the dimensions of the loop i.e. diameter of the loop pipe, length of the loop, and the heat exchangers length, etc.
- To study the influence of operating parameters such as inclination angle, particle concentration, external fluid temperatures, external fluid mass flow rate of thermal performance of nanofluid based natural circulation loop.
- To study the transient behaviour of NCL.

2.5 Research approach

In the current research, numerical and experimental investigations have been carried out to evaluate the thermal performance of the single-phase natural circulation loop operated with heater and with end heat exchangers. A comparative study has been conducted on NCL with different working fluids.

1. An analytical expression is developed to show the suitability of nanofluid in rectangular natural circulation loops.
2. Experiments were carried out to find the thermo-physical properties, such as thermal conductivity and viscosity.
3. A one-dimensional and three-dimensional mathematical model are developed and the system of equations solved by in-house code (in MATLAB) and commercial software (Ansys-Fluent 14.0), respectively.

4. Based on the numerical results, a test rig was designed and fabricated. Experiments were conducted to study the effect of operating parameters, such as inclination angle, particle concentration, external fluid temperature, external fluid mass flow rate, etc.
5. Experiments were also conducted to study the effect of small perturbations on the stability of the loop fluid in NCL.
6. Comparative studies were conducted by considering the all possible errors while conducting experiments.

2.6 Conclusion

A comprehensive review of literature concerning single phase natural circulation loops and nanofluids has been provided. From an exhaustive exploration of literature, the various parameters that influence thermal performance of NCL and stability behaviour in NCL is known to be (i) geometrical and operating parameters and (ii) the properties of working fluid has been documented in the present chapter. In conclusion, the factors that are useful and provide the appropriate background information for consideration to the present research problems have been provided. The different principal objectives of current research work are provided, which will provide a detailed view on the thesis. The ensuing chapters one devoted to presenting extensive details on the suitability of nanofluids in the natural circulation loop, several synthesis methods of nanofluid preparation, introducing various nanofluid stability approach used in the current work. The study also estimated the necessary thermophysical properties, using empirical correlations available in the literature. Thermal conductivity and viscosity of the nanofluids were experimentally estimated and compared with empirical correlations.

Chapter 3

Nanofluid preparation, thermo-physical properties of nanofluids and suitability of nanofluids in natural circulation loop

In this chapter, the preparations of nanofluids as well as the analytical and experimental measurement of thermo-physical properties of nanofluids are discussed in detail. Experimental studies on viscosity and thermal conductivity of nanofluids are compared with existing empirical correlations, as used in the present research. Furthermore, the suitability of various nanofluids as loop fluids in the natural circulation loop is presented. A qualitative comparison is made between nanofluids and water in terms of pipe diameters and temperature differences to reduce the size of the loop. Based on a simple model, results are obtained in both laminar and turbulent flow conditions considering single-phase flow through the loop.

3.1 Synthesis of nanoparticles

Producing nanoparticles, generating a homogeneous suspension and producing stable nanofluids are the key issues with particle suspended fluids. The method of nanoparticle synthesis and its dispersion depends on the type of bulk material and its properties. With updated technology, various synthesis methods are available to produce the nanoparticles at commercial scale. Some of the synthesis methods to produce nanoparticles are presented and some of them are discussed in the sections that follow.

Thermo-physical properties of a nanofluid are strongly influenced by the successful synthesis and stable suspension of nanoparticles in base fluids. Top-down (break down) approach and bottom-up (build up) approaches are the most familiar methods of nanoparticle synthesis [123]. In the top-down approach, external forces are applied to bulk materials to break them down into fine particles, whereas, in bottom-up approach, atomic transformation or molecular condensation techniques are used.

Nanoparticles are widely synthesized by either of the approaches mentioned in the earlier section. The top-down approach can be sub-divided into dry grinding [124] and wet grinding [125]. In any grinding process, a solid substance breaks into nanoparticles by applying mechanical energy in terms of shock, compression or friction. In dry grinding, the process is carried out in the presence of air or gas, whereas in wet grinding, the process is carried out in the liquid environment. Some of the common dry grinding methods are jet milling [126], hammer milling, shearing milling, roller milling, shock shear milling, ball milling and tumbling milling. Common wet grinding methods are tumbling ball milling, vibratory ball milling [127], planetary ball milling [128], centrifugal fluid milling [129], agitating bead milling, flow conduit bead milling, annular gap bead milling and wet jet milling. It is worth noting that agglomeration of nanoparticles is greater with the dry grinding methods as compared to wet grinding methods .

The bottom-up approach is broadly divided into gaseous phase methods, and liquid phase methods. Chemical vapour deposition [133], [134], physical vapour deposition [134], [135] and thermal decomposition methods [136] come under gaseous phase methods. Chemical vapour deposition and physical vapour deposition methods can produce nanoparticles ranging from 10 nm to 100 nm, whereas thermal decomposition methods can produce 4 nm to 18 nm sized nanoparticles. A thermal decomposition method is widely used for producing metal oxide particles on a commercial scale. Liquid phase methods are further classified into liquid-liquid method and sedimentation methods. Chemical reduction of metal ions is an example of liquid-liquid method. The principal advantage of this method is that, the particles can be produced in different shapes and sizes by using an appropriate reducing agent. Along with these methods, solvo-thermal synthesis [140], spray pyrolysis [141], spray drying are some other typical liquid-liquid methods. While, the sol-gel process is an extensively used sedimentation method, which is used to produce polymer nanoparticles and metal oxide nanoparticles [142]. Detailed classification of nanoparticle synthesis methods is given in fig. 3.1.

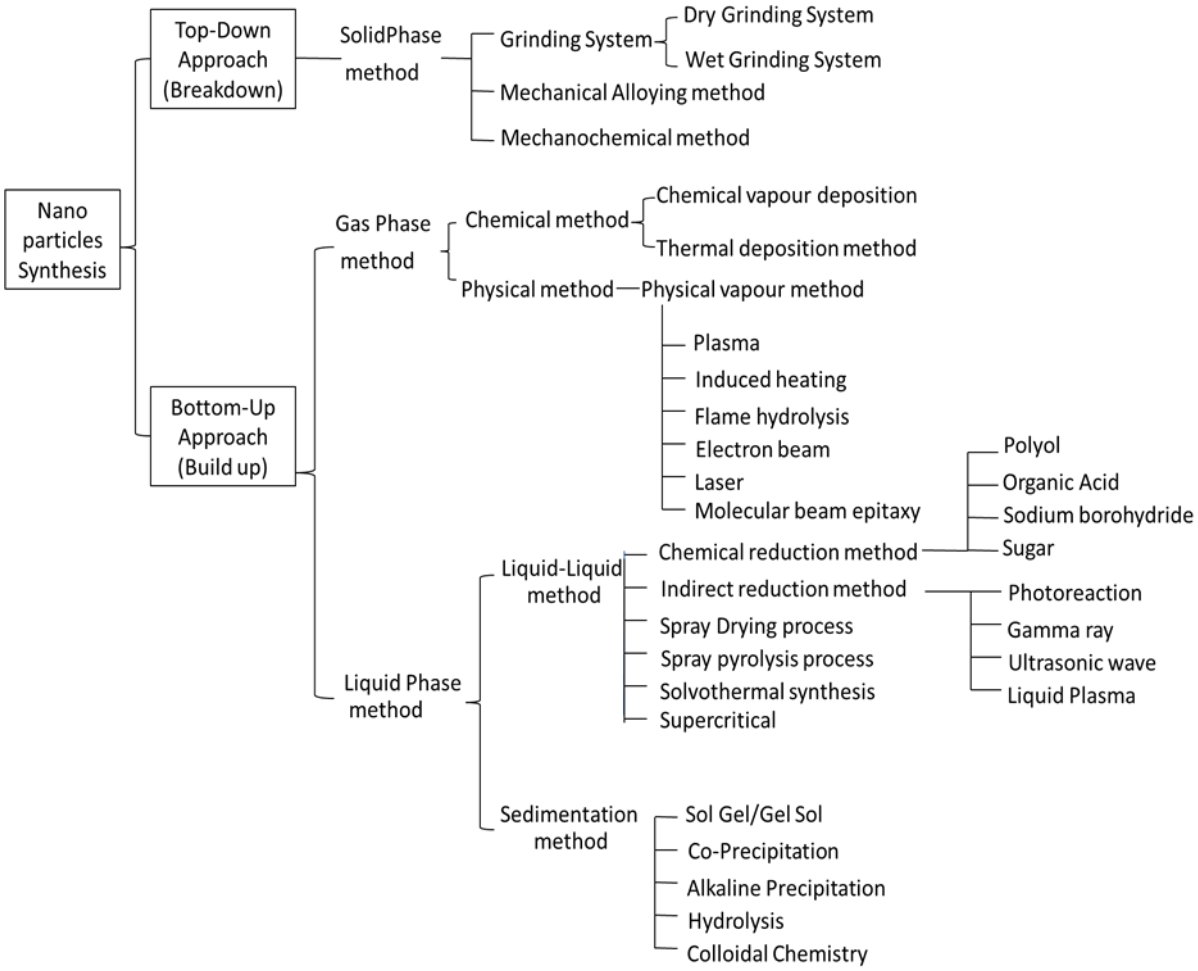

Fig. 3.1 Classification of nanoparticles synthesis methods at a glance [142]

3.2 Nanofluid preparation

Nanofluid preparation is the pivotal stage that decides the stability and thermo-physical properties of a nanofluid. A nanofluid is not a simple mixture of liquid and solid. The prepared nanofluid must possess some essential requirements including durability, stability with minimal agglomeration for considerable duration, and being chemically inert to use nanofluid for real time applications. Two common approaches for the preparation of nanofluids are: one step method and two step method.

3.2.1 One step method

In the one-step method, nanoparticle generation and dispersion in the base fluid were one ago [46], [143]. This is the most suitable method for high thermal conductive metals to avoid oxidation. High stability and uniform dispersions are the principal advantages of this method. The Even rate of agglomeration is relatively low, producing the high concentration

nanofluid at predefined concentration is difficult by this method. In addition, the tedious sequencing of steps like drying, storing, dispersing of the nanoparticles can be avoided. The major drawback of this method is, nanofluids cannot be produced at commercial scale and also it is not a cost effective approach for the production of nanofluids at large scale.

3.2.2 Two step method

In the two-step method, nanoparticles are separately synthesized and suspended in the base fluid independently, with the assistance of mechanical aids in desired concentration [144], [145]. The primary advantage of this method is that the thermophysical properties can be controlled comparatively in a better way than the single-step method. A notable feature of this method is nanoparticles can be produced economically on a large scale. However, the prime difficulty is the unavoidable agglomeration of such particles by virtue of cohesive and Van der Waal forces among the nanoparticles. This agglomeration can be controlled by employing appropriate surfactant or dispersant at critical micelle concentration. The agglomeration can also be minimized by using appropriate mechanical dispersing devices like ultrasonic bath, magnetic stirrer, high-pressure homogenizer and ultrasonic disrupter.

Nanofluids can be prepared by the two step method. To attain the homogeneous and stable dispersion, ultra-sonication can be adapted. By blending an appropriate surfactant in the base fluid agglomeration can be further suppressed.

3.3 Stability of nanofluids

Stability of nanofluids is a key parameter for the consistent functioning of a thermal system at a designed capacity. Therefore, preparation of stable nanofluids for a considerable duration is technical difficulty for researchers. The possible reason for agglomeration of nanofluids is, strong Van der Waal forces and cohesive forces among the nanoparticles. These forces may be the root cause for agglomeration. The agglomerated nanofluid loses its potential to transfer heat by decreasing the Brownian motion of particles. It also deteriorates the flow behaviour by amplifying frictional resistance and consequently increases the pressure drop. Therefore, stable suspension of nanoparticles is essential to get the desired properties.

Fundamental principles for the stable suspension of nanoparticles are (i) Diffusion Principle: nanoparticles are scattered by fluid medium and hence dispersed into it by electric double layer repulsion. (ii) Zeta Potential Principle: the absolute zeta potential value of the nanofluid must be maximized to the extent possible. As the zeta potential diverges from the iso-

electric point, strong repulsive forces will develop among particles and reduces the agglomeration. T.P.Teng et al. [146] observed that Al_2O_3/water nanofluid is stable and showed good thermal conductivity by maintaining pH value of 8.

Some instruments that are commonly used to check the relative stability are sedimentation photographs, zeta potential test, UV-Vis spectrophotometer, SEM (Scanning Electron Microscope), light scattering, and TEM (Transmission Electron Microscope).

From the literature, it is found that a number of effective strategies were developed to minimize the agglomeration. The most common methods are (i) adding surfactant (ii) ultrasonic vibration and (iii) electrostatic stabilization by controlling the pH value. However, the method of adding a suitable surfactant is widely employed by the researchers in the preparation of a stable nanofluid.

3.3.1 Surfactant addition

Surfactant is a surface-active agent, which creates electrostatic repulsion among the nanoparticles in the base fluid to compensate Van der Wall attractions [147]. It enriches the affinity between the nanoparticles and base fluid. These surfactants are complex chemical compounds, which lower the interfacial tension between base fluid and suspended nanoparticles. In addition, they help to stabilize the suspension by increasing the electric double layer repulsion between nanoparticles (one layer is formed on the surface of particles by the corresponding ions within the crystal lattice and a second diffusion layer is formed on the base fluid. When these double-layered particles come closer, repulsive forces develop and thereby diminish the agglomeration). Surfactants chemically convert nanoparticles from hydrophobic to hydrophilic and vice versa, based on the type of host fluid and nanocomposite/nanoparticle. On the other hand, surfactant can also increase the zeta potential of nanofluid, which magnifies the surface charge of dispersed nanoparticles in the host fluid [148], [149]. The conventionally used surfactants are Sodium Dodecyl Benzene Sulfonate (SDBS) [150], [151], Sodium Dodecyl Sulphate (SDS) [148], [152], [153], Cetyl Trimethyl Ammonium Bromide (CTAB) [154], Dodecyle Trimethyl Ammonium Bromide (DTAB) [155], Hexa decetyl trimethyl ammonium bromide (HCTAB), Salt and OlicAcid [156], [157] Sodium Octonate (SOCT) [155], Poly Vinyl Pyrolidone (PVP) [158], [159], Gum Arabic [160] and Octylsilane [161]. To obtain favourable results, selection of appropriate surfactant should be made in conjunction with the combination of nanoparticles and base fluid.

3.3.2 Ultrasonic vibration

It is a standard method for nanofluid stabilization. It is an effective method for homogeneous dispersion of nanoparticles and breaking the agglomeration. Many researchers use this technique, because it is simple and easy. The key principle of this technique is that nanoparticles are continuously subjected to high frequency vibrations and particles are uniformly dispersed in the base fluid. It is to be noted that the surface properties of suspended nanoparticles do not change as in other methods. The optimized duration of sonication depends on the size, type and concentration of nanoparticles. Ultrasonic bath, ultrasonic vibrator and homogenizers are the most common devices to impart ultrasonic vibrations.

The stability of the nanofluid can be measured by the sedimentation rate in terms of particle velocity in the host fluid. According to Stoke's law [162] the speed of nano particle sedimentation can be decreased by decreasing the nanoparticle size (R), increasing host fluid viscosity (μ), and decreasing the density gradient between the nanoparticle and host fluid $(\rho_{np} - \rho_{bf})$. Among all the parameters, the most significant parameter is R. From the theory of colloid chemistry, it is clear that the sedimentation is zero due to Brownian motion of nanoparticle, if the particle size reaches the critical size (R_c) [163]. One can estimate the sedimentation velocity of nanoparticle using eq. (3.1).

$$V = \frac{2R^2}{9\mu}(\rho_{np} - \rho_{bf}) \tag{3.1}$$

From eq. (3.1) of sedimentation velocity, the stability of the nanofluid can increase by reducing the size of nanoparticle (R), reducing the density difference between nanoparticle and base fluid and increasing the viscosity of base fluid.

3.3.3 Electrostatic stabilization

The stability of the nanofluid is directly related to the electro kinetic properties of nanoparticles. An electric charge exists in the atoms in the outer most orbital. This charge is the root cause of the kinetic behaviour of nanoparticles in base fluids. In electrostatic stabilization, stable suspension can be attained by forming an electric static double layer by the ions of particles and host fluid. The diffusion layer is initiated at the iso-electric point at which the zeta potential is zero. As the pH values of solution move away from this iso-electric point, these repulsive forces increase and hence the stability of the nanofluid improves. This electrostatic stabilization method is pH sensitive [164].

3.4 Nanofluid preparation for the current research work

For the current research, all the nanoparticles (Al_2O_3, CuO and SiO_2) with sizes of 30-50 nm are purchased from SISCO Research Laboratory (SRL) Pvt. Ltd., Mumbai, India. The size of particles is assumed to be the same as quoted by the supplier. Distilled water was taken as the base fluid for nanofluid preparation as well as for conducting experiments for comparison of NCL performance. Nanofluids were prepared by the two step method. Nanoparticles were dispersed in the base fluid using an ultra - sonicator (supplied by Electrostatic Industries, India) to break the agglomerated particles and to obtain a stable and homogeneous suspension. The fluid was subjected to continuous sonication for 2 hrs and the sonicator produced ultrasonic waves at 180 W. C-TAB [154] was used as a surfactant to increase the dispersion stability of nanoparticles in base fluid. Both sonication and surfactant were used to control the agglomeration while preparing stable nanofluid. All the nanofluids were prepared at 0.5%, 1.0%, 1.5%, 2%. 2.5% and 3% particle concentrations, which are the suitable particle concentration for heat transfer applications. It is noticed that all the nanofluids have been stable for 72 hours at least without forming any sediment or agglomerating.

Fig 3.2. Preparation of nanofluids by ultra-sonicator (i) Al_2O_3, CuO, SiO_2 nanopowder and C-TAB surfactant (ii) Al_2O_3-water nanofluid (iii) CuO-water nanofluid

3.5 Estimation of thermo-physical properties of nanofluids: Empirical correlations

To precisely measure the performance of a nanofluid based thermal system, accurate information about thermophysical properties of the working fluid is necessary. To evaluate the thermophysical properties of nanofluid analytically, the particles are assumed to be uniformly dispersed in host fluid. These properties depend heavily on the quantity of nanoparticles added to the base fluid. The mass of the nanoparticles required to prepare the nanofluid for a particular volume concentration can be estimated by using eq. (3.2) [43].

$$\emptyset = \frac{V_p}{V_{nf}} = \frac{V_p}{V_p + V_{bf}} = \frac{\frac{m_{np}}{\rho_{np}}}{\frac{m_{np}}{\rho_{np}} + \frac{m_{bf}}{\rho_{bf}}} \times 100 \quad (3.2)$$

Several researchers from the past decades proposed many correlations to precisely evaluate the effective thermo-physical properties of nanofluids by considering different constraints such as particle size, base fluid properties, operating temperature and these correlations are match with experimental results. Most of the existing correlations for nanofluid possess good agreement with the experimental outcomes. Thermo-physical properties such as density, dynamic viscosity, specific heat, thermal expansion coefficient and thermal conductivity of various nanofluids were estimated using empirical correlations which have close approximations with experimental results.

In the current research CuO, Al_2O_3 and SiO_2 nanoparticles with an average particle size of 30-50 nm were considered for the analysis. The particle concentrations for this analysis 0.5%, 1.0%, 1.5%, 2%. 2.5% and 3% were chosen to precisely predict the thermo-physical properties. The properties of water and various nanoparticles are presented in table. 3.1.

Table 3.1 Thermophysical properties of water and various nanoparticles considered for the current research.

Material	Thermal conductivity (W/mK)	Density (kg/m^3)	Specific heat (J/kgK)	Thermal expansion coefficient (K^{-1})
Al_2O_3	40	3900	785.2	8.4×10^{-6}
CuO	69	6350	502.8	9.3×10^{-6}
SiO_2	1.4	2648	692	0.5×10^{-6}
Water	0.6	997	4181.3	2.5×10^{-4}

3.5.1 Density

Density of nanofluid is estimated based on the principle of the mixture rule and it can be calculated by using eq. (3.3) [43]. Vajjha et al. [165] made a comparison between experimental values of density and prediction via eq. (3.3) for Al_2O_3, CuO and SiO_2 nanofluids. They observed good agreement between the measured and predicted values. Hence, eq. (3.3) is used as a general correlation to estimate density of all types of nanofluids in the present work.

$$\rho_{nf} = \left(\frac{m}{V}\right)_{nf} = \frac{m_{bf} + m_{np}}{V_{bf} + V_{np}} = \frac{\rho_{bf} V_{bf} + \rho_{np} V_{np}}{V_{bf} + V_{np}} = \emptyset\, \rho_p + (1 - \emptyset)\rho_{bf} \quad (3.3)$$

$$where, \emptyset = \frac{V_p}{V_p + V_{bf}}$$

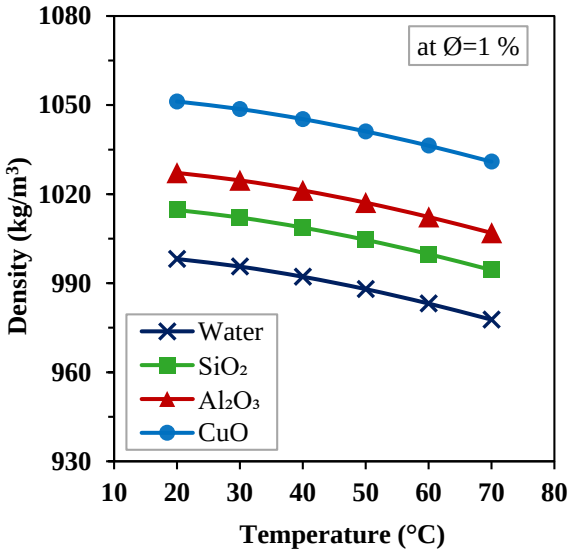

Fig. 3.3 Variations of density of nanofluids with temperature

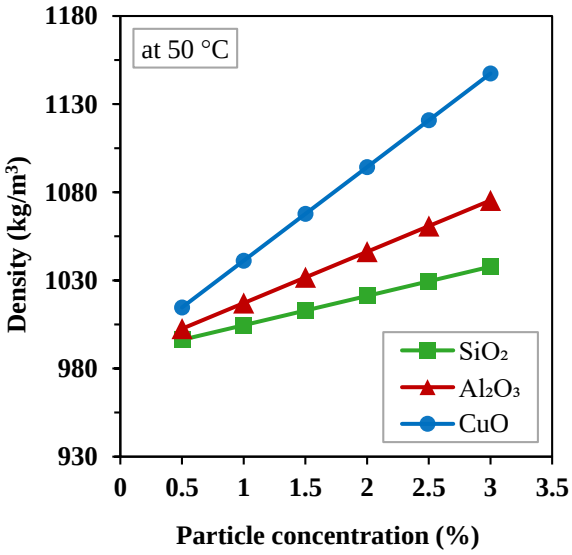

Fig. 3.4 Density variation of different nanofluids in particle concentration

The influence of temperature and particle concentration on the density of various nanofluids is described in fig. 3.3 and fig. 3.4 respectively. The density of all nanofluids decreases with increase in temperature, as shown in fig 3.3. It is clear from fig. 3.4 that the density of all nanofluids is linearly increasing with particle concentration. It is noticed from eq. (3.2) that the density of the nanoparticle material directly influences the density of nanofluid. It can be observed from table 3.1 that copper oxide has the highest density, which consequently causes higher density of CuO/water nanofluid compared to other nanofluids.

3.5.2 Heat Capacity

Heat capacity is a quantitative measure of heat transfer in a NCL. Specific heat of the nanofluid is found to decrease in proportion to the increment of particle concentration. This reduction in heat capacity leads to an increase in the exit temperature of the working fluid at the heat source in NCL. The heat capacity of nanofluids can be estimated from the principle of mixture rule by using eq. (3.4) [43].

$$C_{p,nf} = \frac{(1-\emptyset)\rho_{bf}C_{p,bf}+\emptyset\rho_p C_{p,p}}{\rho_{nf}} \qquad (3.4)$$

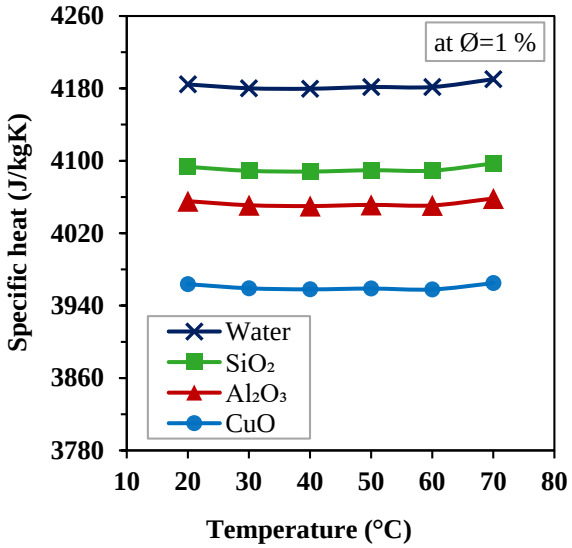

Fig. 3.5 Variation of specific heat of CuO/water nanofluid with temperature

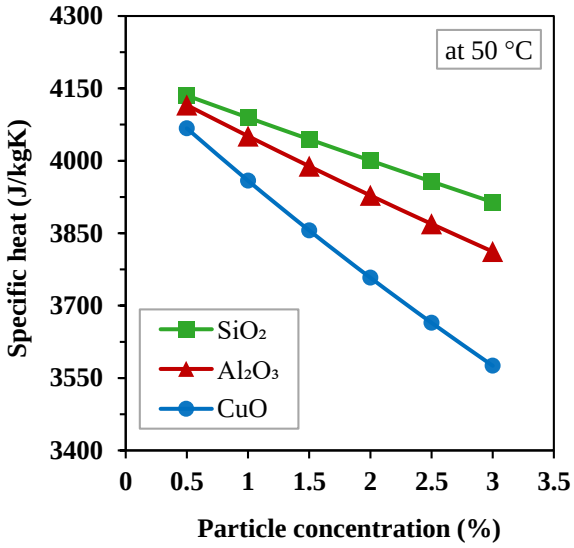

Fig. 3.6 Specific heat variation of different nanofluids with particle concentration

The effect of temperature on the specific heat of nanofluids at 1% particle concentration is elucidated in fig. 3.5. The specific heat does not vary much with temperature for all fluids described in fig. 3.5. The influence of particle concentration of the specific heat of various nanofluids at 50 °C is described in fig. 3.6. It can be observed from fig 3.6 that the specific heat is inversely varying with the particle concentration and it is true for all nanofluids taken up in this research. The nanofluids have a lowest specific heat and need low quantity of energy to raise the unit temperature. Similar results can be observed for density as well as for specific heat from many studies [166], [167].

3.5.3 Thermal expansion coefficient

Khanafer et al. [168] developed an empirical relation to estimate thermal expansion coefficient of nanofluids which is given in eq. (3.5):

$$\beta_{nf} = \beta_{nf}\left[\frac{1}{1+\frac{(1-\emptyset)\rho_{bf}}{\emptyset\ \ \rho_p}}\frac{\beta_p}{\beta_{bf}} + \frac{1}{1+\frac{\emptyset\ \ \rho_p}{(1-\emptyset)\rho_{bf}}}\right] \tag{3.5}$$

Wang et al. [169] suggested a simple relation to estimate the thermal expansion coefficient of the nanofluid and it is given in eq. (3.6):

$$\beta_{nf} = \emptyset\,\beta_p + (1-\emptyset)\beta_{bf} \tag{3.6}$$

Nayak et al. [170] conducted an experimental study to determine the thermal expansion coefficient of water based nanofluids. Their results show that the thermal expansion coefficient

increases with particle concentration and temperature. Khanafer et al. [171] theoretically measured the thermal expansion coefficient of various nanofluids using eqs. (3.5) and (3.6) and these values were compared with the experimental data of Ho et al. [172]. They concluded that eq. (3.5) had good agreement with experimental data of Ho et al. [172]. Therefore, in the present work eq. (3.5) was used to estimate the thermal expansion coefficient of various nanofluids at different concentrations and temperatures.

3.5.4 Viscosity

In many heat transfer applications, fluid flow properties also play a crucial role in effective thermal management. In NCL also, the flow behaviour of a nanofluid is influenced by the dynamic viscosity of the working fluid. Thus, viscosity of nanofluids receives equal priority as thermal conductivity. Plenty of correlations are available in the open literature to estimate the dynamic viscosity of nanofluid. Some of the favourable correlations, which will closely predict the dynamic viscosity of nanofluids to the experimental outcomes, are presented in this section.

Einstein [173] developed a correlation to estimate the effective viscosity of solution having spherical solid particles in the base fluid using hydrodynamic equations and it is given in eq. (3.7).

$$\mu_{nf} = (1 + 2.5\emptyset)\mu_{bf} \tag{3.7}$$

Brinkman [174] modified Einstein's correlation for use in particle concentrations of 4% and it is shown in eq. (3.8).

$$\mu_{nf} = (1 - \emptyset)^{2.5}\mu_{bf} \tag{3.8}$$

Batchelor [175] further modified Einstein's correlation by considering the effect of Brownian motion as given in eq. (3.9):

$$\mu_{nf} = (1 + 2.5\emptyset + 6.2\emptyset^2)\mu_{bf} \tag{3.9}$$

Nguyen et al. [176] briefly describes the impact of particles size and temperature on the viscosity of a nanofluid. The viscosity of a nanofluid proportionally increased with the size of the nanoparticle and is reduced with an increase in temperature. The viscosity of nanofluid at different particle sizes can be estimated using the equations below:

$$\mu_{nf} = (1.475 - 0.319\emptyset + 0.0512\emptyset^2 + 0.009\emptyset^3)\mu_{bf} \qquad for\ d_p = 29nm \tag{3.10}$$

$$\mu_{nf} = (1 + 0.025\emptyset + 0.015\emptyset^2)\mu_{bf} \qquad for\ d_p = 36nm \tag{3.11}$$

$$\mu_{nf} = (0.904\exp(0.1483\emptyset)\mu_{bf} \qquad for\ d_p = 47nm \qquad (3.12)$$

Equation (3.13) presents the influence of temperature on the viscosity of nanofluids, while Eq. (3.14) considers the particle concentration along with the temperature of working fluid [177].

$$\mu_{nf} = (2.1275 - 0.01275T + 0.00027T^2)\mu_{bf} \qquad (3.13)$$

$$\mu_{nf} = 4.682\left(\frac{T_\alpha}{T_{nf}}\right)^{0.00049} \emptyset^{0.1794}\mu_{bf} \qquad (3.14)$$

3.5.5 Thermal conductivity

It is the one of the notable thermophysical properties, which govern heat transfer characteristics of a nanofluid. By suspending high thermal conductive solid particles in base fluid the net thermal conductivity of the nanofluid increases due to convection currents between base fluid and solid particles. Many researchers have proposed numerous correlations to predict and explain the peculiar enhancement of thermal conductivity by considering various parameters. Maxwell [30] is the pioneer in this area who proposed a theoretical model to determine the effective thermal conductivity of solid particle suspensions in liquids, which is the base correlation to determine the thermal conductivity of nanofluids till date. This model is effective for homogeneously dispersed low concentration nanofluids. It is drawing the attention of many researchers for its theoretical soundness and practical applications.

$$k_{nf} = k_{bf}\left\{\frac{[k_{np}+2k_{bf}-2\emptyset(k_{bf}-k_{np})]}{[k_{np}+2k_{bf}+\emptyset(k_{bf}-k_{np})]}\right\} \qquad (3.15)$$

Bruggeman [178] proposed a correlation for spherical nanoparticles by considering the influence of nano clusters on thermal conductivity of nanofluid, and it is given by:

$$k_{nf} = \frac{1}{4}(3\emptyset - 1)k_{np} + \left[(2 - 3\emptyset)k_{bf}\right] + \frac{k_{bf}}{4}\sqrt{\Delta} \qquad (3.16)$$

where, $\Delta = \left[(3\emptyset - 1)^2\left(\frac{k_{np}}{k_{bf}}\right)^2 + [(2 - 3\emptyset)^2 + 2(2 + 9\emptyset - 9\emptyset^2)]\left(\frac{k_{np}}{k_{bf}}\right)\right]$

Koo and Kleinstreuer [179] introduced a new correlation to precisely predict the thermal conductivity of nanofluid by considering both the effects of static and dynamic motion of nanoparticles. In their analysis, Maxwell [30] model is considered as static part where dynamic motion of nanoparticles is ignored; therefore, a Brownian motion term is introduced to account for the dynamic motion nanoparticles in base fluid.

$$k_{nf} = k_{static} + k_{Brownian} \qquad (3.17)$$

$$k_{static} = k_{bf}\left\{\frac{k_{np}+2k_{bf}+2\emptyset(k_{np}-k_{bf})}{k_{np}+2k_{bf}-\emptyset(k_{np}-k_{bf})}\right\} \quad (3.18)$$

$$k_{Brownian} = 5X10^4\beta\emptyset\rho_{bf}C_{p,bf}\sqrt{\frac{k_BT}{\rho_{np}d_{np}}f} \quad (3.19)$$

$$k_{nf} = k_{bf}\left\{\frac{k_{np}+2k_{bf}+2\emptyset(k_{np}-k_{bf})}{k_{np}+2k_{bf}-\emptyset(k_{np}-k_{bf})}\right\} + 5X10^4\beta\emptyset\rho_{bf}C_{p,bf}\sqrt{\frac{k_BT}{\rho_{np}d_{np}}f} \quad (3.20)$$

Where, β was introduced for discussing the interaction between bulk fluid and nanoparticle, f represented the temperature depending on thermal conductivity

$$\beta = 0.0137(100\emptyset)^{-0.8229} \quad \emptyset < 1\% \quad (3.21)$$

$$\beta = 0.0017(100\emptyset)^{-0.0841} \quad \emptyset > 1\% \quad (3.22)$$

$$f = (-134.63 + 1722.3\emptyset) + (0.4075 - 6.04\emptyset)T \quad (3.23)$$

Vast literature is available on the influence of various parameters on thermal conductivity. Summary is given below.

(i) Particle concentration: It follows a linear relationship with thermal conductivity [180]

(ii) Particle material: By suspending the nanoparticles in base fluid, nanoclusters are formed around the nanoparticle and these causes for the enhancement of thermal conductivity. The size of nanoclusters depends on the type of particle material. The nanoparticles, which are capable of forming the larger nanoclusters should possess higher thermal conductivity [47]. The enhanced thermal conductivity of hybrid nanofluid may be the driving parameter for improving the heat transfer rate and sustain the interest of researchers to use them in many thermal applications [28], [32].

(iii) Base fluid: By suspending the nanoparticles in base fluid, an electronic double layer develops around the nanoparticle and the thickness of the double layer depends on the type of base fluid and suspended particles [181]. The key parameters that affect the thermal conductivity of nanofluid are dynamic viscosity and thermal conductivity of based fluid. Relatively less thermal conductive base fluid will exhibit high thermal conductivity ratio [32]. On the other hand, high viscous fluids possess stable nanofluid, but this obstructs the Brownian motion of the nanoparticles, as a result of which it reduces the thermal conductivity of a nanofluid. Systematic experimental work, however, is needed to establish the impact of base fluid on thermal conductivity of a nanofluid.

(iv) Particle size: Brownian motion of the nanoparticle is one of the root-causes for enhanced thermal conductivity of nanofluid. As particle size reduces, nanoparticles move at a faster rate and hence colloidal motion increases, and improves the energy transport within the liquid medium [182].

(v) Particle shape: Most of the nanoparticles are produced either in spherical or in cylindrical shape. Cylindrical shaped particles would exhibit more thermal resistance than spherical particles. The credible reason could be A long cylinder offers more thermal resistance to heat flow in the axial direction and therefore cylindrical shape particles have less heat transfer than spherical shape particles [183].

(vi) Temperature: Temperature will dramatically influence the thermal conductivity of nanofluid. As the temperature increases, the Brownian motion of nanoparticle also increases, and thus, the thermal conductivity of a nanofluid also increases [184]. However, any raise in temperature may also affect the size of nanoclusters and thickness electric double layer. Therefore, thermal conductivity of nanofluid follows the decreasing trend at elevated temperatures [185].

(vii) Acidity of nanofluid: The electrostatic repulsive forces of nanoparticles depend on the pH value of nanofluid. As the pH value of nanofluid moves away from iso-electric static point, the repulsive forces between the nanoparticles and base fluid also increase and hence the stability as well as thermal conductivity of a nanofluid increase [164], [186].

3.6 Estimation of the viscosity and thermal conductivity: Experimental study

Among all the thermophysical properties, thermal conductivity and viscosity are key properties, which govern the heat transfer and flow behaviour of a nanofluid. Many engineering applications demand a trade-off between dynamic viscosity and thermal conductivity of a nanofluid. Enhanced thermal transport properties along with minimal augment of viscosity are favourable for better thermal performance of an NCL. Both viscosity and thermal conductivity of water and all nanofluids have been experimentally measured. Experiments were conducted at different particle concentrations from 0.5% to 3% over 20 $^{\circ}$C to 70 $^{\circ}$C temperature range.

3.6.1 Viscosity Measurement

The dynamic viscosity of water, and nanofluids at different particle concentrations and temperatures were measured using a Rheolab QC rotational rheometer (Anton Paar supplier, India) as shown in fig. 3.7. The apparatus is equipped with a peltier temperature controlled thermostatic bath with computer interface to control and measure the rheological behaviour of nanofluid at different temperatures. The apparatus can measure the viscosity over a range of 1 to 10^9 cP and over a temperature range of -20 $^{\circ}$C to 180 $^{\circ}$C. The computer interface facilitates the collation of measured data and to vary the temperature of working fluid. For reliability of measurements, viscosity of distilled water is experimentally measured and compared with the standard data taken from REFPROP tables [187]. The experimental readings have close approximations with standard data, with less than 2 % deviation, over the considered range of temperatures. The nanofluid is placed between concentric cylinders of the rheometer. The outer cylinder is rotated by external means, while the inner cylinder remains stationary. When the outer cylinder rotates, the torque is transmitted to inner stationary member through a thin liquid film of nanofluid formed between the cylinders. Based on the speed of rotation, and thickness of fluid film (gap between cylinders), one can measure the viscosity of fluid from its Newtonian behaviour [188].

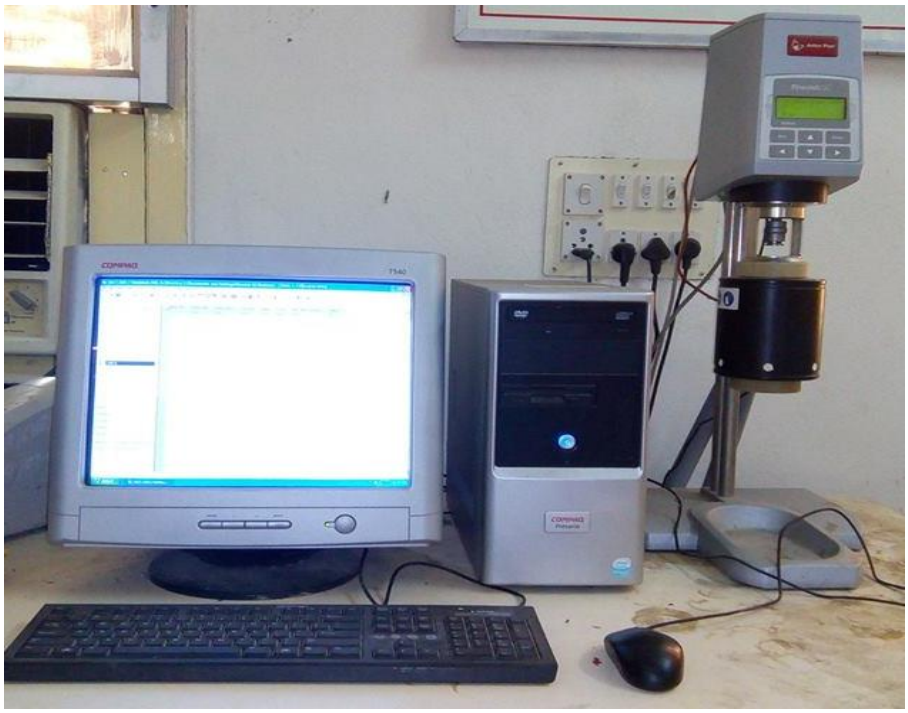

Fig. 3.7 Photographic view of Rheometer with computer interface

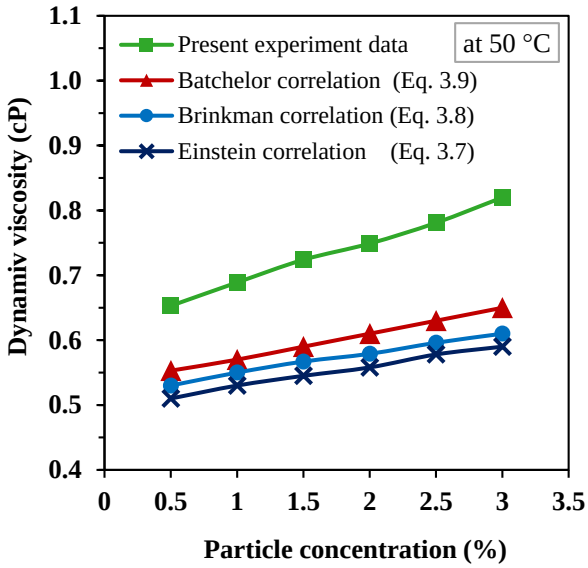

Fig. 3.8 Comparison of empirical and experimentally measured viscosity of CuO/water nanofluid

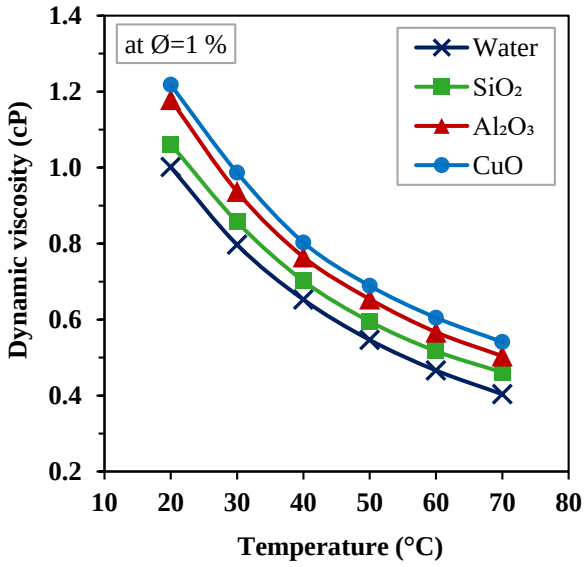

Fig. 3.9 Experimentally measured viscosity of water and different nanofluids as a function of temperature

The viscosity of a CuO-water nanofluid at different particle concentrations is experimentally measured and compared with several existing empirical correlations. Figure 3.8 shows the variation of empirically estimated and experimentally measured viscosity of a CuO/water nanofluid as a function of particle concentration. It can be observed from the experimental results that viscosity of a nanofluid increases with particle concentration and this increment is relatively more at higher concentrations. The increasing particle concentration amplifies the entanglement and resistance between adjacent layers and leads to an increase in the viscosity of a nanofluid. Many other factors related to intermolecular interactions at the microscopic level also play an indirect role in the enhancement of dynamic viscosity of a nanofluid. The probable reason for the augmenting of nanofluid viscosity is that the nanoparticles are loaded into base fluid, with larger interfacial/contact area of nanoparticles with base fluids promoting greater shear rates and consequently responsible for higher viscosity [177]. Yet another possible reason may be that the inter-particle forces among the particles cause higher shear rates and subsequently, an increase of viscosity. It can be observed from fig. 3.8 that there is a notable deviation between measured and analytical results. Among all the empirical correlations, the Bachelor correlation i.e. eq. (3.9) has a low deviation with experimental values. Therefore, Bachelor correlation i.e. eq. (3.9) was used to estimate the dynamic viscosity of various nanofluids in the present work. It is observed from fig. 3.8 that at a temperature of 50 $^{\circ}$C, dynamic viscosity of CuO-water nanofluid is increased from 0.546 cP

(for distilled water) to 0.653 cP, 0.689 cP, 0.724 cP, 0.749 cP, 0.781 cP and, 0.82 cP for particle volume concentration of 0.5%, 1%, 1.5%, 2%, 2.5% and 3.0% respectively.

In view of the fact that NCL has to operate over a range of temperatures, dynamic viscosity of nanofluids is measured at different temperatures. The variation in dynamic viscosity of distilled water and various nanofluids (CuO-water, Al_2O_3-water, and SiO_2-water) with the temperature at 1% particle concentration is presented in fig. 3.9. The viscosity of all nanofluids is decreasing with an increase in temperature and this decrement is relatively more at high temperatures. As the temperature of nanofluid increases, Van Der Waals forces of attractions gradually cease and lead to a reduction in the viscosity of a nanofluid [189].

Correlation proposed to estimate the viscosity of nanofluids:

Experimental investigations are needed for validating the various empirical correlations used to estimate the viscosity of a nanofluid. Though, plenty of correlations are available in open literature, most of the correlations are not able to precisely predict the viscosity of nanofluid with close approximation to measured values. Because, the correlations available in the literature, considers the particle concentration as a sole parameter that influence the nanofluid viscosity , but the properties of nanoparticle material are not taken into account. However, few correlations considered the temperature as an influencing parameter [176], [177]. It is clear from fig. 3.10 that the empirical correlations are under estimating the viscosity of nanofluid. Therefore, to precisely predict the viscosity of nanofluid a new correlation has been developed by considering the all possible influencing parameters. In the developed correlation particle concentration, temperature and density of the nanoparticle are also taken into account and the developed correlation is:

$$\frac{\mu_{nf}}{\mu_{bf}} = 1 + a\phi^b \left(\frac{T_{nf}}{T_0}\right)^c \left(\frac{\rho_{nf}}{\rho_{bf}}\right)^d \qquad (3.24)$$

Constants of the developed correlation for different nanofluids of viscosity are presented in table 3.2.

Table 3.2 Correlation constants for different nanofluids

Nanofluid/ correlation constant	a	b	c	d
CuO/water	0.1762	0.0901	1.5472	9.9762

It is clear from the constants of correlations that the density of nanoparticle has significant influence on viscosity of nanofluid.

For the proposed correlation, from the curve fit, regression coefficient is 0.9512. It can be observed that the data would correlated with 96% of the data is with the curve fit range. Therefore, it is noted to worthy that, the proposed correlation is capable to precisely estimate the viscosity of water based mono nanofluids as well as hybrid nanofluids with a single equation.

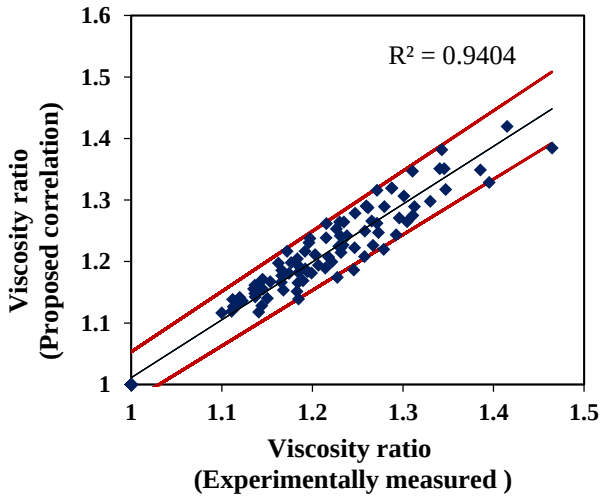

Fig. 3.10 Viscosity ratio for experimental measurements & proposed correlation

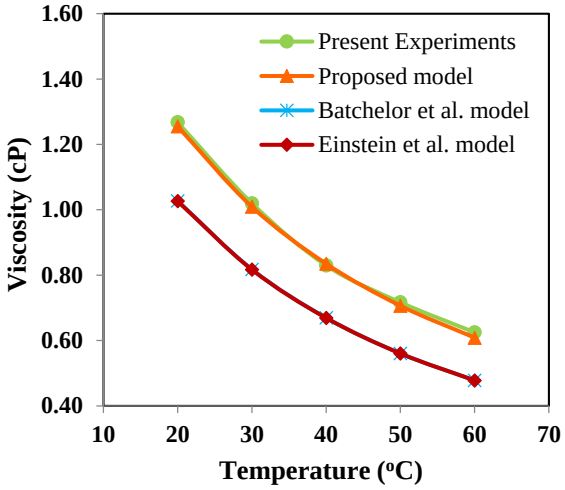

Fig 3.11 Comparison of proposed and existing correlations.

Comparisons were made between proposed correlation and various empirical relations available in the open literature and presented in fig. 3.11. It can be observed from Fig. 3.11 that the proposed correlation has good agreement with the experimental results.

3.6.2 Thermal conductivity measurement

Thermal conductivity of all working fluids (water and nanofluids) considered in the current work were experimentally measured using thermal conductivity analyzer (TPS 500S, Therm. Test Inc., Fredericton, Canada), which is shown in fig. 3.12(a). The instrument is equipped with different types of sensors with software module interface to measure the thermal conductivity of different materials like bulk materials, powders, thin films, and wide range of liquids including nanofluids. The apparatus works based on transient plane source principle and follows ISO 22007-2.2 standards. In the current work, 7552 Kapton sensor of 2 mm diameter was used to measure thermal conductivity of nanofluids at different particle concentrations. The

equipment was supported with a thermostatic bath to facilitate measurement of the thermal conductivity over a wide range of temperatures, from -20 ˚C to 200 ˚C.

Fig. 3.12(a) Thermal conductivity Analyzer

Fig. 3.12(b) Conductivity measuring sensor

To measure the thermal conductivity of nanofluid, Kapton sensor was immersed in the nanofluid filled attachment, so that both sides of the sensor had identical environment. The arrangement was kept idle for 20 min to reach thermal equilibrium state and then thermal conductivity was measured from the software interface module. Each sample was tested three times under identical temperature conditions and averages of the readings were considered for the further analysis. The sensor-sample arrangement is as shown in fig. 3.12 (b).

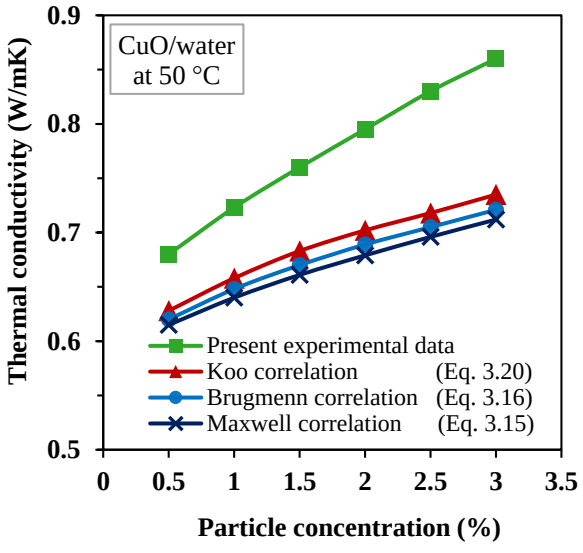

Fig. 3.13 Variation of thermal conductivity of CuO/water nanofluid with particle concentration

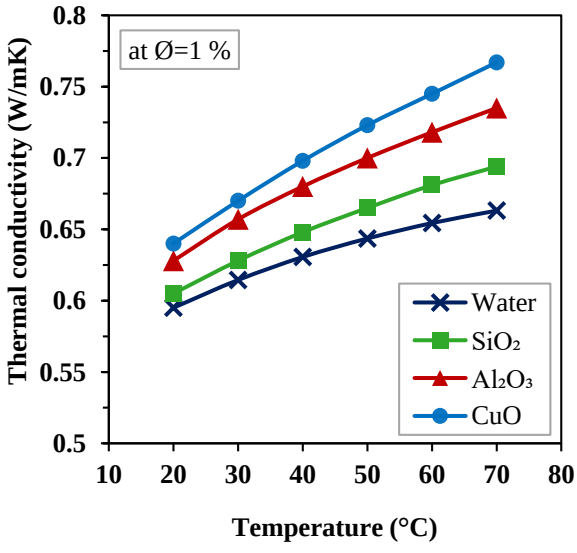

Fig. 3.14 Thermal conductivity of various nanofluids as a function of temperature

Thermal conductivity of CuO/water nanofluid at different particle concentrations was experimentally measured and the results were compared with the empirical correlations

available in the literature as shown in fig. 3.13. It can be observed from fig. 3.13 that the thermal conductivity of CuO/water nanofluid is progressively increasing with the particle concentration and it is amplifying at higher concentrations. As the particle concentration increases, the mean free path of the nanoparticles is decreased, and this leads to lattice vibrations which are commonly known as percolation effect [192]; that may also be one of the root causes for the consequential enrichment of nanofluid thermal conductivity. The maximum deviation between experimental and empirical correlations of Maxwell i.e. eq. (3.15), Brugmenn, i.e. eq. (3.16), and Koo i.e. eq. (3.20) is 18%, 16% and 10% respectively. This may be because of the empirical models that were not considered the root causes of anomalous enhancement of thermal conductivity like Brownian motion, specific surface area, interfacial liquid layering, and surface chemistry, which will take part in the enhancement of thermal conductivity of a nanofluid. However, among all the correlations, the Koo correlation i.e. eq. (3.20) has a low deviation vis-a-vis experimental value for thermal conductivity because it includes Brownian motion effect. Therefore, in the present research the Koo correlation i.e. eq. (3.20) was used to estimate thermal conductivity of various nanofluids.

Figure 3.14 shows the enhancement of thermal conductivity of nanofluids with the temperature at 1% particle concentration. It is clearly observed from fig. 3.14 that the thermal conductivity of any fluid increases with temperature. This is because the inter particle cohesive forces and corresponding viscosity are diminished with a rise in temperature which causes Brownian motion. The increased random movement of nanoparticles promotes micro convection between nanoparticle and base fluid and leads to enhancement the thermal conductivity of nanofluid. As elucidated in fig. 3.14 thermal conductivity of CuO/water nanofluid increases with temperature. The enhancement of thermal conductivity depends on the properties of base fluid as well as nanoparticle material [193]. It can be observed from table 3.1 that the bulk material of copper oxide (CuO) has higher thermal conductivity than other materials. Therefore, the maximum enhancement of thermal conductivity is obtained for CuO/water nanofluid. The thermal conductivity of CuO/water nanofluid is enhanced by 15.67% at 1.0% particle concentration and 70 °C temperature when compared with water.

3.7 Suitability of nanofluids in NCL

A natural circulation loop can be modelled using a simple one dimensional model or a detailed three dimensional model. Based on the type of model selected, the governing equations

are obtained by applying mass, momentum and energy balance equations to the loop (refer fig 3.16 for control volume analysis).

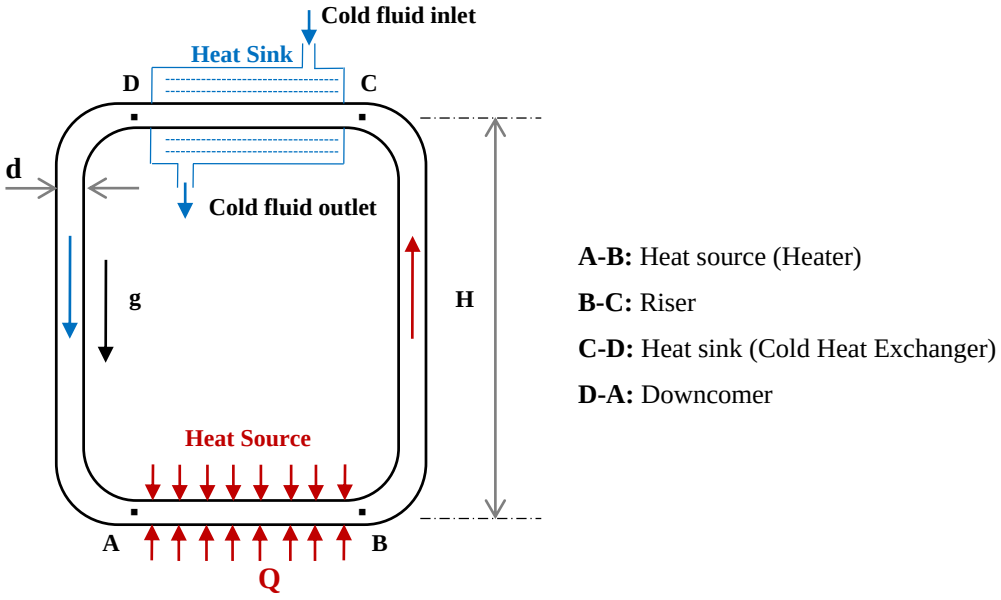

Fig. 3.15 Representation of geometrical and operating parameters

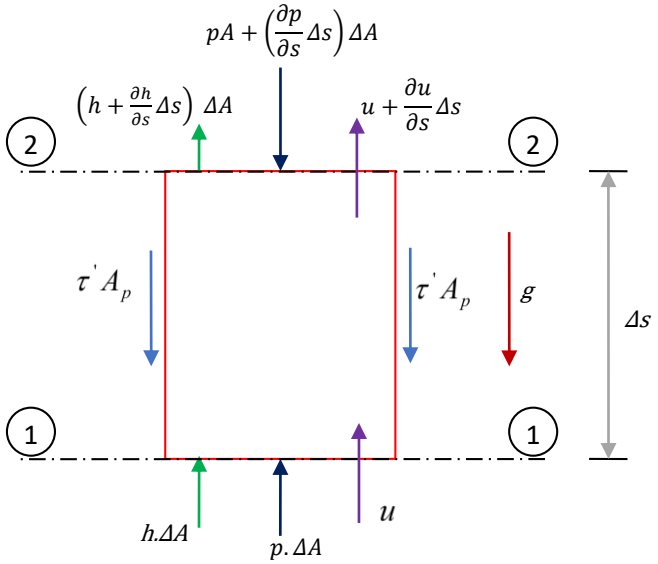

Fig. 3.16 Control volume of the fluid in riser

Momentum equation:

For incompressible, steady and one dimension flows, the momentum equation can be written as follows:

$$\rho\, \Delta A\, u \frac{\partial u}{\partial s} = -\frac{\partial p}{\partial s}\Delta s\, \Delta A - \rho g\, \Delta s\, \Delta A - \tau_w A_p \qquad (3.25)$$

Dividing both sides with ΔA

$$\rho\, u\frac{\partial u}{\partial s} = -\frac{\partial p}{\partial s}\Delta s - \rho g\, \Delta s - \tau_w \frac{A_p}{\Delta A} \tag{3.26}$$

$$\rho\, u\frac{\partial u}{\partial s} = -\frac{\partial p}{\partial s}\Delta s - \rho g\, \Delta s - \tau_w \frac{(\pi d \Delta s)}{\left(\frac{\pi}{4}d^2\right)} \tag{3.27}$$

$$\rho\, u\frac{\partial u}{\partial s} = -\frac{\partial p}{\partial s}\Delta s - \rho g\, \Delta s - \frac{4\tau_w}{d}\Delta s \tag{3.28}$$

$$\rho\, u\frac{\partial u}{\partial s} = -\frac{\partial p}{\partial s} - \rho g - \frac{4\tau_w}{d} \tag{3.29}$$

Now. Substitute, $\tau_w = \frac{1}{2} f \rho u^2$ in the above equation

$$\rho\, u\frac{\partial u}{\partial s} = -\frac{\partial p}{\partial s} - \rho g - \frac{2f\rho u^2}{d} \tag{3.30}$$

Using an order of magnitude analysis,

$$\frac{\rho u^2}{L} \sim \frac{\rho u^2}{d}$$

$as\ L \gg d$, the minimal pressure changes can be neglected.

Energy equation:

From the steady and one dimensional heat conduction equation,

$$\rho\, C_p u\frac{\partial T}{\partial s} - k\frac{\partial^2 T}{\partial s^2} = 4\frac{q}{d_h} - 4\frac{h}{d_h}(T - T_o) + \frac{1}{A}\int \varphi\, dA \tag{3.31}$$

Where, *'q'* indicates heat transfer per unit area, *'k'* and *'C_p'* are thermal conductivity and specific heat of the fluid, *'h'* is heat transfer coefficient, *'T_w'* is the wall temperature and 'φ' is the viscous dissipation function.

In the above energy equation, axial conduction term and viscous dissipation terms are $\left(q_a = k\frac{\partial^2 T}{\partial s^2}\right)$ and $\left(q_v = \frac{1}{A}\int \varphi\, dA\right)$ respectively.

Now consider left side part of the above equation and do an order of magnitude analysis,

$$\rho C_p u\frac{\Delta T}{L} \sim k\frac{\Delta T}{L^2}$$

$$\frac{\rho C_p}{k}\frac{u}{L} \sim \frac{1}{L^2}$$

$$\frac{\rho C_p}{k} uL \sim 1$$

$$\left(\frac{uL}{\nu}\right)\left(\frac{\nu}{L}\right) \sim 1$$

$$(Re)(Pr) \gg 1$$

The product of Reynolds number (Re) and Prandtl number (Pr) is far greater than 1. Therefore, the axial conduction term $\left(k\frac{\partial^2 T}{\partial s^2}\right)$ can be neglected in energy equation.

Therefore, the energy equation is simplified after neglecting axial conduction term as follows:

$$\rho\, C_p u \frac{\partial T}{\partial s} = 4\frac{q}{d_h} - 4\frac{h}{d_h}(T - T_w) + \frac{1}{A}\int \varphi\, dA \tag{3.32}$$

Let consider, $(nq) = 4\frac{q}{d_h} = 4\frac{h\,(T-T_w)}{d_h}$ and $(C_1\, u^2) = q_v = \frac{1}{A}\int \varphi\, dA$

Now, apply an order of magnitude analysis to above energy eq. (3.32),

$\left(\rho C_p u \frac{\Delta T}{L}\right)$ (nq) (nq) $(C_1\, u^2)$

u $\left(\frac{nqL}{\rho C_p \Delta T}\right)$ (nq) $(C_1\, u^2)$

(nq) $C_1\left(\frac{nqL}{\rho C_p \Delta T}\right)^2$

$C_1 = \left(\frac{nq(\rho C_p \Delta T^2)}{(nq)^2 L^2}\right)$

$$C_1 = \frac{1}{nq}\left(\frac{\rho C_p}{k}\,\frac{k\Delta T}{L}\right)^2 \tag{3.33}$$

$$C_1 = \frac{1}{nq}(\alpha\, q_a)^2 \tag{3.34}$$

As discussed above, the axial conduction term (q_a) is neglected because it has very low value of an order of magnitude. Therefore the term $(q_a)^2$ will be very small. Hence, the viscous term can be neglected in the energy equation.

Therefore, based on an order of magnitude analysis, generally, for single-phase flows, the flow is assumed to be incompressible as the pressure changes are negligible compared to the system pressure. Further, for the sake of simplicity, the Boussinesq approximation is used in the governing equations for the buoyancy term. In addition, the viscous dissipation and axial conduction terms are assumed to be negligible for most of the commonly encountered natural circulation loops [56]. Under these assumptions and neglecting inertia terms in the momentum equation and heat losses in the riser and downcomer, it can be shown that the balanced volumetric flow rate (V) in the loop is given by [56]:

$$V = \left(\frac{2\beta g H Q}{\rho C_p Y}\right)^{1/3} \tag{3.35}$$

where Q is the total heat transfer rate at the heat source or heat sink, Δz is the difference between elevations of the centres of the heat source and heat sink. The above equation is shown to be exactly valid for the case of uniform heat flux or for a linear temperature distribution in the heat source and sink [56]. All the geometric parameters are represented in fig. 3.15. Using the above equation, it can be further shown that the temperature difference across the heat source/sink (ΔT) is given by:

$$\Delta T = \left(\frac{Q}{\rho C_p}\right)^{2/3} \left(\frac{Y}{2g\beta\Delta z}\right)^{1/3} \quad (3.36)$$

In the above equations, Y is the overall resistance parameter defined by:

$$Y = 4\left(\frac{L_t}{d \cdot A_{cs}^2}\right) f_c \quad (3.37)$$

where L_t is the total circulation length, d and A_{cs} are the hydraulic diameter and cross-sectional area of the loop (assumed to be equal throughout the loop) and f_c is the friction factor which depends on the flow regime. Generally, depending upon the Reynolds number, either fully developed laminar flow or fully developed turbulent flow correlations are used to estimate the friction coefficient even though studies show that neither may be completely applicable in natural convection loops [56]. The characteristic velocity required for calculation of Reynolds number is obtained by dividing the volumetric flow rate by the cross-sectional area. For the sake of comparison of different working fluids, it is assumed that the loop is uniform and is circular in cross-section. In addition, the following correlations are used for estimating friction factor for laminar and turbulent flows:

$$f_c = \frac{16}{Re_{eff}} \quad \text{(Laminar flow)} \quad (3.38)$$

$$f_c = 0.079 \times {Re_{eff}}^{-0.25} \quad \text{(Turbulent flow)} \quad (3.39)$$

where, effective Reynolds number, 'Re_{eff}' is given by:

$$Re_{eff} = \left(\frac{\rho d}{\mu}\right)\left(\frac{V}{A_{cs}}\right) \quad (3.40)$$

Equations (3.35) to (3.40) were used to compare different nanofluids with water. Here the comparison is made in terms of the required tube diameters. Keeping the heat input, temperature drop across the heat source, loop height and total length same, it can be shown that the ratio of the required diameter of the loop when water is used as the loop fluid to that with nanofluid as the loop fluid (d_w/d_{nf}) is given by [84]:

$$\frac{d_w}{d_{nf}} = \left(\frac{\mu_w}{\mu_{nf}}\right)^{1/4} \left(\frac{\rho_{nf}}{\rho_w}\right)^{1/2} \left(\frac{C_{nf}}{C_w}\right)^{1/4} \left(\frac{\beta_{nf}}{\beta_w}\right)^{1/4} \quad \text{for laminar flow} \quad (3.41)$$

$$\frac{d_w}{d_{nf}} = \left(\frac{\mu_w}{\mu_{nf}}\right)^{1/19} \left(\frac{\rho_{nf}}{\rho_w}\right)^{8/19} \left(\frac{C_{nf}}{C_w}\right)^{7/19} \left(\frac{\beta_{nf}}{\beta_w}\right)^{4/19} \quad \text{for turbulent flow} \quad (3.42)$$

Figure 3.17 shows the variation of diameter ratio with temperature at the inlet to the riser for laminar and turbulent flows respectively, considering a single-phase liquid flow. It can be

seen that both for laminar and turbulent flows, the required pipe diameters are much smaller when nanofluids are used as working fluid in the loop. It is evident from fig.3.17 that the use of SiO_2-water, Al_2O_3-water and CuO-water nanofluids in place of water results in the pipe diameter can be reduced by 8%, 10.55% and 12.35%, respectively, at 70 °C temperature for turbulent flows. This is attributed mainly to the higher density and low specific heat of nanofluids compared to water at the same temperature. Thus, the use of nanofluid in place of water offers compactness to NCL. Particularly, replacement of water with CuO-water nanofluid provide more compactness.

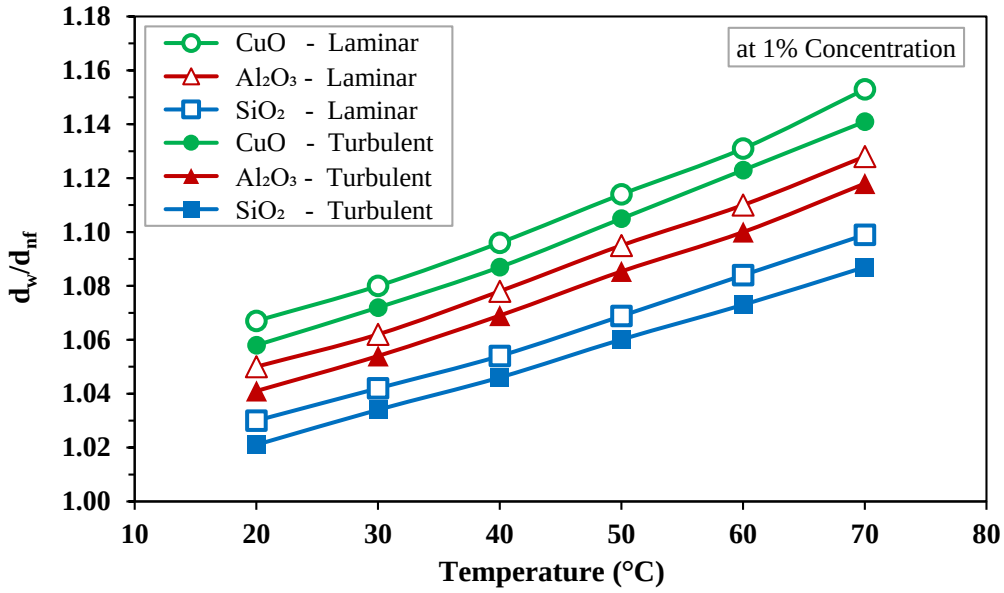

Fig. 3.17 Comparison between water and different nanofluids in terms of pipe diameters at 1% particle concentration

The variation of diameter ratio with particle concentration at 50 °C temperature for laminar and turbulent flows is presented in fig. 3.18. It is observed from fig.3.18 that both for laminar and turbulent flows the pipe diameter ratio (d_w/d_{nf}) is increasing the particle concentration. The diameter ratio is more for CuO-water nanofluid than for other nanofluids (SiO_2-water and Al_2O_3-water) due to its higher density, low specific heat at fixed concentration and temperature. The diameter ratio of water to CuO-water nanofluid is increased by 4.12% and 2.32% when compared with the diameter ratio of water to SiO_2-water and water to Al_2O_3-water nanofluids respectively at 3% concentration for turbulent flows. Furthermore, it is implied from fig. 3.18 that in using SiO_2-water, Al_2O_3-water and CuO-water nanofluids in place of water, the pipe diameter can be reduced by 12.28%, 13.79% and 15.75% respectively at 3% concentration for turbulent flows.

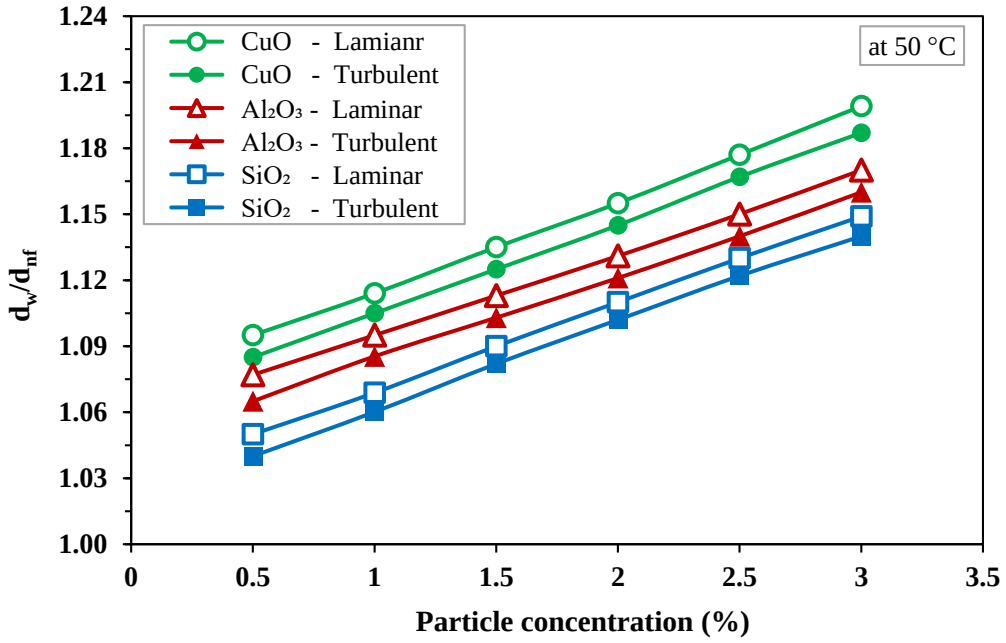

Fig. 3.18 Comparison between water and different nanofluids in terms of pipe diameters at 50 °C temperature

For the same heat input, loop length, elevation between the heat source and sink and tube diameter, temperature difference across heat source/sink is given by:

$$\Delta T = \left(\frac{1}{\rho C_p}\right)^{2/3} \left(\frac{f_c}{\beta}\right)^{1/3} \tag{3.43}$$

Substituting the friction factor correlations for laminar and turbulent flows in the above Eq. (3.43), we get:

$$\frac{\Delta T_w}{\Delta T_{nf}} = \left(\frac{\mu_w}{\mu_{nf}}\right)^{1/3} \left(\frac{\rho_{nf}}{\rho_w}\right) \left(\frac{C_{nf}}{C_w}\right)^{2/3} \left(\frac{\beta_{nf}}{\beta_w}\right)^{1/3} \quad \text{for laminar flow} \tag{3.44}$$

$$\frac{\Delta T_w}{\Delta T_{nf}} = \left(\frac{\mu_w}{\mu_{nf}}\right)^{1/12} \left(\frac{\rho_{nf}}{\rho_w}\right)^{3/4} \left(\frac{C_{nf}}{C_w}\right)^{2/3} \left(\frac{\beta_{nf}}{\beta_w}\right)^{1/3} \quad \text{for turbulent flow} \tag{3.45}$$

Figure 3.19 shows the variation of ratio of temperature drop/rise of different fluids with temperature for laminar and turbulent flows. From fig. 3.19 it is seen that use of nanofluids in place of water results in less temperature difference across heat exchangers. In designing heat exchangers, it is preferable to keep the temperature difference of the fluid minimum to reduce the exergy losses due to heat transfer. From the property variation of water and nanofluids with temperature, it is observed that the coefficient of thermal expansion (β) of nanofluids increases with temperature. Therefore, it is evident from fig.3.19 that the use of SiO_2-water, Al_2O_3-water

and CuO-water nanofluids in place of water, the temperature difference can be reduced by 3.66%, 8.5% and 11.19% respectively at 70 °C temperature for turbulent flows. Furthermore, use of CuO/water nanofluid in place of water results in very low temperature difference than with other nanofluids.

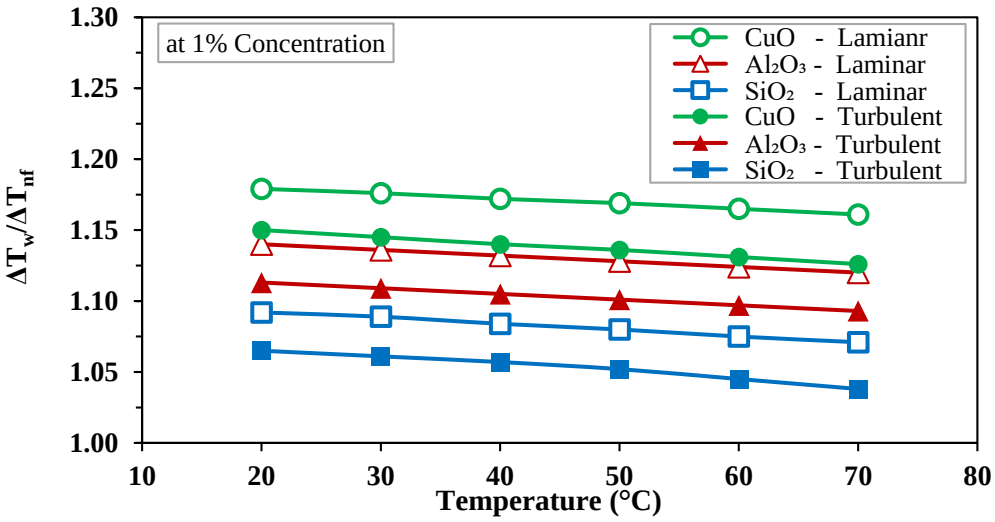

Fig. 3.19 Comparison between water and different nanofluids in terms of temperature rise/drop at 1% particle concentration

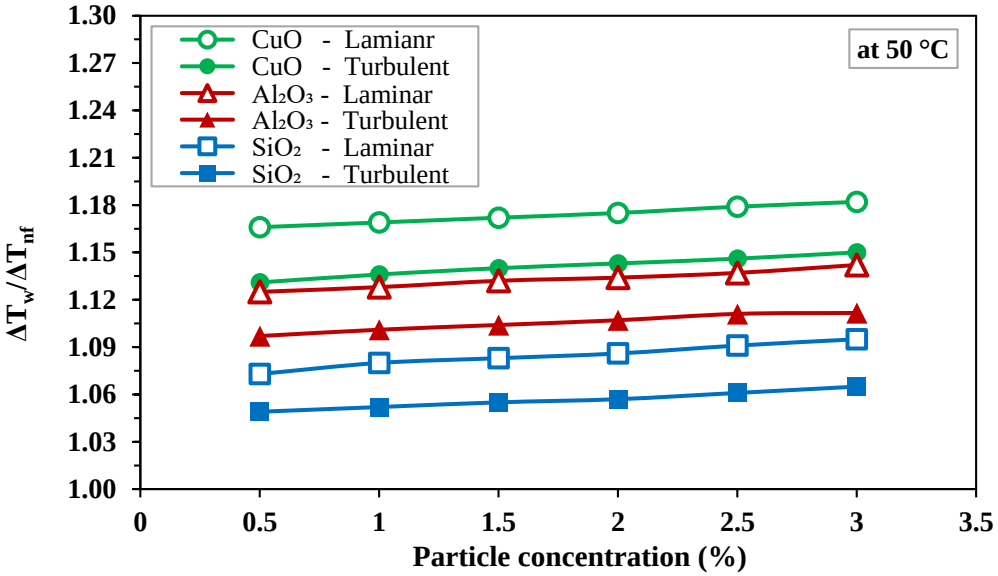

Fig. 3.20 Comparison between water and different nanofluids in terms of pipe diameters at 50 °C temperature

The influence of particle concentration on temperature difference across the heat exchanger in 50°C temperature for laminar and turbulent flows is presented in fig. 3.20. It is observed from fig. 3.20 that both for laminar and turbulent flows the ratio of temperature difference ($\Delta T_w/\Delta T_{nf}$) increases with particle concentration. The temperature difference ratio

is more for CuO-water nanofluid than for other nanofluids (Al_2O_3-water and SiO_2-water) due to its higher thermal expansion coefficient at fixed concentration and temperature. The temperature difference ratio of water to CuO-water nanofluid is increased by 3.45% and 7.98% when compared with diameter ratio of water to Al_2O_3-water and water to SiO_2-water nanofluids, respectively, at 3% concentration for turbulent flows. At last, it is concluded from fig. 3.20 that the use of SiO_2-water, Al_2O_3-water and CuO-water nanofluids in place of water can reduce the temperature gradient by 6.10%, 10.03% and 13.04% respectively, at 3% concentration for turbulent flows.

3.8 Conclusion

This chapter discussed the various synthesis methods that were used to produce nanoparticles. It addressed themes pertaining to different nanofluid preparation methods and various techniques to prepare the stable nanofluid. This chapter also investigated the estimation of thermo-physical properties of nanofluids from the empirical correlations available in the literature. It also compared the experimentally measured values of thermo-physical properties with empirical correlations. Results show that experimental results of thermo-physical properties of nanofluids are in good agreement with empirical correlations. Therefore, the empirical correlations are used in further study for estimation of thermo-physical properties of nanofluids.

Furthermore, in this chapter, a comparative study is presented between different nanofluids and conventional fluid (water) that can be used in single-phase natural circulation loops for solar, nuclear and electronic cooling applications. The following observations were reached:

1. For the same temperature difference across the heat exchanger, both for laminar and turbulent single-phase liquid flows, the required pipe diameters are smaller when nanofluids (SiO_2-water, Al_2O_3-water and CuO-water) are used in place of water. Of the fluids considered here, CuO-water nanofluid required least pipe diameter at fixed temperature and concentration.
2. For the same geometry and heat input, the temperature difference across heat exchangers is least for the systems using nanofluids both for laminar and turbulent flows.
3. Since nanofluids have enhanced thermo-physical properties, they may be considered as a suitable fluid in natural convection loops for solar and nuclear heat transfer applications.

Based on the above observations, further studies were carried out on nanofluid (SiO_2-water, Al_2O_3-water and CuO-water) based natural circulation loops. These are presented in subsequent chapters that follow.

Chapter - 4

Steady-state analysis of nanofluid based natural circulation loop using 1-D numerical modelling

In the present chapter, the theoretical analysis on steady-state performance of rectangular natural circulation loop that uses water and various nanofluids as loop fluid is presented. Also, since analytical models exist for simple cases, the results obtained from the numerical method used in the present work can be easily validated.

4.1 Mathematical formulation

In the present analysis, a one-dimensional (1-D) mathematical model is formulated to study the performance of nanofluid based single-phase NCL with end heat exchangers. Figure 4.1 shows a rectangular NCL with hot heat exchanger (HHE) as a heat source and cold heat exchanger (CHE) as a heat sink and these heat exchangers are connected by two parallel vertical legs named as riser and downcomer. As NCL is buoyancy driven, the heat source is always kept below the heat sink. The loop is placed vertically with respect to the gravity vector. In this loop, the working fluid, also called the loop fluid, absorbs heat from the heat source and rises up, loses heat in the heat sink and returns back to the heat source through the downcomer.

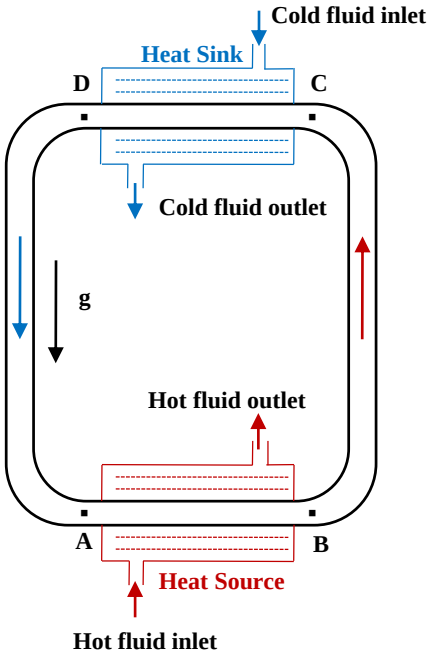

A-B: Hot Heat Exchanger (HHE)

B-C: Riser

C-D: Cold Heat Exchanger (CHE)

D-A: Downcomer

Fig. 4.1. Schematic diagram of a rectangular natural circulation loop

The following assumptions are considered to simulate the fluid in a single-phase NCL.

- The loop is operated in steady-state mode.
- There is no phase change throughout the loop i.e. only sensible heat transfer takes place in the heat source and heat sink.
- Nanofluid is a homogenous (single-phase) fluid.
- Nanoparticles and base fluid are in thermal equilibrium.
- Vertical legs are adiabatic.
- In the energy equation, axial conduction and viscous dissipation effects are neglected.

4.1.1 Conservation equations

The 1-D conservation equations under steady-state condition for single-phase NCL can be written as follows:

Conservation of mass:

$$\frac{\partial(\rho u)}{\partial s} = 0 \qquad (4.1)$$

Conservation of momentum:

The momentum equation is derived for NCL model by balancing the forces acting on the fluid element with the assumptions stated earlier. All the variations in the properties are considered

along the coordinate 's' running along the loop length. The pressure gradient at every section of the loop is derived separately by modifying the general momentum equation. The resulting equation is given by:

$$\frac{\partial(\rho u^2)}{\partial s} = -\frac{\partial p}{\partial s} - \rho g - \frac{2}{d} f \rho u^2 \qquad (4.2)$$

Equation (4.2) is valid for the riser section where the fluid is in upward motion. But the fluid flow is downwards in the downcomer section, hence the gravitational pressure head acts in the direction of the flow. So, the sign of 'ρg' term in eq. (4.2) changes in the downcomer section. The momentum equation for downcomer is obtained after changing the sign of a gravitational head term in the momentum equation (i.e. eq. 4.3).

$$\frac{\partial(\rho u^2)}{\partial s} = -\frac{\partial p}{\partial s} + \rho g - \frac{2}{d} f \rho u^2 \qquad (4.3)$$

Conservation of Energy:

The energy equation also has been derived separately for each section of the system.

Downcomer and Riser:

$$\frac{\partial Q}{\partial s} = m\left(\frac{\partial h}{\partial s} + \frac{\partial}{\partial s}\left(\frac{u^2}{2}\right) + g\right) \qquad (4.4)$$

Where $\frac{\partial Q}{\partial s}$ is the heat transferred from or to the loop fluid in the riser and downcomer sections. Since both the downcomer and riser sections are assumed to be perfectly insulated, $\frac{\partial Q}{\partial s} = 0$. Then eq. (4.4) can be expressed in terms of enthalpy gradient as:

$$\frac{\partial h}{\partial s} = -\frac{\partial}{\partial s}\left(\frac{u^2}{2}\right) - g \qquad \text{for riser and downcomer} \qquad (4.5)$$

The temperature gradient at HHE can be obtained by the following expressions:

$$\dot{m_{lf}} C_{p,lf} \frac{\partial T_{lf}}{\partial s} + \frac{(UA_{sa})_{hhe}}{L_h}\left(T_{lf} - T_{in,hw}\right) = 0 \qquad \text{for loop fluid} \qquad (4.6)$$

$$\dot{m_{hw}} C_{p,hw} \frac{\partial T_{hw}}{\partial s} + \frac{(UA_{sa})_h}{L_h}\left(T_{in,hw} - T_{lf}\right) = 0 \qquad \text{for external fluid} \qquad (4.7)$$

The temperature gradient at CHE can be obtained by the following expressions:

$$\dot{m_{lf}} C_{p,lf} \frac{\partial T_{lf}}{\partial s} + \frac{(UA_{sa})_{che}}{L_c}\left(T_{lf} - T_{in,cw}\right) = 0 \qquad \text{for loop fluid} \qquad (4.8)$$

$$\dot{m_{cw}} C_{p,cw} \frac{\partial T_{cw}}{\partial s} + \frac{(UA_{sa})_c}{L_c}\left(T_{i,cw} - T_{lf}\right) = 0 \qquad \text{for external fluid} \qquad (4.9)$$

4.1.2 Friction factor and heat transfer correlations

On external fluid (water) side:

Stephan [194] developed a correlation for laminar flow (Re ≤ 2300) at constant temperature boundary condition, which is used here to estimate the heat transfer coefficient inside the annulus and it is expressed in eq. (4.10):

$$Nu = Nu_{\infty} + \left[1 + 0.14\left(\frac{d_{out}}{d_{in}}\right)^{-1/2}\right]\frac{0.19\left(Pe \cdot d_{hy}/L\right)^{0.8}}{1 + 0.117\left(Pe \cdot d_{hy}/L\right)^{0.467}} \quad (4.10)$$

Where $Nu_{\infty} = 3.66 + 1.2\left(\frac{d_{out}}{d_{in}}\right)^{-1/2}$ is the Nusselt number for fully developed flow.

Gnielinski [195] correlation is used to estimate the heat transfer coefficient for turbulent flows (Re > 2300) and it is given by:

$$Nu = \frac{\left(f_c/2\right)\left(\mathrm{Re} - 1000\right)\mathrm{Pr}}{1 + 12.7\left(f_c/2\right)^{1/2}\left(\mathrm{Pr}^{2/3} - 1\right)} \quad (4.11)$$

For laminar region the friction factor is expressed as

$$f = \frac{16}{Re} \quad (4.12)$$

The reasons behind considering the hydrodynamic developed flow are

(i) System size

(ii) Steady state operation.

On loop fluid (water) side:

In the case of water as loop fluid, for laminar flow (Re ≤ 2300) in a smooth circular tube, Shah [196] suggested an expression to obtain the Nusselt number as given in eq. (4.14).

$$Nu = 1.61 \times \left(Re \cdot Pr \cdot \frac{d_i}{L}\right)^{1/3} \quad (4.14)$$

On loop fluid (nanofluid) side:

In case of nanofluid as loop fluid, for laminar flow in circular tube, Yimin Xuan [197] came up with a relation to estimate Nusselt number by eq. (4.15).

$$Nu_{nf} = 0.4328\left(1.0 + 11.285\emptyset^{0.754}Pe_{nf}^{0.218}\right)Re_{nf}^{0.333}Pr_{nf}^{0.4} \quad (4.15)$$

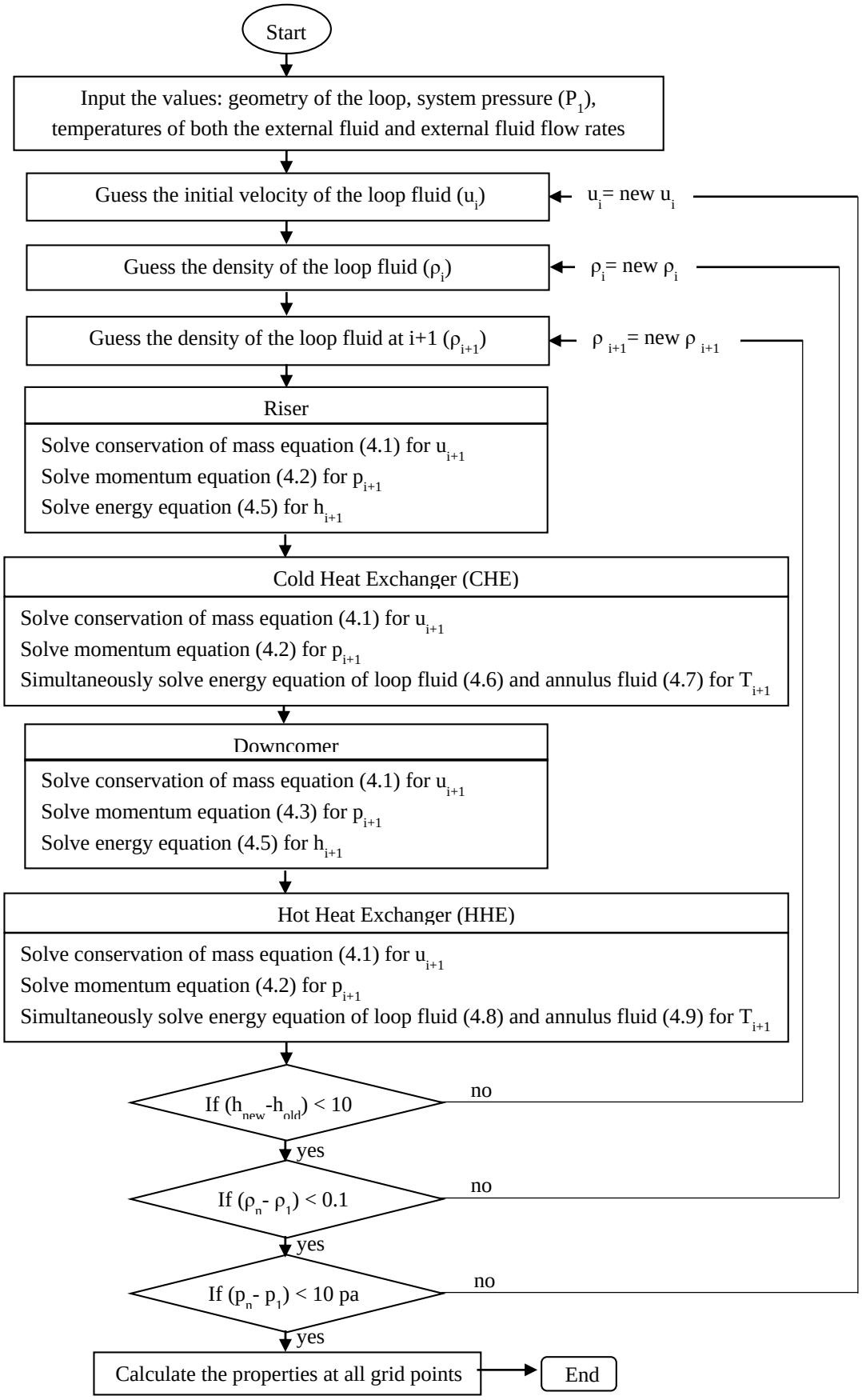

Fig.4.2 Flowchart to solve set of all conservation equations

Table 4.1. Geometrical and operating parameters

Parameter	Value
Length of the heat exchangers	1 m
Loop height	1 m
Total loop length	4 m
Loop pipe inner diameter	0.015 m
Loop pipe wall thickness	0.0016 m
Inner diameter of both heat exchangers	0.0215 m
Mass flow rates of annulus fluids in HHE & CHE	0.05 Kg/s
Inlet temperature of hot water	40 °C
Inlet temperature of cold water	20 °C
Particle volume concentration	1 %

4.1.3 Solution methodology

For solving all conservation equations and to simulate the fluid in single-phase NCL, a computer code is written in MATLAB. Conservation equations are discretized by finite difference method. International association for the properties of water and steam (IAPWS-IF 97) data is adopted in the developed code for estimating properties of the water. Three water nanofluids (Al_2O_3, CuO and SiO_2) at 1% volume concentration were chosen for the present study. In HHE and CHE, water was chosen as external fluid. In this study, 1.01325 bar was taken as fluid pressure for all working fluids. To solve the set of equations one has to specify the required heat transfer rate, dimensions of the loop (height, diameters of downcomer and riser), pressure and temperature at riser inlet (point B in fig. 4.1). An iterative procedure is then adapted to arrive at a balanced mass flow rate and temperature difference across the heat sink and source. The effect of each independent parameter is studied by varying it over a given range, while keeping the other parameters constant. Perfect algorithm was formulated to solve the set of conservation equations and it is shown in fig. 4.2.

4.2 Results and discussion

All the results were obtained by solving the complete set of conservation equations stated earlier. Figure 4.3 shows the temperature profiles of the various loop fluids along the loop. It indicates that the temperature of the loop fluid is not varied in downcomer and riser sections because these two sections are assumed as adiabatic. A steep increase in the

temperature has been observed in HHE in which loop fluid absorbs convective heat from the hot fluid and the reverse is observed in CHE. Also, it is very clear from fig. 4.3 that high temperature can be observed for CuO-water nanofluid than for Al_2O_3-water and SiO_2-water due to its low specific heat and high thermal conductivity.

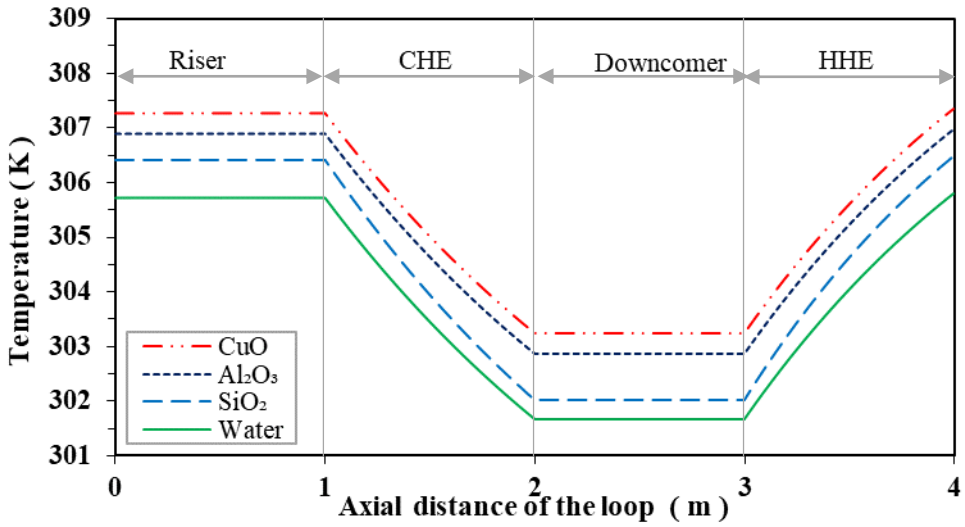

Fig. 4.3. Temperature variation along the loop length

4.2.1 Effect of loop height

To study the influence of loop height on the performance of rectangular NCL, a simulation program is run by varying the loop height from 0.5 m to 3 m while the remaining parameters are kept constant as per given table 4.1. Figures 4.4 and 4.5 show that in increasing the loop height, the steady-state mass flow rates and heat transfer rates are increasing, respectively, for all loop fluids because the buoyancy force in riser section increases with loop height. This buoyancy enhancement leads to an increase in the mass flow rate which in turn increases the Reynolds number because the diameter of the pipe is kept constant. As Reynolds number increases, the heat transfer coefficient in the heat exchanger increases. Thus, though the heat transfer area is constant, an increase in heat transfer coefficient results in a higher heat transfer rate.

Vijayan et al. [198] developed a correlation to estimate the steady state mass flow rate of the loop fluid in NCL and this correlation was successfully used for nanofluids by Nayak et al. [99]. Therefore, the present numerical results are validated with the analytical results obtained by using Vijayan's correlation, which is given in eq. (4.16). Figure 4.4 shows that the present numerical results are in good agreement with analytical results for all loop heights.

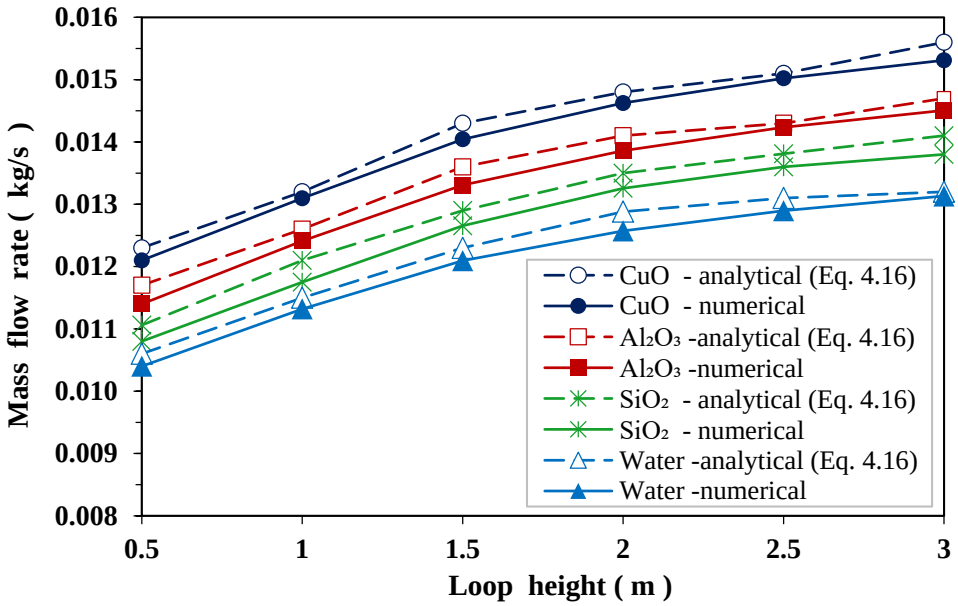

Fig. 4.4. Variation of steady state mass flow rate of the loop fluid with loop height

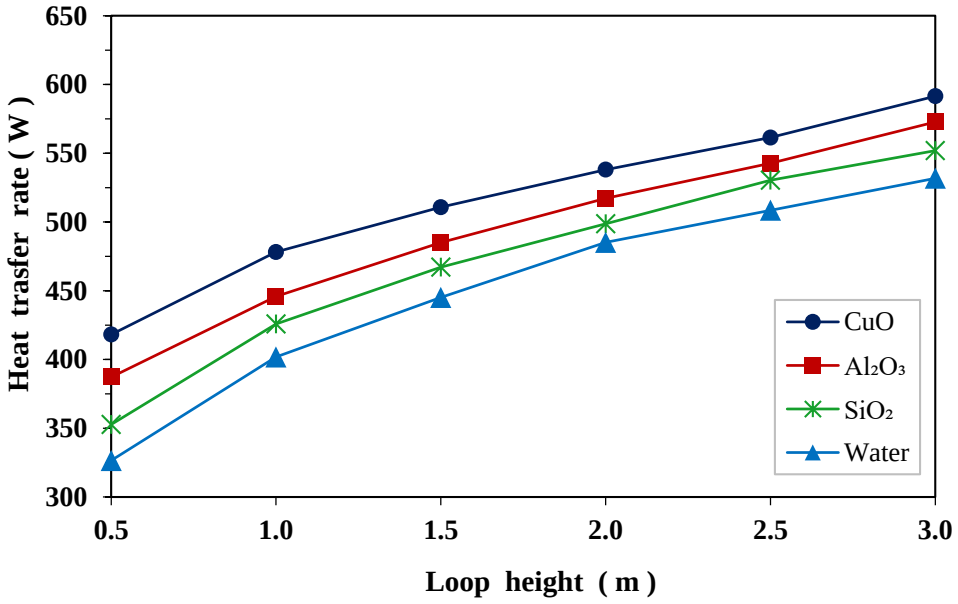

Fig. 4.5. Influence of loop height on heat transfer rate for different loop fluids

$$m_{ss} = \left(\frac{2g\Delta\rho HQd^{b}A_{cs}^{2-b}\rho_{l}}{P\Delta T\mu_{r}^{b}N_{G}C_{p}}\right)^{\frac{1}{3-b}} \tag{4.16}$$

4.2.2 Effect of heat exchanger length

Figures 4.6 and 4.7 show the influence of heat exchanger length on mass flow rate and heat transfer rates of the NCL, respectively. The lengths of both CHE and HHE are assumed to

be equal and these are varied simultaneously by keeping all remaining parameters constant, as given in table 4.1.

For all the loop fluids, as heat exchanger length increases from 1 m to 19 m, balanced mass flow rate decreases due to an increase in pressure drop and it is shown in fig. 4.6. From fig. 4.7 it can be observed that initially the heat transfer rate increases with length due to the increased heat transfer area, and it reaches a peak, after which it starts decreasing slightly due to the reduced heat transfer coefficient. It is concluded from fig.4.7 that the heat transfer rate reaches a peak at a heat exchanger length of 9 m, 11 m, 13 m and 13 m for CuO-water, Al_2O_3-water, SiO_2-water nanofluids and pure water, respectively; thereafter no variation is observed in heat transfer rate with length. So, these values can be considered as the optimum heat exchanger length for the given input data.

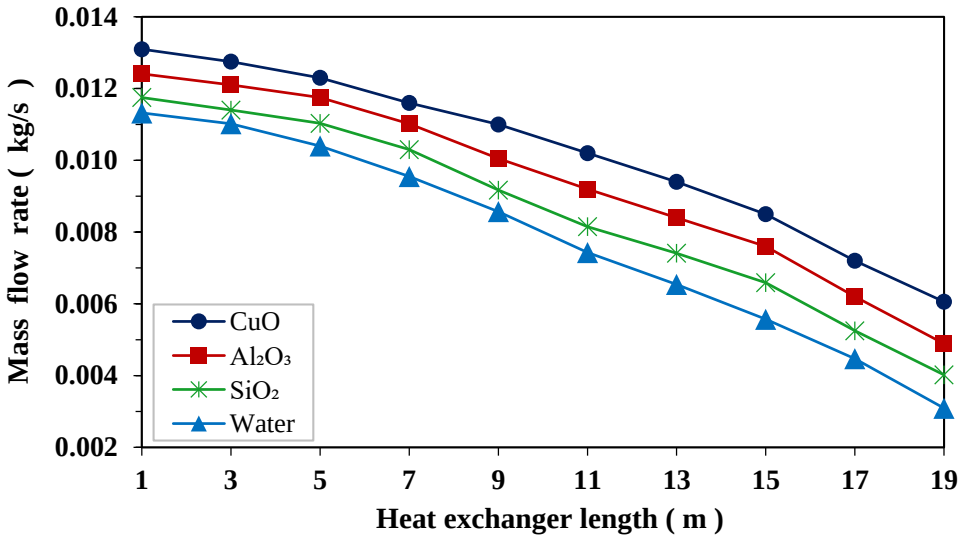

Fig. 4.6. Variation of loop fluid mass flow rate with heat exchanger length

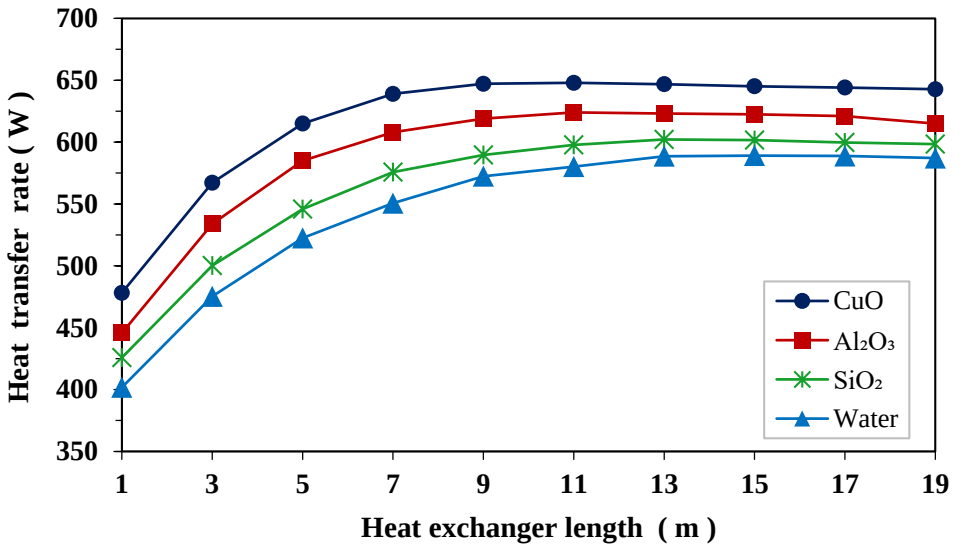

Fig. 4.7. Variation of heat transfer rate with heat exchanger length

4.2.3 Effect of diameter of the pipe

The influence of pipe diameters on the performance of the NCL was studied in detail by considering three different cases.

Case-I:

In the first case, the diameter of the loop pipe at HHE, CHE, downcomer and riser sections are assumed to be same, and they were varied simultaneously and the results are presented in fig. 4.8. In this case, only pipe diameter is varied and all the remaining parameters were kept constant as given in table 4.1. Therefore, as expected the mass flow rate and heat transfer rate of any working fluid increases with pipe diameter. For this case, no optimum diameter could be obtained for the working fluids considered in this study.

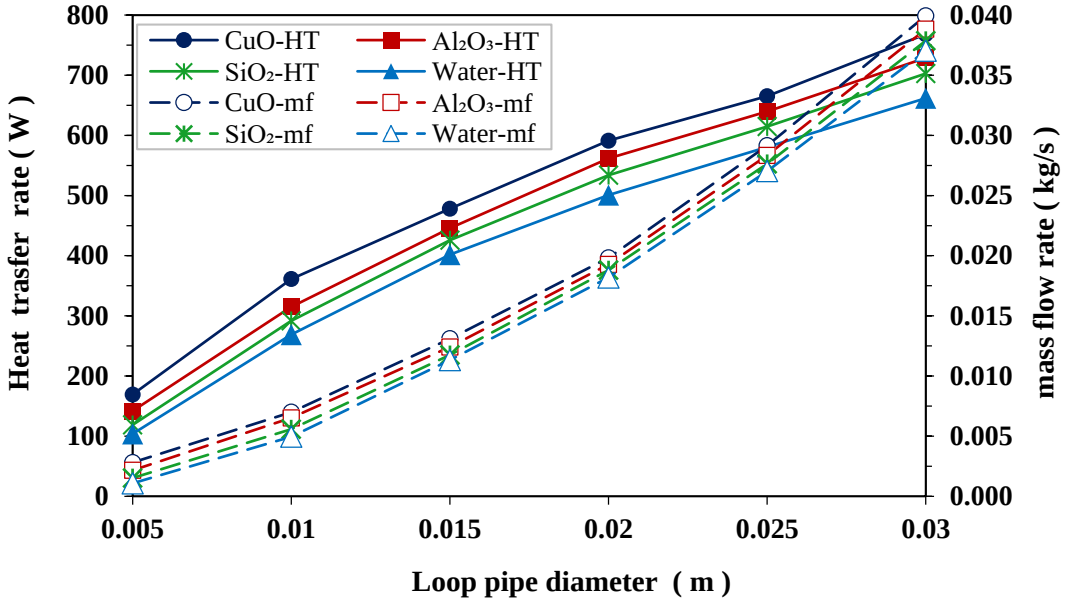

Fig. 4.8. Variation of heat transfer rate and mass flow rate with loop pipe diameter

Case-II:

In the second case, diameters of downcomer and riser were varied simultaneously and loop pipe diameter at HHE and CHE sections were kept constant, as shown in table 4.1. the results obtained for Al_2O_3-water and CuO-water nanofluids are shown in fig. 4.9 and fig. 4.10, respectively. From figs. 4.9 and 4.10 it is observed that the heat transfer rate increases from 203 W to 475 W and from 221 W to 488 W for Al_2O_3-water and CuO-water nanofluids, respectively, with a simultaneous increase in the riser and downcomer diameters from 0.005m to 0.03m. The steady state mass flow rates are less at lower diameters due to high frictional resistance. This decreases

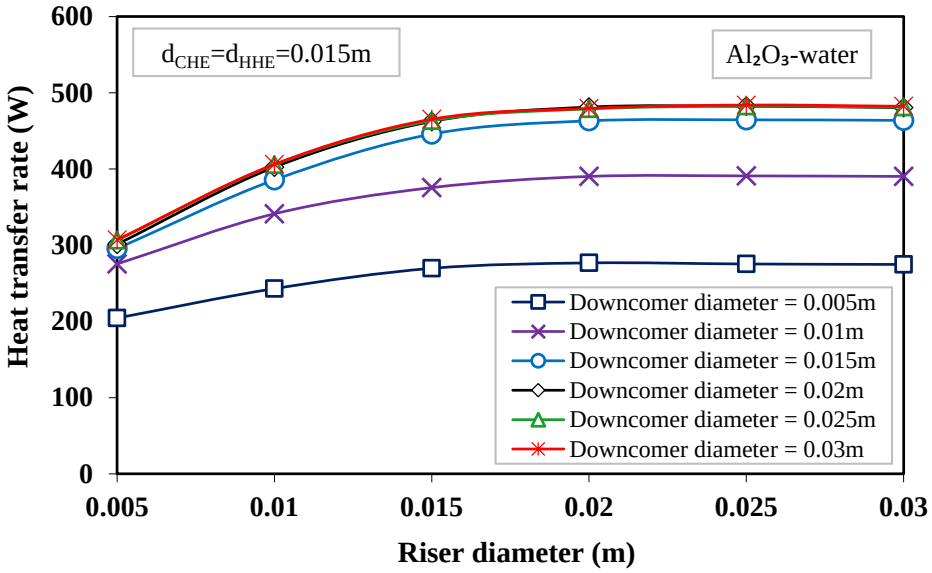

Fig. 4.9. Influence of downcomer and riser diameter on heat transfer rate for Al_2O_3-water nanofluid

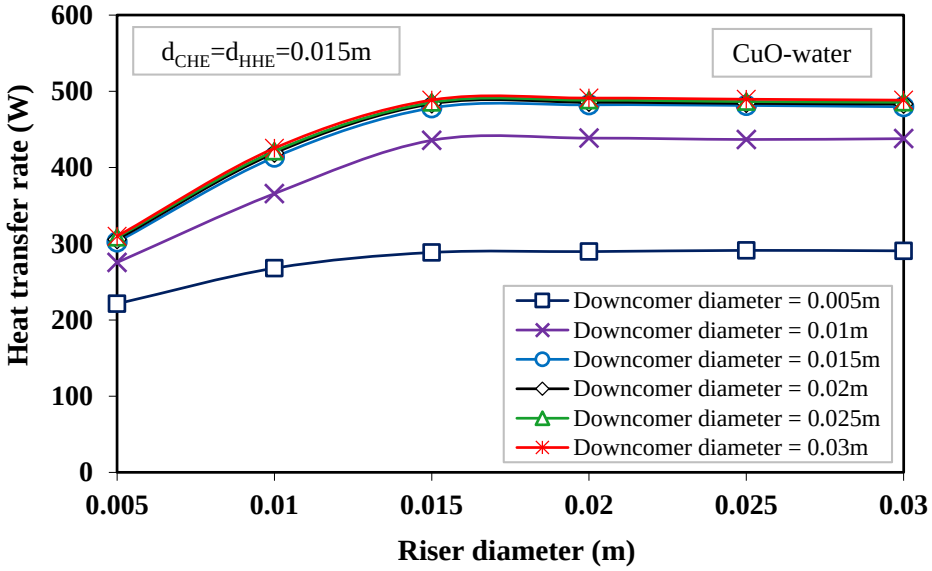

Fig. 4.10. Influence of downcomer and riser diameter on heat transfer rate for CuO-water nanofluid

the loop performance. The frictional pressure drop decreases with an increase in the diameter and after a certain value this decrement is negligible, even with an increase in the diameter; therefore, after a certain value of downcomer and riser diameters, the constant mass flow rate is attained which results in a constant heat transfer rate. From fig. 4.9 it can be observed that for all the downcomer diameter values, the heat transfer rate did not vary much when the riser diameter was increased beyond about 0.02 m, which indicates an optimum riser diameter using

Al_2O_3-water nanofluid and for all riser diameter values, the heat transfer rate is not varied much when the downcomer diameter is increased beyond 0.02 m which indicates an optimum downcomer diameter using Al_2O_3-water nanofluid. Similarly, for CuO-water nanofluid, an optimum diameter value of both riser and downcomer is 0.015 m, as can be observed from fig 4.10. Therefore, for nanofluids which are considered in the present study, 15 mm can be considered as an optimum diameter value for both downcomer and riser sections for the given set of data.

Case-III:

In case III, the diameter of the loop pipe at HHE and CHE sections was varied simultaneously by keeping downcomer and riser diameters constant as per given in table 4.1. It can be observed from fig. 4.11 that for any loop fluid the mass flow rate and heat transfer rates are increasing with heat exchanger diameter and within the range studied, no optimum diameter was attained for any loop fluid.

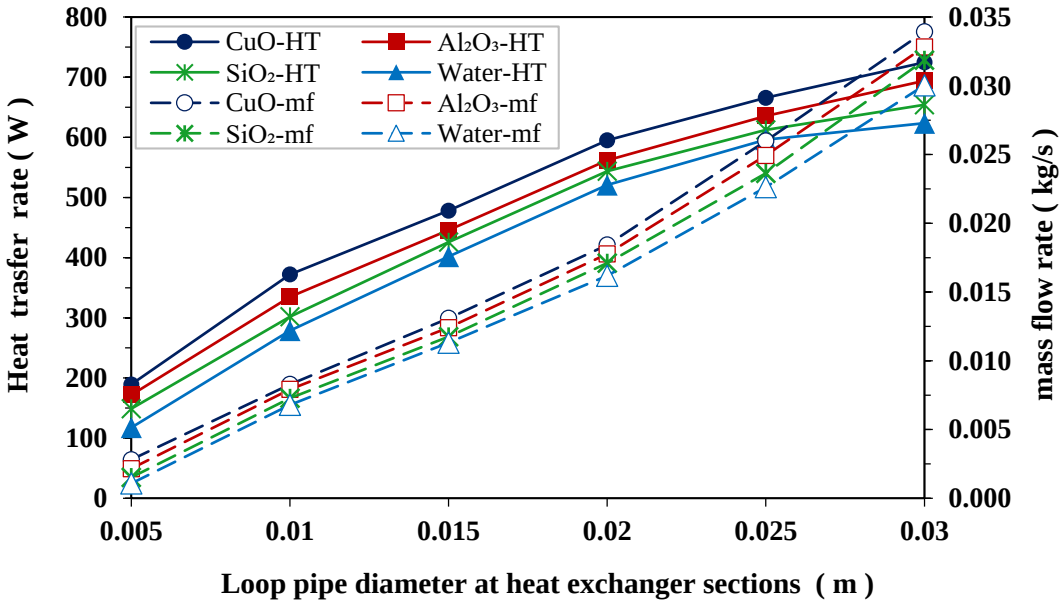

Fig. 4.11. Variation of mass flow rate and heat transfer rate with heat exchanger diameter

4.2.4 Hot/cold water flow rates

To study the influence of external fluid flow rates on the performance of the NCL, CuO-water and Al_2O_3-water nanofluids, the nanofluids were considered as loop fluids and results were compared with each other. The results were obtained by varying one parameter at a time while keeping other parameters constant. The variation of heat transfer rate with external fluid flow rates is shown in fig. 4.12. It is observed from fig. 4.12 that, the heat transfer rate increases

with hot and cold water flow rates. At lower values of water flow rates, the heat transfer rate increases due to increased heat transfer coefficient on the water side, but after reaching a certain value, this increment in heat transfer rate becomes small as heat transfer resistance on water side becomes small for both HHE and CHE. Furthermore, the average temperatures of heat addition to loop fluid increase with increase in water flow rate in HHE. Similarly, the average temperature at which heat is removed from the loop fluid decreases with higher water flow rates in CHE. The properties of CuO-water and Al_2O_3-water nanofluids are also influenced by temperature effects, which in turn affect the heat transfer rate and mass flow rate.

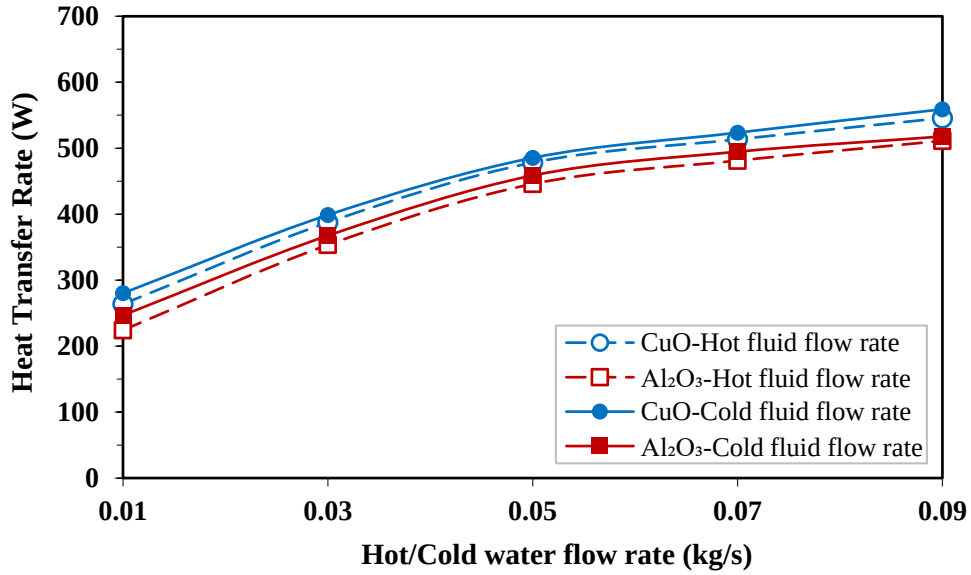

Fig. 4.12. Effect of hot/cold water flow rates on heat transfer rate

4.2.5 Hot/cold water inlet temperatures

The effect of hot and cold water inlet temperatures on the heat transfer rate is shown in fig. 4.13. It is observed from fig. 4.13 that the heat transfer rate increases with an increase in hot water inlet temperature or decrease in cold water inlet temperatures, respectively. It is also observed from fig. 4.13 that inlet temperatures of external fluids have a much stronger effect on loop heat transfer rate compared to fluid flow rates. The increased heat transfer rate due to an increase in hot water inlet temperatures in HHE increases the temperature difference of loop fluid at HHE which in turn increases the buoyancy. However, in general, the inlet temperatures of the external fluids depend on the system load and specific application.

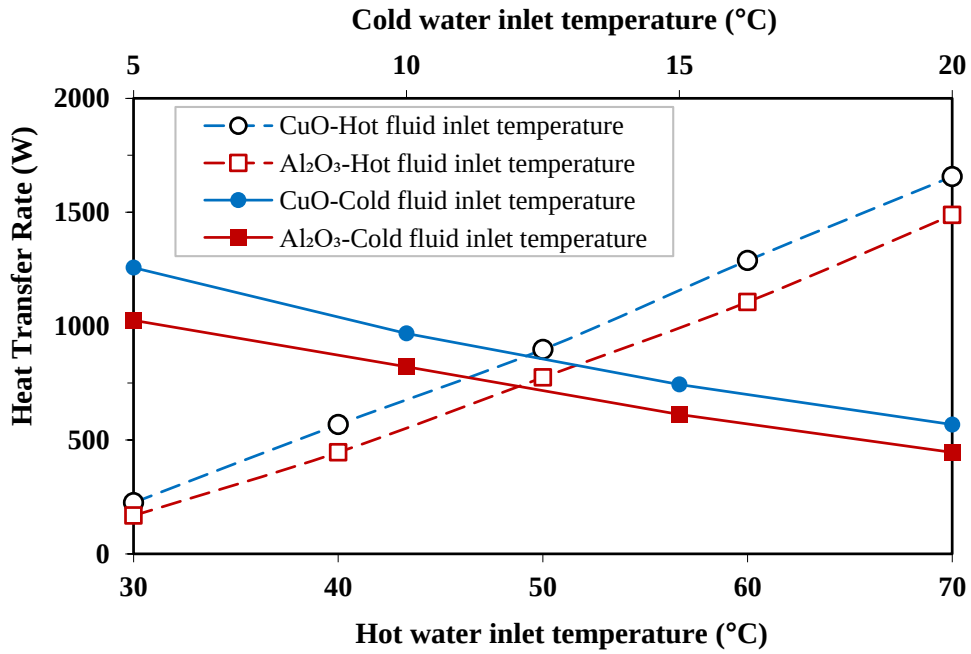

Fig. 4.13. Variation of heat transfer rate with hot/cold fluid inlet temperatures

4.2.6 Optimum values of various parameters in tabular form

Based on the above studies, the optimum values of various geometrical parameters were presented in Table 4.1.

Table 4.2. Optimum values of various geometrical parameters

Fluid/Parameter	Water	SiO_2-water	Al_2O_3-water	CuO-water
Diameter of the riser	0.015 m	0.015 m	0.015 m	0.015 m
Diameter of the downcomer	0.015 m	0.015 m	0.015 m	0.015 m
Loop pipe diameter at heat source and heat sink	No optimum value	No optimum value	No optimum value	No optimum value
Heat exchanger length	13 m	13 m	11 m	09 m
Loop Height	No optimum value	No optimum value	No optimum value	No optimum value

4.3 Conclusion

In chapter 4, the steady-state analysis of single phase rectangular NCL with end heat exchangers is developed using 1-D numerical modelling and the following conclusions have been drawn from the numerical results.

- All the numerical results validated with the analytical results obtained using published correlations.
- For a given set of operating parameters, an optimum heat exchanger length is found to be around 9 m, 11 m, 13 m and 13 m for CuO-water, Al_2O_3-water, SiO_2-water nanofluids and pure water, respectively.
- For a given set of operating parameters, an optimum diameter of the loop pipe is found to be around 0.015m for any working fluid.
- The mass flow rate of the external fluids is not influenced much by the heat transfer rate of the loop. However, the loop heat transfer rate is strongly influenced by the temperatures of the external fluids.

Based on the above discussions, it is clear that CuO-water nanofluid possess higher mass flow rates and heat transfer rate than other nanofluids. Therefore, further study has been carried out with CuO-water nanofluid at different particle concentrations.

Chapter - 5

Heat transfer analysis of nanofluid based NCL using 3D numerical modelling

A three-dimensional (3-D) modelled geometry is essential to estimate the system performance by considering some critical parameters such as influence of local buoyancy, bends in geometry, and axial conduction. Therefore, in the present chapter, numerical investigation has been carried out to study the influence of particle concentration, loop inclination angle and multiple channels on thermal performance of the CuO-water nanofluid based single phase rectangular NCL. For this study, a 3-D NCL model was developed and simulated using ANSYS-Fluent 14.0. All the numerical results were validated with the published data.

5.1 Numerical methodology

Figure 5.1(a) shows the schematic diagram of a rectangular NCL with heater, riser, cooler and downcomer. The rotation of the loop in the YZ plane is shown in fig. 5.1(b). The loop fluid is heated at the heating section with a constant heat flux condition and cooled at the cooling section by isothermal wall temperature condition. Buoyancy is created by the temperature gradients that cause the fluid to circulate in the loop. The geometrical parameters and material specifications are given in table 1. The following assumptions are made to formulate a 3-D NCL model in ANSYS-Fluent 14.0.

- The loop is operated in steady state mode.
- No slip boundary condition is applied near the walls.
- Riser and down comer sections are fully adiabatic.
- The flow is under laminar flow condition.
- The nanofluid is incompressible and the nanoparticles have uniform size and shape.

5.1.1 Governing equations

The conservation equations of mixture model are solved using the commercial software, Ansys-Fluent 14.0. The continuity, momentum and energy equations of mixture model are as follows [199]:

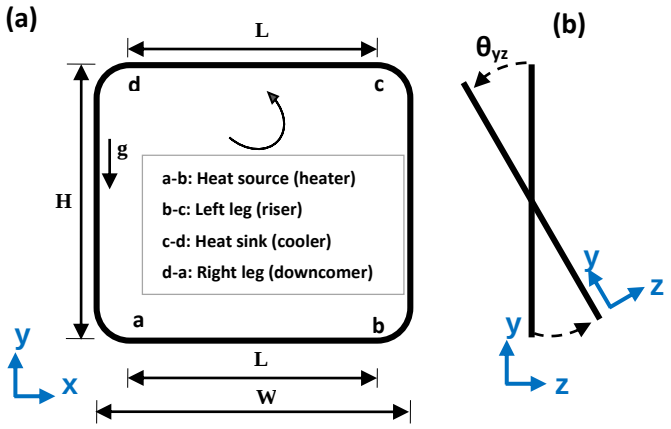

Fig. 5.1. (a) Schematic diagram of the geometrical NCL model and (b) rotation of the loop in YZ plane

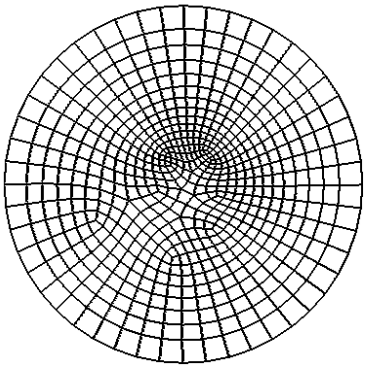

Fig. 5.2. Mesh of a loop fluid at cross section of the heater

Continuity equation:

$$\nabla \cdot \left(\rho_m \vec{V}_m\right) = 0 \tag{5.1}$$

Momentum equation:

$$\nabla \cdot \left(\rho_m \vec{V}_m \vec{V}_m\right) = -\nabla p + \nabla \cdot \left[\mu_m \left(\nabla \vec{V}_m + \nabla \vec{V}_m^T\right)\right] + \left(\rho_m \vec{g}\right) + \vec{F} + \nabla\left(\emptyset_w \rho_w \vec{V}_{dr,w} \vec{V}_{dr,w} + \emptyset_p \rho_p \vec{V}_{dr,p} \vec{V}_{dr,p}\right) \tag{5.2}$$

Energy equation:

$$\nabla \cdot \left(\left(\emptyset_w \vec{V}_w \left(\rho_w h_w + p\right)\right) + \left(\emptyset_p \vec{V}_p \left(\rho_p h_p + p\right)\right)\right) = \nabla \cdot \left(K_{eff} \nabla T\right) \tag{5.3}$$

It is to be noted that the thermo-physical properties of the nanofluid are calculated by the mixture rule [199]and the Stokes number [199] can be estimated by:

$$\mathrm{St} = \frac{\tau_p}{t_s} \tag{5.4}$$

where the particle response time (τ_p) and the system response time (t_s) are:

$$\tau_p = \frac{\rho_p d_p^2}{18\mu_w} \tag{5.5}$$

$$t_s = \frac{L_c}{V_s} \tag{5.6}$$

The average heat transfer coefficient and Rayleigh number are obtained by,

$$h_{avg} = \frac{Q}{A_s \times (T_w - T_b)} \tag{5.7}$$

$$Ra = \frac{(g\beta q" d^4 \rho^2 C_P)}{(\mu \times k^2)} \tag{5.8}$$

Table 5.1 Geometrical specifications of the model.

Parameter	**Value (unit)**
Diameter of the loop	0.015 (m)
Loop pipe wall thickness	0.0016 (m)
Total length of the loop (L_t)	5.44 (m)
Length of the heater (L_H) and cooler (L_C)	1.4 (m) each
Loop height (H)	1.26 (m)
Width of the loop (W)	1.46 (m)
Loop pipe wall material	copper

5.1.2 Boundary conditions

For the simulations, constant wall heat flux condition was imposed on the heater over a range of 500-2500 W with 500 W being step size and isothermal uniform wall temperature of 293 K considered at the cooler. Riser and downcomer were assumed to be perfectly insulated.

5.1.3 Solution methodology

A 3-D geometric model of the NCL was developed in ANSYS-14.0 workbench module and simulated with water and CuO-water nanofluid. The entire simulations were carried out under steady state conditions. The implicit coupled condition was imposed. The governing

equations were discretized by the finite volume method. Semi Implicit Method for Pressure Linked Equations (SIMPLE) algorithm was used to couple the pressure and velocity. The momentum and energy equations were iterated by using the second order upwind scheme. The pressure term in the momentum equation was solved by pressure staggering option (PRESTO) scheme. To neglect the influence of boundary layer at the pipe walls, no-slip boundary condition was applied. Axial conduction along the pipe wall and viscous dissipation rate of the loop fluid were incorporated. The continuity and momentum equations converged by reaching the velocity and pressure residuals to 10^{-3} and the energy equation converged when its residual reaches to 10^{-6}.

Rashidi et al. [200] numerically compared single phase and two phase models (Volume of fluid, Eulerian and Mixture models) of nanofluid heat transfer in wavy channel. They concluded that the two phase models show better performance than the single phase model. Particularly, the mixture model data perfectly matched with experimental data. According to the Fluent manual, Stokes number (St) is helpful to choose an appropriate model among all available models such as volume of fluid (VOF), mixture and Eulerian models for simulating two phase flows. If St > 1, the Eulerian model is most suitable and if St << 1 or St ≈ 1, any of the models can be used. But the mixture model is computationally inexpensive and widely used to simulate nanofluid flows. In the present study, the Stokes number was estimated using eq. (5.4) and its value is around 12×10^{-4} and hence the mixture model is employed to simulate a nanofluid based NCL.

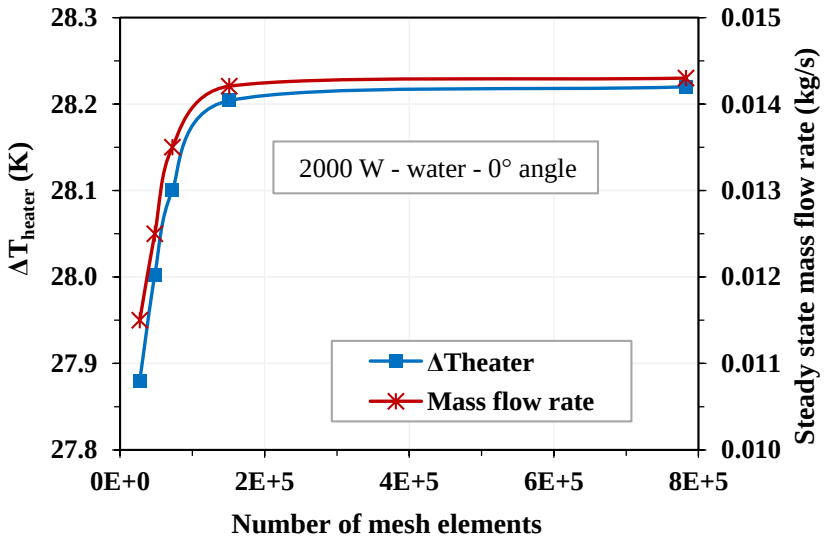

Fig. 5.3. Mesh sensitivity analysis

5.1.4 Mesh sensitivity analysis

The meshing of the loop fluid at a cross section of the loop pipe is shown in fig. 5.2. Previous researchers [201], [202] proposed a method for mesh verification. On refining the element size, the number of elements in the mesh are increased. This element size plays a vital role in the simulation results. Therefore, in order to test mesh sensitivity, five different element sizes were considered and the results were analyzed. For the mesh sensitivity test, the simulations were carried out with water as the working fluid and at 2000 W of power input without inclination angle. Figure 5.3 shows the influence of a number of elements on two independent variables such as steady state mass flow rate and temperature difference of the loop fluid at the heater. The effect of the number of elements on the temperature gradient and mass flow rate is presented in table 5.3. By increasing the number of elements from 150,920 to 782,784, the difference in temperature gradient across the heater was reformed by 0.06% and the mass flow rate difference by only 0.5%. Therefore, the mesh with 150,920 number of elements was considered for the simulations in order to use the computational time effectively.

Table 5.2. Thermo-physical properties of water and CuO nanoparticle at 298 K

Property (unit)	Water (from NIST)	CuO nanoparticle
ρ (kg/m^3)	997.05	6350
C_p (J/kg K)	4181.3	502.8
k (W/m K)	0.60652	69
β (per K)	0.000257	9.3×10^{-6}

Table 5.3. Mesh result details

No. of elements	Number of nodes	ΔT_{heater}	m (kg/s)
782784	918684	28.220	0.014300
150920	133280	28.204	0.014206
72350	65304	28.100	0.013500
48000	48960	28.002	0.012500
27250	39240	27.880	0.011500

5.1.5 Validation

On the developed 3-D NCL model, all the simulations were carried out at a steady state condition and the results were validated with the analytical results of Vijayan's correlation [198] which is given in eq. (4.16) and it was used for nanofluids by Nayak et al. [99].

Figure 5.4 shows that the simulation results of the developed model matched the analytical results in terms of mass flow rate of the loop fluid. The maximum difference between the simulation and analytical results is lower than 8.6% that is considerable, making it evident that, while developing the geometry and carrying the numerical simulations, all the possible influencing parameters of mass flow rate are considered.

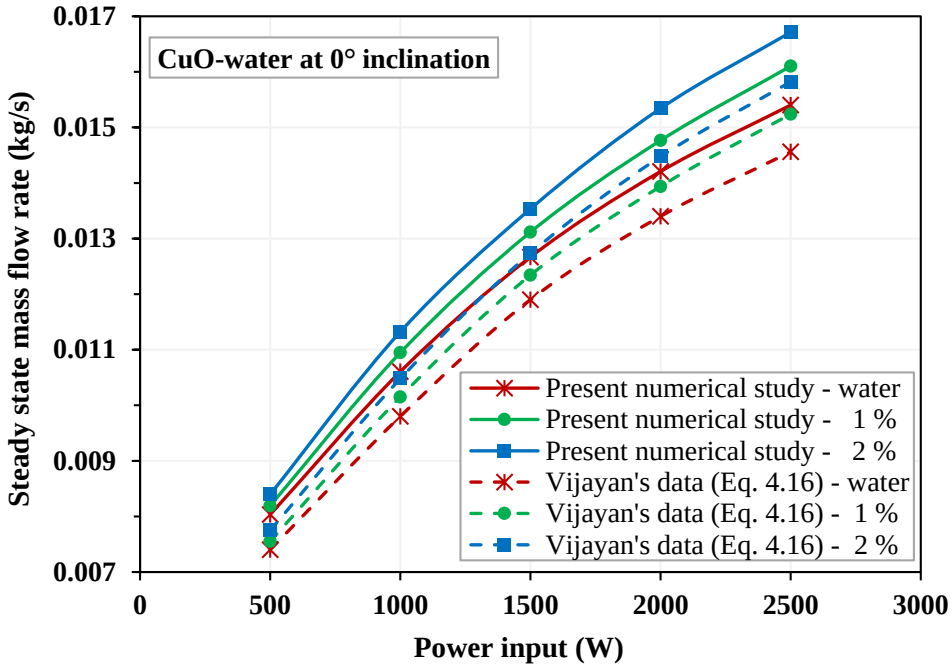

Fig. 5.4. Validation of numerical results with Vijayan's data [198]

5.2 Results and discussion

In the present chapter, numerical investigations were carried out for various power inputs (500 W to 2500 W) at the heater section. A constant temperature (293 K) wall boundary condition was imposed at the cooler section. The NCL was operated with water and CuO-water nanofluid as loop fluids. The performance of the loop was studied at different particle volume concentrations, various loop inclination angles and with multiple channels.

5.2.1 Influence of the particle concentration on thermal performance of the NCL

To investigate the influence of particle concentration on heat transfer and fluid flow characteristics, the NCL was operated with CuO-water nanofluid as loop fluid at different particle volume concentrations of 1%, 3%, 5% and 6%, and the performance was compared with water as loop fluid.

Steady state mass flow rate:

The mass flow rate of loop fluid in NCL under steady state condition was obtained at various power inputs and different particle volume concentrations. It is well known that mass flow rate of the loop fluid increases with an increase in power input at the heat source. Figure 5.5 shows explicitly the variation of flow rate of water and CuO-water nanofluid with power input. By increasing the power input, a higher density gradient is developed between the heat

source and heat sink which causes an enhanced mass flow rate. It is noticed from fig. 5.5 that the mass flow rate of CuO-water nanofluid is more than that of the water. It is observed from fig. 5.5 that the mass flow rate of the loop fluid is enhanced from 4.56% to 18.18% by varying the particle concentration from 1% to 5% when compared with water. But when the particle concentration is increased upto 6%, the mass flow rate is decreased by 3.26% when compared with 5% concentration.

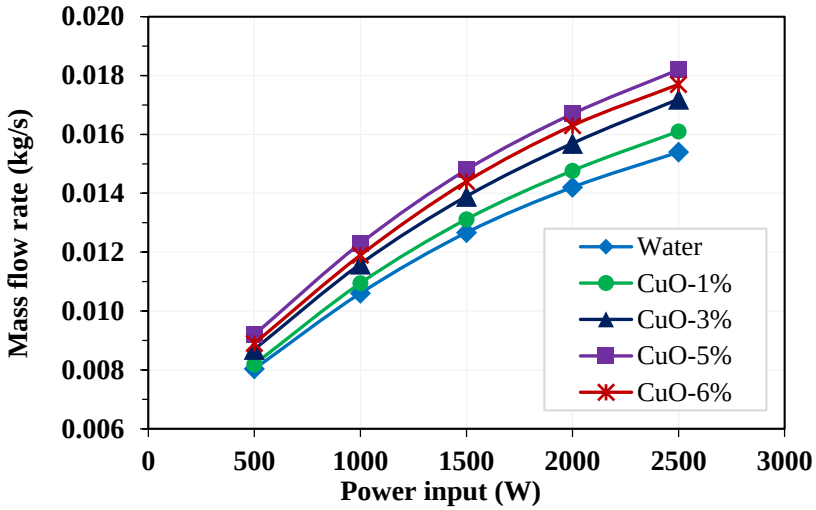

Fig. 5.5. Variation of steady state mass flow rate with power input

The mass flow rate of the loop fluid in the NCL is solely influenced by buoyancy effects. This buoyancy effect can be enhanced either by decreasing the viscous resistive forces or by improving the buoyancy driving forces. The thermo-physical properties of the fluid influence the viscous forces. Particularly for nanofluid, viscosity has more emphasis resistive forces. As the viscosity of the nanofluid is a function of the particle volume concentration, its effect cannot be neglected. Therefore, another way to improve the buoyancy driving forces is either by increasing the temperature or by regulating the thermo-physical properties of the fluid. As the particle concentration increases, the effective density of the nanofluid is increased and the specific heat (C_p) is reduced. By suspending the nanoparticles in the base fluid, the net specific heat of the nanofluid is reduced [16] as well as thermal expansion coefficient (β) of the nanofluid is increased [17] and hence the temperature of the loop fluid increases for the same power input. In the simulations, the specific heat of the CuO-water nanofluid is estimated by the mixture rule and the result reveals that, specific heat of the nanofluid is reduced by 2.87%, 8.83% and 14.96% at 1%, 3% and 5% particle volume concentrations respectively when compared with water. This decrease in specific heat gives a larger temperature rise in the fluid at the same power input. The temperature rise gives large change in the density gradient

between the heat source and heat sink which causes an increase in the mass flow rate. In addition to this, thermal expansion coefficient of the nanofluid is also an important parameter for the mass flow rate enhancement. The thermal expansion coefficient is more for nanofluids when compared with water. With increasing the particle concentration, the thermal expansion coefficient also increases. This may provide a physical reason for the increase of mass flow rate with the addition of nanoparticles by up to 5% concentration in the water. As the particle concentration increases from 5% to 6%, the percentage increment in the viscosity is more than the percentage decrement in the specific heat and therefore, the viscous forces dominate the buoyancy forces. This may be the reason for the decrement in the mass flow rate by the addition of nanoparticles beyond 5% particle concentration in water. Therefore, for NCL model, particle concentration at 5% is considered to be the optimum value.

Average Nusselt number:

The average Nusselt number at the heat source is estimated based on the area weighted average wall function heat transfer coefficient. The wall function heat transfer coefficient at the heat source is obtained from the simulation results. At the heat source, a variation of the average Nusselt number with power input and particle volume concentration is shown in fig. 5.6. The addition of high thermal conductive nanoparticles in the inherently poor conductive water, the effective thermal conductivity of the nanofluid increases. Therefore, for a given power input, the convective heat rate between the wall and the bulk fluid is more for the nanofluid, which results in an increase in its average heat transfer coefficient. This increment in average heat transfer coefficient causes the enhancement of the average Nusselt number.

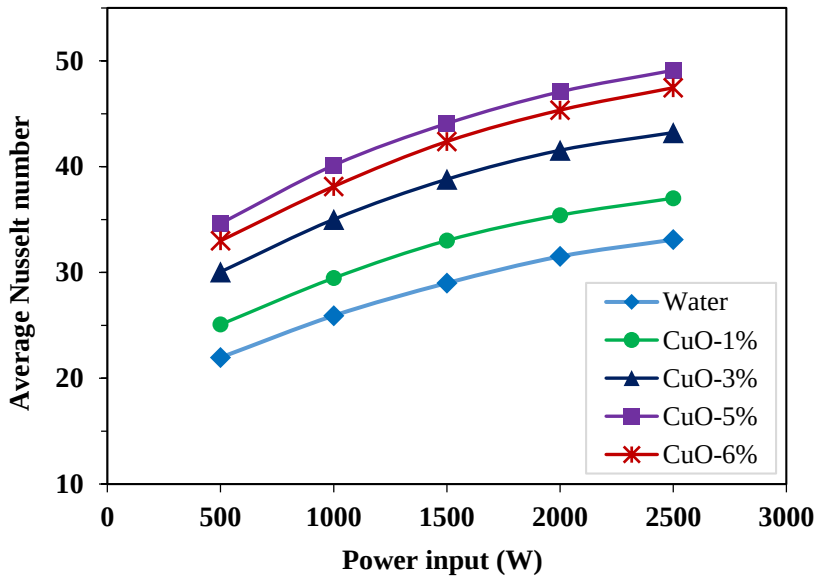

Fig. 5.6. Variation of Nusselt number with power input at heat source

5.2.2 Effect of loop inclination angle on thermal performance of the NCL

To study the influence of the loop inclination angle, the loop is simulated with CuO-water nanofluid at two different particle concentrations (1% and 2%) and at various loop inclination angles and the results are compared with water. Figure 5.7 shows the developed NCL model with inclination.

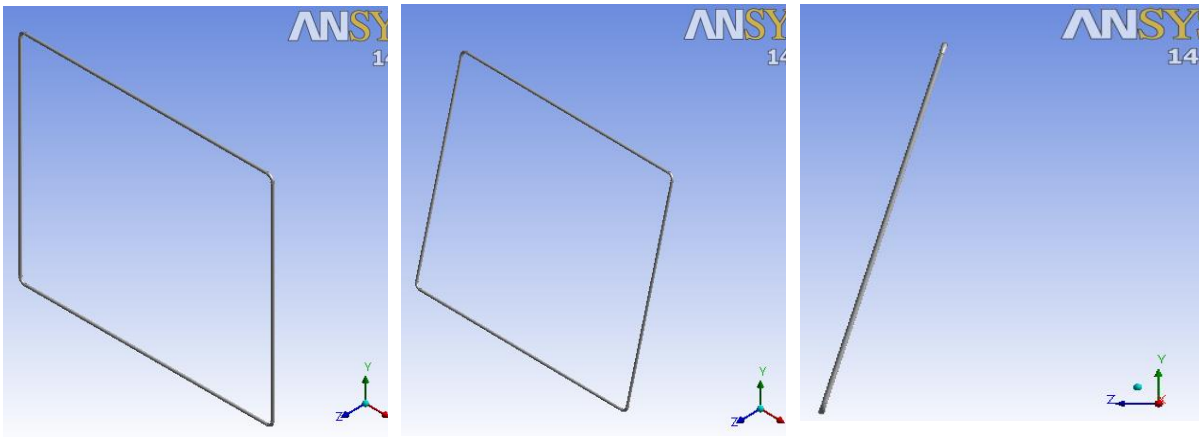

(a). The geometry of inclined NCL model without inclination

(b). The geometry of inclined NCL model (front view)

(c). The geometry of inclined NCL model (side view)

Fig. 5.7. The geometry of inclined NCL model with and without inclination angle

Effect of power input, particle concentration and inclination angle on steady state mass flow rate:

The variation of steady state mass flow rate of the loop fluid in NCL at different power inputs and particle concentrations is described in fig. 5.8. It is well known that the mass flow rate of the loop fluid increases with power input. By increasing the power input, a higher density gradient is developed between the heater and cooler sections, which enhances the mass flow rate. For a given power input, the mass flow rate of CuO-water nanofluid is higher than that of water. By suspending the nanoparticles in the base fluid, the net specific heat of the nanofluid is reduced by 4.28% and 7.85% at 1% and 2% particle volume concentrations, respectively, when compared with water. This decrease in specific heat gives larger temperature rise in the fluid at the given power input. The temperature rise results in a large change in density gradient between the heater and cooler sections, which causes an increase in the steady state mass flow rate. In addition to this, the thermal expansion coefficient of the nanofluid is also an important parameter for mass flow rate enhancement. The thermal expansion coefficient is more for

nanofluids than for water. When increasing the particle concentration, thermal expansion coefficient increases and this increment causes an improvement in the driving force. This may provide a physical reason for the increase of mass flow rate with particle concentration. It is observed from fig. 5.8 that the mass flow rate of the loop fluid is enhanced by 4.93% and 10.15% at 1% and 2% particle concentration, respectively, when compared with water at high power input and 15° loop inclination angle.

Figure 5.9 shows the variation of steady state mass of flow rate with loop inclination angle. The steady state mass flow rate decreases with loop inclination angle. As the loop inclination angle increases, the effective loop height decreases, which leads to a reduction in the gravitational acceleration that is related to the cosine of the inclination angle. This could be a possible reason for increasing the mass flow rate with loop inclination angle. It is observed from fig. 5.9 that the steady state mass flow rate is decreased by 34.57%, 33.74% and 31.51% for water, CuO-water nanofluid at 1% and 2% particle concentrations, respectively, by varying the loop inclination angle from 0° to 60° at 2000 W power input.

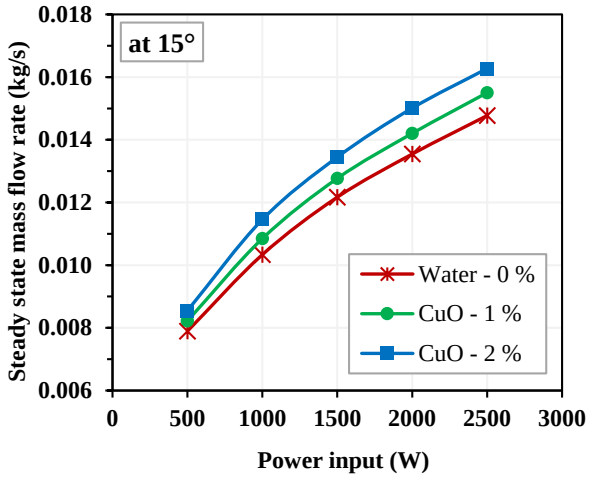

Fig. 5.8. Variation of steady state mass flow rate at heater with power input

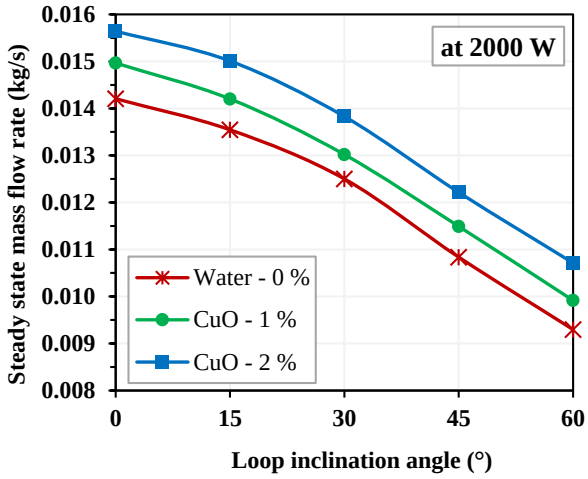

Fig. 5.9. Variation of steady state mass flow rate with loop inclination angle

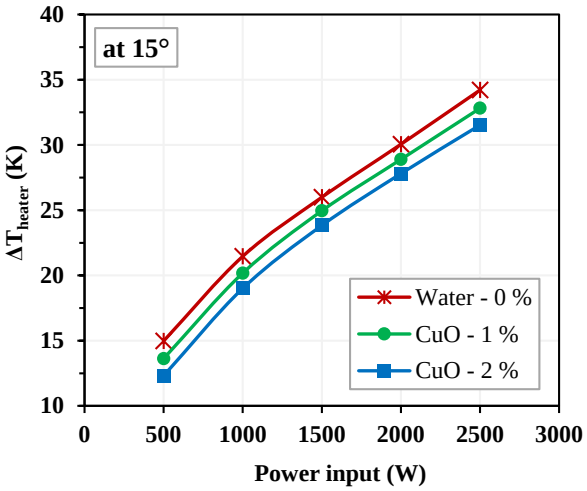

Fig. 5.10. Variation of temperature gradient at heater with power input

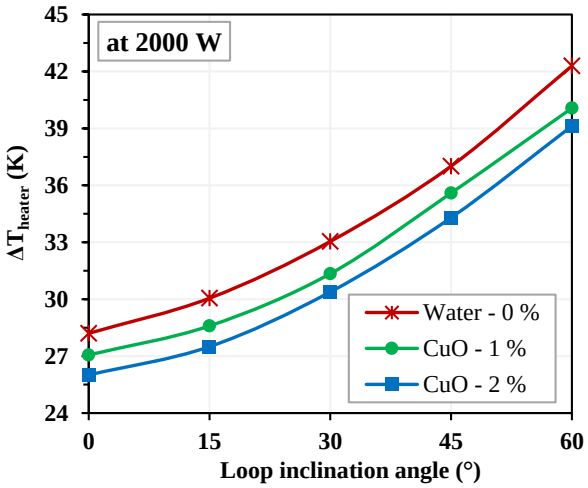

Fig. 5.11. Variation of temperature gradient at heater with loop inclination angle

Effect of power input, particle concentration and inclination angle on temperature gradient at heater:

The analysis has been carried out to study the temperature difference of the loop fluid at the heater for different power inputs, loop inclination angles and particle concentrations. Figure 5.10 shows the temperature gradient at the heater for different power inputs and particle concentrations at 15° loop inclination angle. It is noticed from fig. 5.10 that the temperature gradient of the loop fluid increases with power input. The temperature gradient is diminished by 4.08% and 7.86% at 1% and 2% particle concentrations, respectively, when compared with water at a high power input and 15° inclination angle. The steady state mass flow rate enhancement causes a decrease in temperature gradient with particle concentration at a given power input.

Figure 5.11 shows the effect of inclination angle and particle concentration on the temperature gradient at the heater section for a given power input of 2000 W. Figure 5.11 illustrates that temperature difference increases with inclination angle, and decreases with particle concentration. One possible reason may be that as the loop inclination angle increases, the effective loop height reduces, which leads to lowering of gravitational acceleration, and the corresponding mass flow rate. The lower mass flow rate of the loop fluid causes the temperature gradient to rise at the heater section. From fig. 5.11 it is seen that the temperature gradient is increased by 27.98%, 28.23% and 28.77% for water, CuO-water nanofluid at 1% and 2% particle concentrations, respectively, by varying the loop inclination angle from 0° to 60° at 2000 W power input.

Figure 5.12 shows the temperature contours of loop fluid at the heater entrance and exit for different power inputs and particle concentrations at 15° inclination angle. It is observed that there is a uniform temperature distribution at the heater entrance for all considered loop fluids at a low power input. On the contrary, at the exit of the heater, the average temperature of the loop fluid increases with the power input and particle concentration. As the power input increases, the density of the fluid decreases, and thus the low density fluid in the heater section moves upward due to buoyancy and causes generation of high temperature zone at the top portion in heater as described in fig. 5.12. In the same way, as the particle concentration increases, the percentage of the high temperature zone also increases. The possible root cause for the generation of high temperature zones is decrease in specific heat and increasing thermal expansion coefficient with particle concentration.

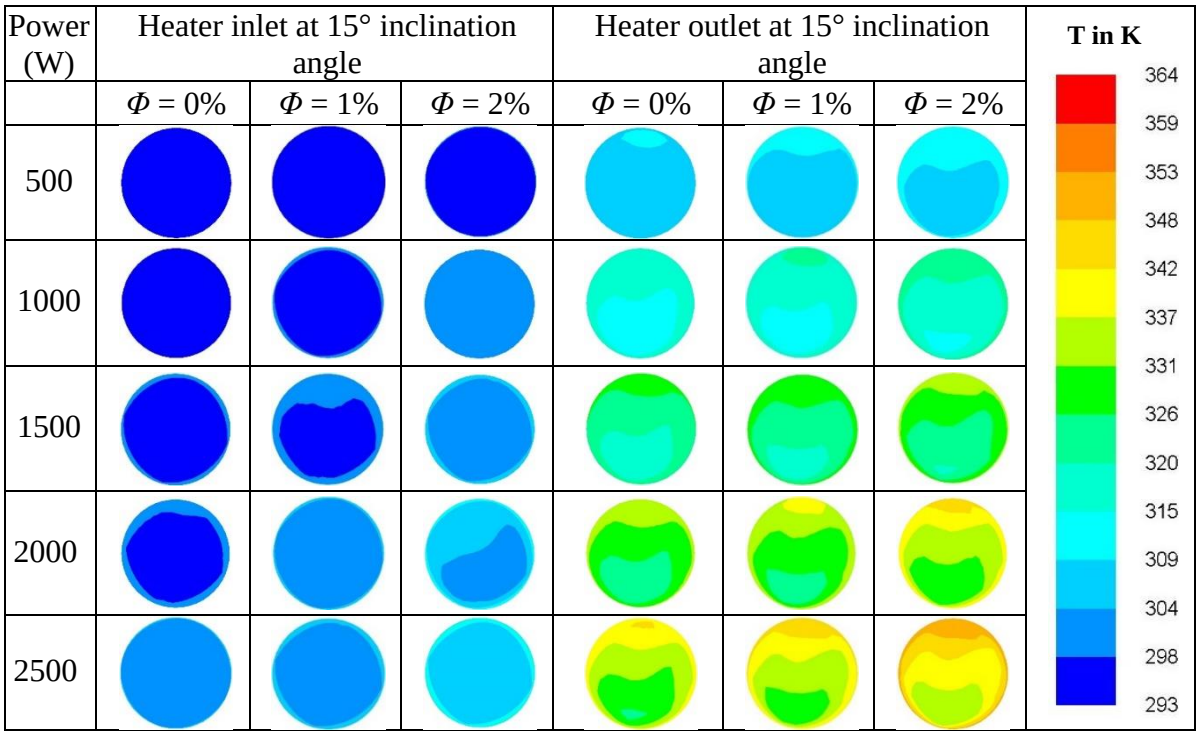

Fig. 5.12. Temperature (in K) contours plot for different partcile concentrations at 15° loop inclination angle.

Figure 5.13 shows the temperature contours at the entrance and exit of the heater section at 1% particle concentration for different power inputs and loop inclination angles. The distribution is non uniform at the heater exit for all inclination angles at higher power inputs; however, the distribution is uniform at lower power inputs. It can be observed from fig. 5.13 that the temperature of the loop fluid decreases at the heater inlet and increases at the heater outlet with inclination angle. As a result, the temperature gradient at the heater section increases

with loop inclination angle as described in fig. 5.13. The temperature contours of loop fluid at the middle of the riser and downcomer are presented in fig. 5.14. It can be observed that for the same heat input, as inclination increases, fluid temperature increases. Three dimensional representation of the loop geometry with CuO-water nanofluid is presented in fig. 5.15 and 5.16. Figure 5.15 shows the temperature of the loop fluid thought the loop at 500W and 1% particle concentration. Similarly, fig. 5.16 shows temperature of the loop fluid thought the loop at 2500W and 1% concentration.

Power (W)	Heater inlet at Φ = 1% particle concentration					Heater outlet at Φ = 1% particle concentration				
	0°	15°	30°	45°	60°	0°	15°	30°	45°	60°
500	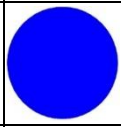	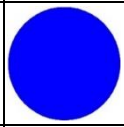	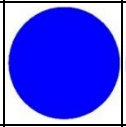	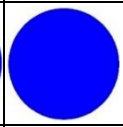	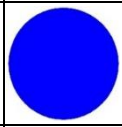	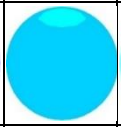	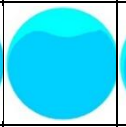		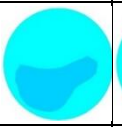	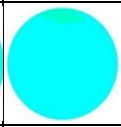
1000	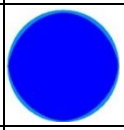	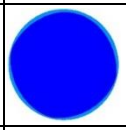	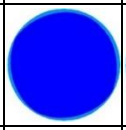	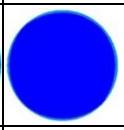	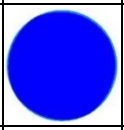	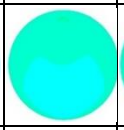	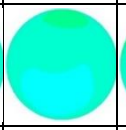	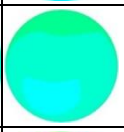	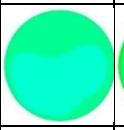	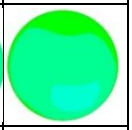
1500	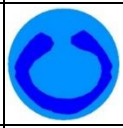	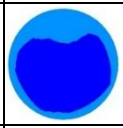	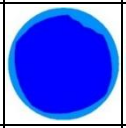	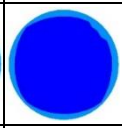	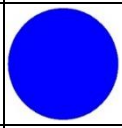	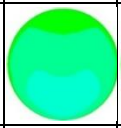	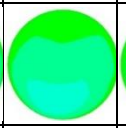	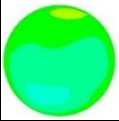	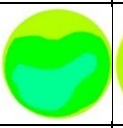	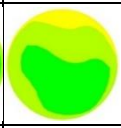
2000	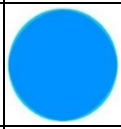	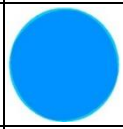	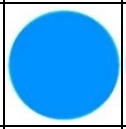	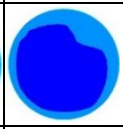	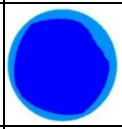	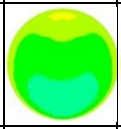	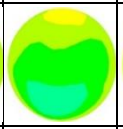		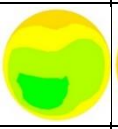	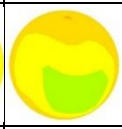
2500										

Fig. 5.13. Temperature (in K) contours plot for different inlcination angles at 1% particle concentration. (Refer fig. 5.12 for temperature scale).

Power (W)	Downcomer center at Φ = 1% particle concentration					Riser center at Φ = 1% particle concentration				
	0°	15°	30°	45°	60°	0°	15°	30°	45°	60°
2500										

Fig. 5.14. Temperature contours plot at the cross section of the riser centre and the downcomer centre for different inclination angles at 1% particle concentration. (Refer fig. 5.12 for temperature scale)

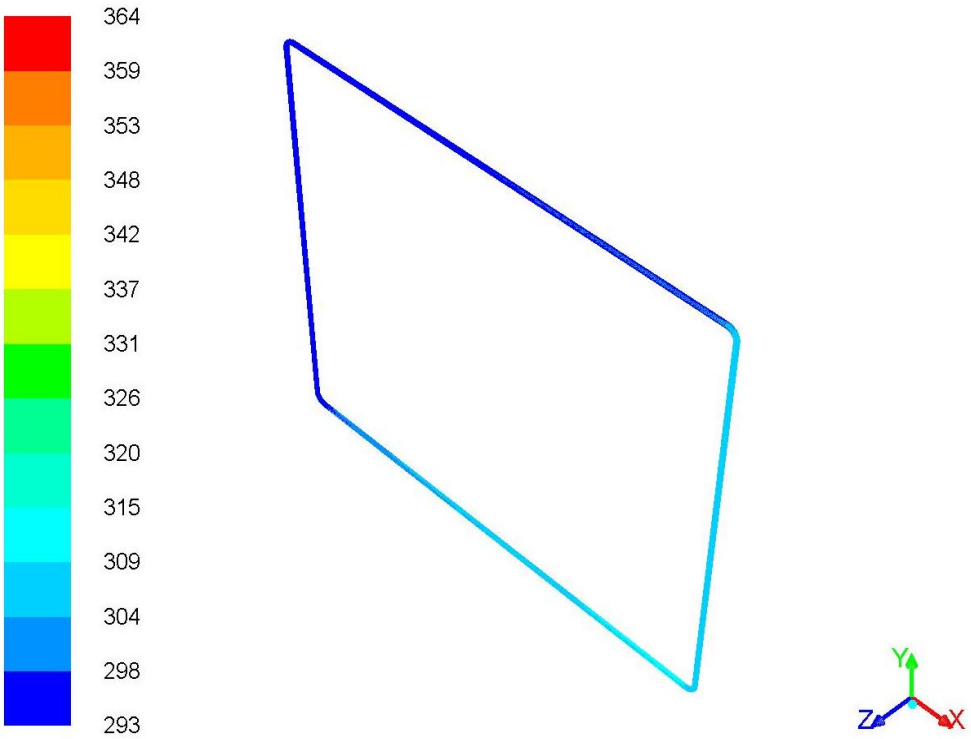

Fig 5.15 The three dimensional representation of the temperature of CuO-water nanofluid at 500W for 1% concentration

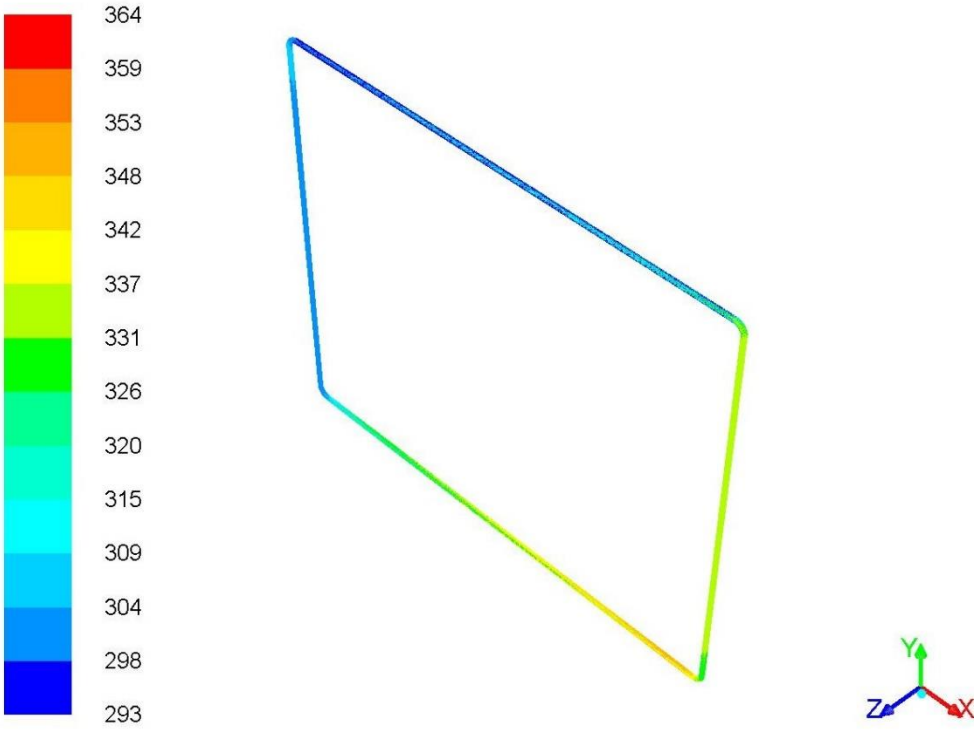

Fig 5.16 The three dimensional representation of the temperature of CuO-water nanofluids at 2500W for 1% concentration

Effect of power input, particle concentration and loop inclination angle on average heat transfer coefficient:

Figure 5.17 shows the effect of particle concentration and power input on the average heat transfer coefficient. The average heat transfer coefficient of the loop fluid at heater section is estimated using eq. (5.7). As illustrated in fig. 5.17, the average heat transfer coefficient is enhanced with power input and particle concentration. The CuO-water nanofluid has higher thermal conductivity than water and the thermal conductivity increases with particle concentration. Therefore, the difference between average wall temperature and average bulk fluid temperature at the heater section increases with particle concentration, which results in an increase in the average heat transfer coefficient of loop fluid. This could be one possible reason for the heat transfer enhancement with the particle concentration. It is noticed from fig. 5.17 that the average heat transfer coefficient is enhanced by 29.63% and 54.55% at 1% and 2% particle concentrations, respectively, when compared with water at high power input and 15° loop inclination angle.

The effect of inclination angle on average heat transfer coefficient at heater section is illustrated in fig. 5.18. The average heat transfer coefficient is decreasing with loop inclination angle. The net height of the loop decreases with a loop inclination angle which results in a decrease of the net gravitational acceleration effect. This reduced gravitational effect causes a decrease in mass flow rate and corresponding Reynolds number. This reduced Reynolds number leads to a decrease in Nusselt number and corresponding heat transfer coefficient. It is noticed from fig. 5.18 that the average heat transfer coefficient decreases by 0.83%, 0.94% and 1.05% for water, CuO-water nanofluid at 1% and 2% particle concentrations, respectively, by varying the loop inclination angle from 0° to 15° at 2000 W power input. Further, by increasing the loop inclination angle up to 60°, the average heat transfer coefficient decreases by 14.29%, 10.97% and 10.27% for water, CuO-water nanofluid at 1% and 2% particle concentrations, respectively. Therefore, from fig. 5.18 it can be concluded that the loop inclination angle at 15° has limited influence on the average heat transfer coefficient.

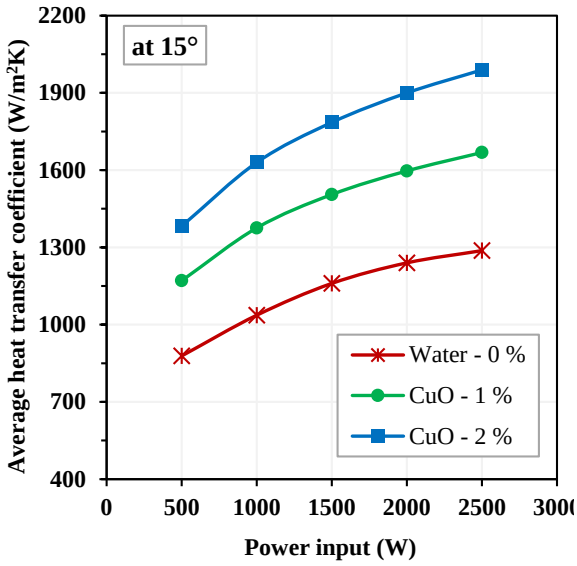

Fig. 5.17. Variation of average heat transfer coefficient at the heater with power input

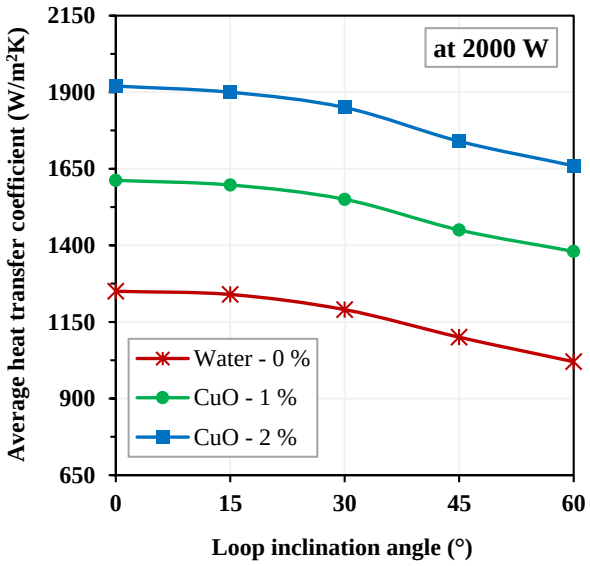

Fig. 5.18. Variation of average heat transfer coefficient at heater with inclination angle

Effect of power input, particle concentration and loop inclination angle on Rayleigh number:

Rayleigh number is an important dimensionless parameter which is helpful to study the buoyancy effect of natural circulation flows. The Rayleigh number of a working fluid can be estimated using eq. (5.8). It can be noticed from this equation that, for a given geometry, the Rayleigh number purely depends solely on the thermophysical properties of the working fluid. Figure 5.19 demonstrates the influence of power input and particle concentration on Rayleigh number. As can be seen from fig. 5.19, the Rayleigh number of the working fluid increases with the power input and particle concentration as well. The thermal expansion coefficient of the nanofluid is much and specific heat of the nanofluid is relatively lower than the water, which results in an increase in the average temperature of the loop fluid at the heater for a nanofluid. However, this temperature rise in the heater section leads to the production of high buoyancy forces which dominate viscous forces. Therefore, the resultant high buoyancy could be a reason for increasing Rayleigh number in the nanofluid and it further increases with the particle concentration.

The influence of inclination angle on Rayleigh number is presented in fig. 5.20. For a fixed power input, the Rayleigh number diminishes with loop inclination angle. As the loop inclination angle increases, the net height of the loop is reduced by the cosine angle which reduces the gravitational acceleration effect. It is observed from fig. 5.20 that by increasing the inclination angle from 0° to 15° the Rayleigh number decreases by 1.05%, 1.10% and 1.70% for water, CuO-water nanofluid at 1% and 2% particle concentrations, respectively. In addition, increasing the loop inclination angle by up to 60°, the Rayleigh number is reduced by 23.09%, 22.12% and

21.69% for water, CuO-water nanofluid at 1% and 2% particle concentrations, respectively. The effect of inclination angle on Rayleigh number is relatively low at lower inclinations as shown in fig. 5.20. Therefore, lower inclination angles of up to 15° may be acceptable without affecting the Rayleigh number.

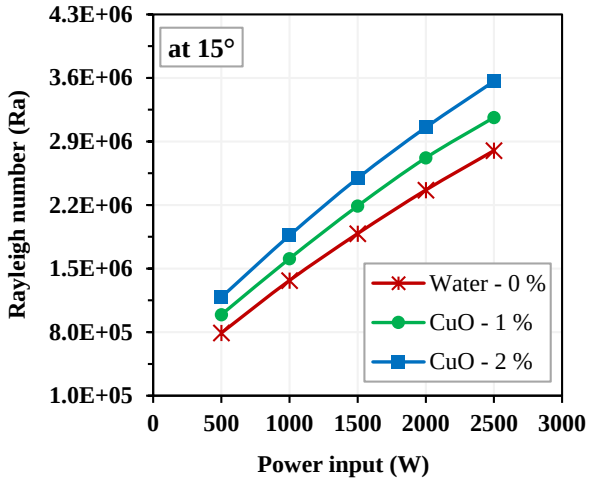

Fig. 5.19. Variation of Rayleigh number with power input

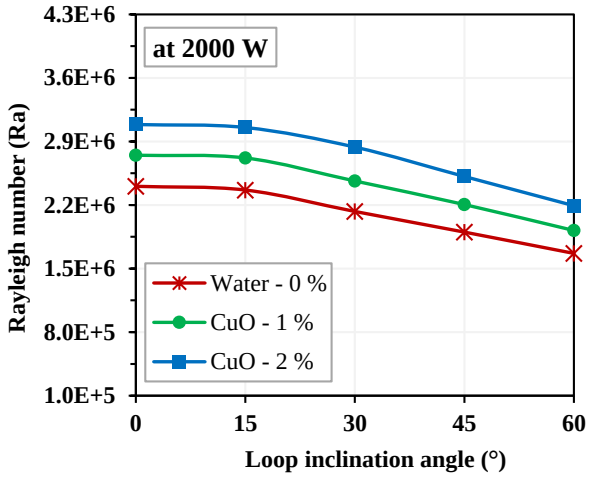

Fig. 5.20. Variation of Rayleigh number with loop inclination angle

Effect of power input, particle concentration and inclination angle on effectiveness of the loop:

Effectiveness is a non-dimensional parameter for transparency on the enhancement in heat transfer rate. For a given geometry, effectiveness is the ratio of actual heat transfer [$m_{ss} \times C_{p,h} \times (T_{ho} - T_{hi})$] to maximum possible heat transfer [$m_{ss} \times C_{p,c} \times (T_{ho} - T_{cw})$] and this relation is developed by [35]. Figure 5.21 shows the effect of power input and particle concentration on the effectiveness of NCL. Figure 5.21 summarizes the effectiveness of NCL, which proportionally increases with particle concentration. Figure 5.21 shows the effectiveness is improved by 5.70 % and 10.68 % at 1% and 2% particle concentrations, respectively, when compared with water at high power input. Figure 5.22 shows the effect of loop inclination angle on effectiveness at a given power input of 2000 W. The effectiveness of NCL is increased by 18.63%, 18.97% and 19.83% for water, 1% and 2% particle concentrations, respectively, at 60° inclination angle when compared with a vertical configuration (i.e. 0° inclination angle).

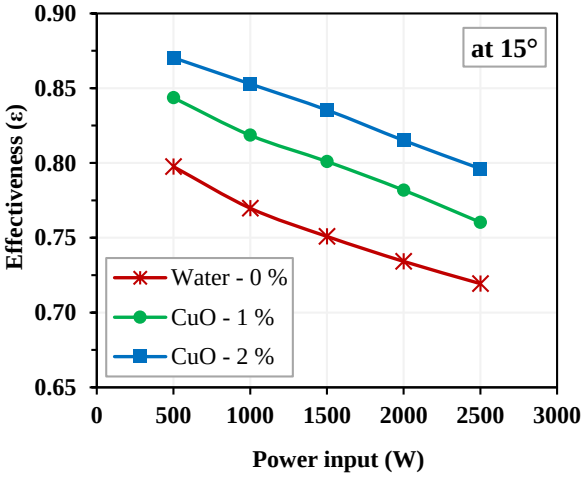

Fig. 5.21. Variation of effectiveness of NCL with power input

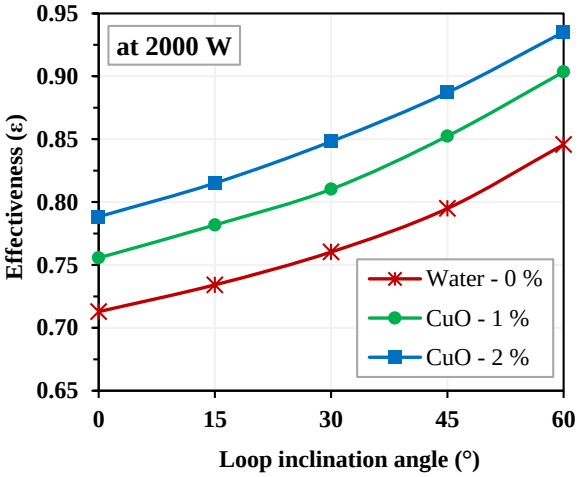

Fig. 5.22. Variation of effectiveness of NCL with loop inclination angle

5.2.3 Effect of multiple channels on thermal performance of the NCL

In the present section, the influence of multiple channels (double riser and double downcomer-DRDD) on heat transfer and fluid flow characteristics of nanofluid based NCL was investigated. For this investigation the CuO-water nanofluid at different concentrations was considered as loop fluid and the results were compared with that of water. Figures 5.23 and 5.24 show the schematic diagram and mesh of a rectangular NCL with multiple channels respectively. This kind of model is suitable for solar water heating systems, geothermal heat extraction systems and electronic chip cooling systems. The geometrical specifications of NCL with multiple channels are given in table 5.4 and all the remaining specifications are the same as given in table 5.1.

Table 5.4. Geometrical specifications of the NCL model with multiple channels

Parameter	Value (unit)
Total length of the DRDD loop	8.24 m
Width of the DRDD loop	1.56 m

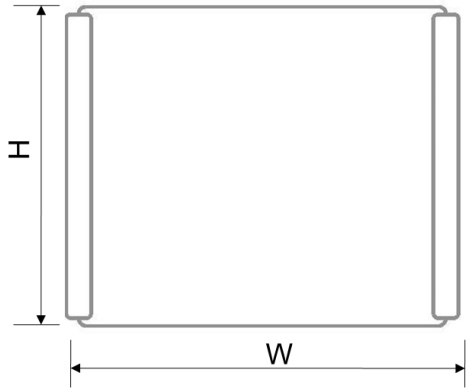

Fig. 5.23. Schematic diagram of the geometrical DRDD-NCL

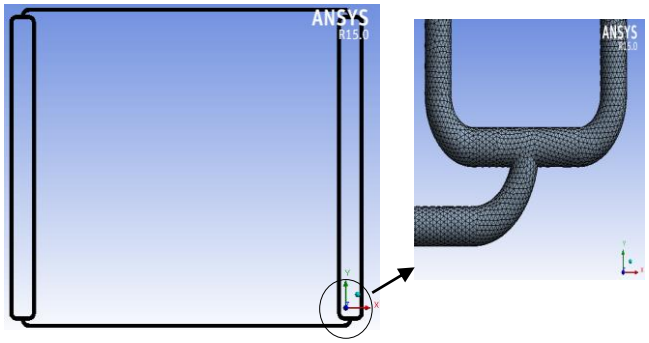

Fig. 5.24. Mesh of a loop fluid in DRDD-NCL at bend

Validation:

The simulation results of the current study were compared with the analytical approach of Vijayan's correlation [75] which is given in eq. (5.10). Figure 5.25 illustrates that the simulation results follows the same trend with the analytical results of Vijayan's correlation in terms of steady state Reynolds number and modified Grashof number. It is observed from fig. 5.25 that the analytical approach was close to Reynolds number, though this deviation was less than 10%.

$$Re_{ss} = 0.1768 \left[\frac{Gr_m}{N_G}\right]^{0.5} \tag{5.10}$$

The modified Grashof number (Gr_m) and effective loss coefficient (N_G) can be calculated by eqs. (5.11) and (5.12) respectively [75]:

$$Gr_{m,lf} = \frac{\left(g\ \beta_{lf}\ \rho_{lf}^2\ d^3\ \mathrm{Q_h}\ H\right)}{\left(A_{cs}\ \mu_{lf}^3\ \mathrm{C_{p,lf}}\right)} \tag{5.11}$$

$$N_G = \frac{L_t}{d} \tag{5.12}$$

Comparison of NCL performance with single channel and multiple channels in terms of steady state mass flow rate:

The decrease in specific heat and increase in thermal expansion coefficient with particle concentration gives a large temperature rise in the fluid at the same heat input. This temperature rise gives a large change in density gradient between the heat source and heat sink, which causes an increase in the mass flow rate. Figure 5.26 shows that the steady state mass flow rate of the

loop fluid in multiple channel (double riser double downcomer-DRDD) NCL was increased by 2.5% when compared with single channel (single riser single downcomer-SRSD) NCL.

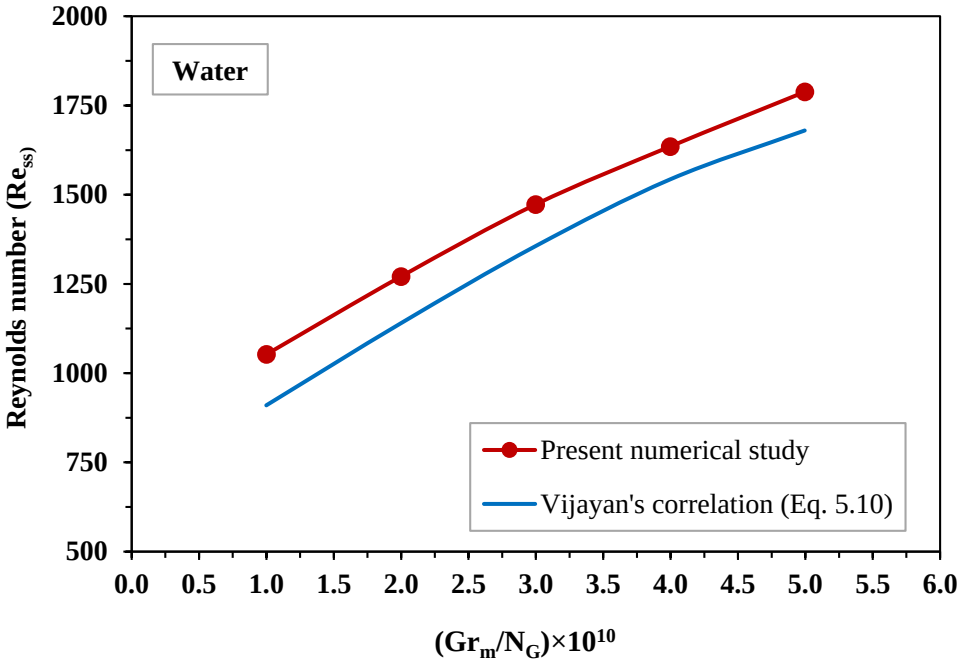

Fig. 5.25. Validation of numerical results with Vijayan's correlation [75]

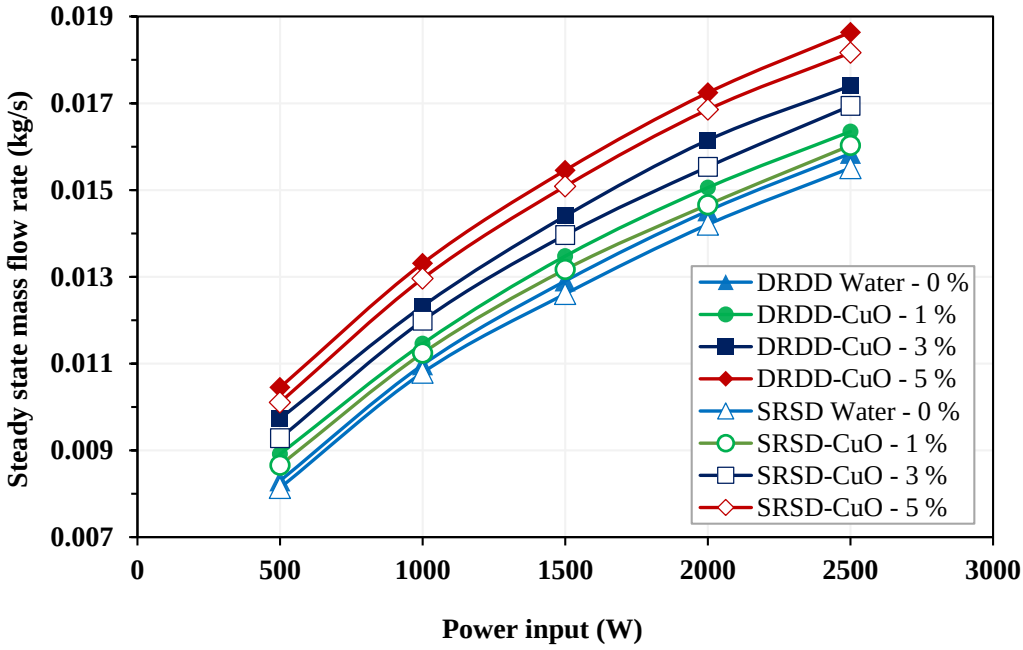

Fig. 5.26. Variation of mass flow rate with power input

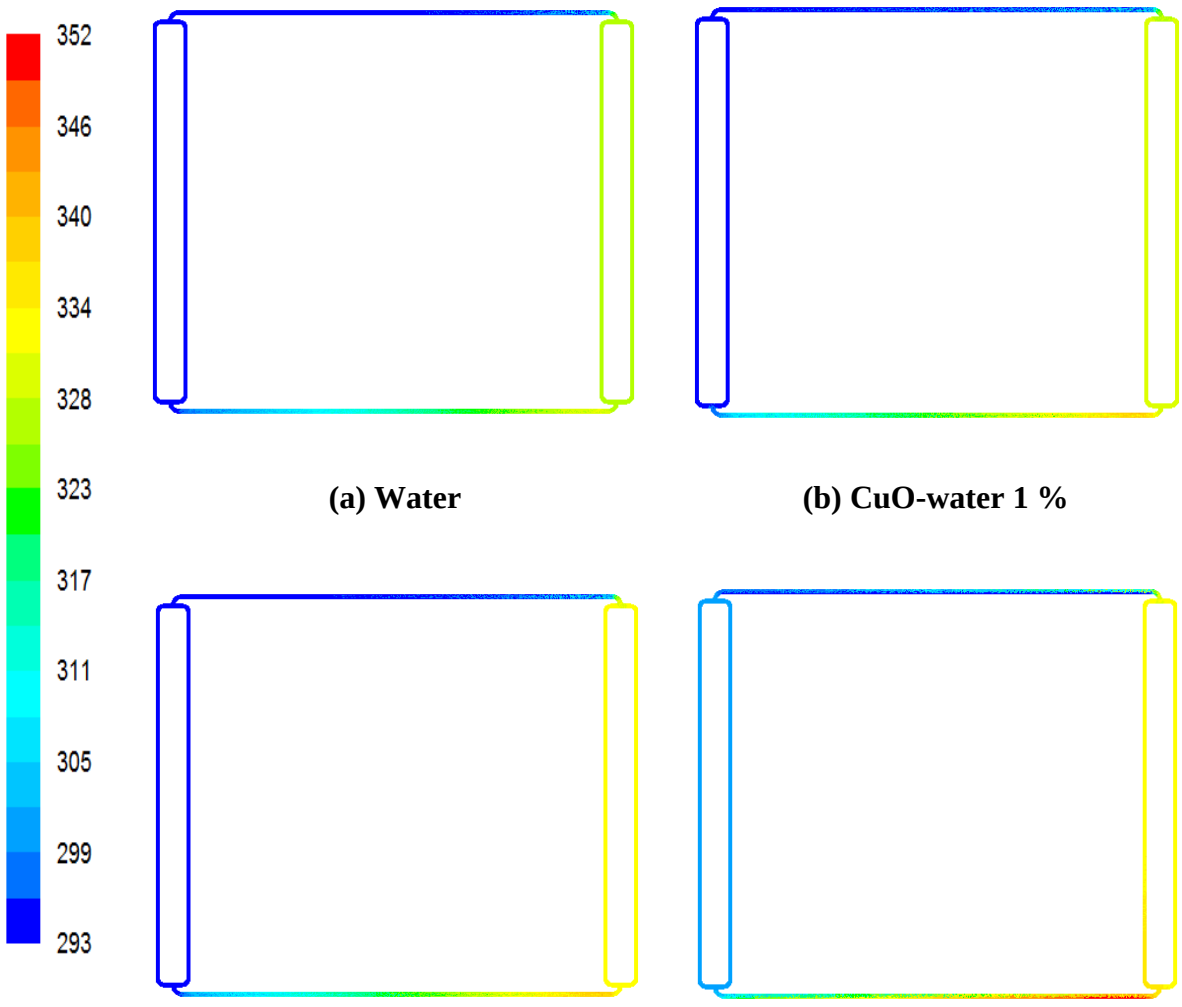

Fig. 5.27. Temperature (K) contours plot of multiple channel type NCL at 2000 W

Temperature contours of the loop fluid throughout the loop:

Figure 5.25 shows the temperature contour profile of the loop fluid at different particle concentrations. It can be observed from fig. 5.27 that the temperature of the loop fluid decreases at heater inlet and increases at the heater outlet with particle concentration. Therefore, the temperature gradient at heater increases with particle concentration.

Effect of multiple channels on average heat transfer coefficient:

Figure 5.26 shows the effect of multiple channels on the average heat transfer coefficient. The average heat transfer coefficient of the loop fluid at the heater section is estimated using eq. (5.7). As illustrated in fig. 5.28, the average heat transfer coefficient enhances with power input

and particle concentration. The CuO-water nanofluid has higher thermal conductivity than water and this thermal conductivity increases with particle concentration. Therefore, the convective heat rate between the wall and the bulk fluid at the heater section increases with particle concentration, which results in an increase in the average heat transfer coefficient of the loop fluid. This could be one possible reason for the heat transfer enhancement with particle concentration.

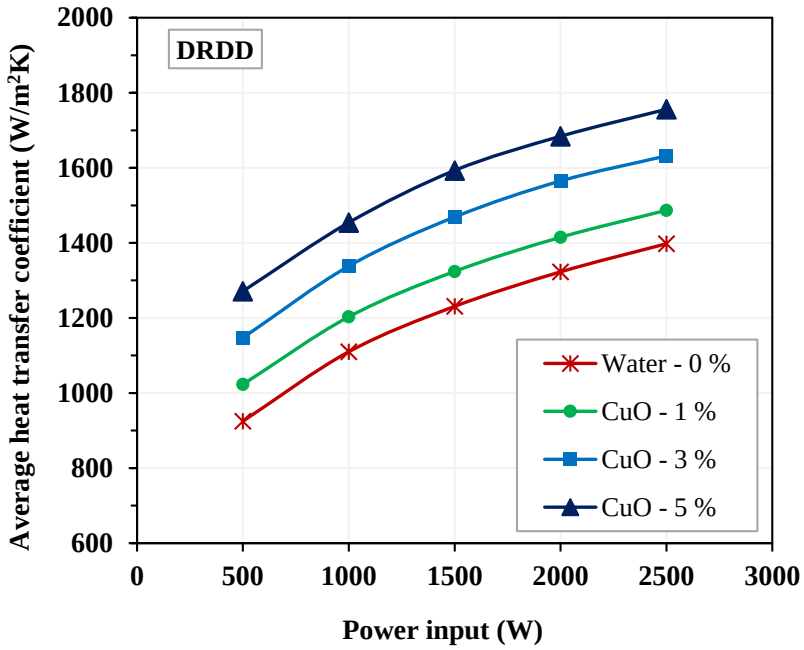

Fig. 5.28. Variation of average heat transfer coefficient with power input

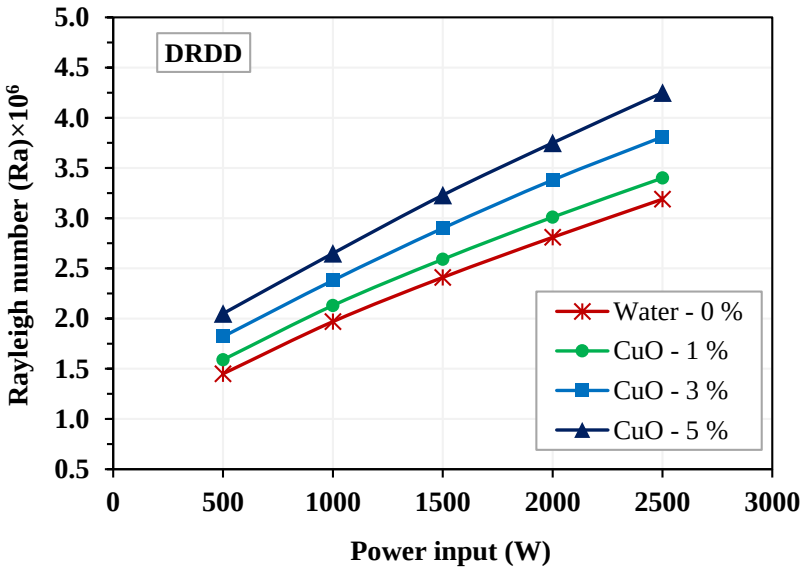

Fig. 5.29. Variation of Rayleigh number with power input

Effect of multiple channels on Rayleigh number:

Figure 5.29 shows the influence of multiple channels on Rayleigh number. It can be seen from fig. 5.29 that the Rayleigh number of the working fluid increases with power input and particle concentration. The temperature rise in the heater section leads to higher buoyancy force and that dominates the viscous force. Therefore, higher buoyancy could be a reason for a increase in Rayleigh number with the nanofluid and it further increases with the particle concentration which can be observed in fig. 5.29.

5.3 Conclusion

The steady-state analysis of a single phase rectangular NCL with heater as a heat source was carried out using 3-D numerical modelling in Ansys-Fluent 14.0. Based on the numerical results the following conclusions have been drawn.

- The steady state mass flow rate of the NCL increases with heat input and decreases with the loop inclination angle.
- If the particle volume concentration increased from 0% to 5%, then the mass flow rate of the loop fluid increased by 26%, but with any further increase in particle concentration, the mass flow rate decreased due to viscous forces dominating the buoyancy forces. Therefore, for this kind of NCL model, 5% particle concentration can be considered as optimum value.
- Effectiveness increases with particle concentration and inclination angle. Therefore, the effectiveness of a nanofluid based NCL is more than a water based NCL.
- At a given power input and fixed inclination angle, the average heat transfer coefficient of the nanofluid is enhanced with the particle concentration. Moreover, the average heat transfer coefficient is influenced by the loop inclination angle.
- Rayleigh number is reduced with the inclination angle; however, the effect of inclination angle is relatively minor for up to 15°. Therefore, lower inclination angles of up to 15° are preferable without a significant effect on Rayleigh number.
- The performance of the NCL with multiple channels (DRDD) was enhanced by 2.5% when compared with single channel (SRSD) in terms of the mass flow rate.

Chapter - 6

Experimental studies on nanofluid based single phase NCL

In chapter 4, one-dimensional theoretical results of nanofluid based natural circulation loop with end heat exchangers were presented. In chapter 5, three-dimensional simulation results of nanofluid based natural circulation loop with heater as heat exchanger have been presented. Although experimental results are available in the open literature on NCL with water as a working fluid, test results on nanofluid based systems are very few. Hence, in the present chapter, experimental studies have been conducted to understand the working fluid behaviour in NCL with heater as a heat source and with heat exchanger as a heat source and to validate the numerical model which is described in earlier chapters. Experiments were carried out on an instrumental test facility which was designed for use with nanofluid as working fluid.

6.1 Experimental studies on nanofluid based NCL with heater as heat source

6.1.1 Experimental facility

A detailed schematic diagram of the experimental facility used for this study is shown in fig. 6.1. The photographic view of the experimental test rig is presented in fig. 6.2. The system consists of a heater at the bottom and tube-in-tube cold heat exchanger at top. These two are connected by two parallel vertical legs called riser and downcomer. A smooth stainles

steel tube with 15.1 mm external diameter 12.7 mm internal diameter is chosen for the loop pipe. To prevent heat leak from or to the ambient, the entire loop was insulated with 4 mm thick asbestos rope. The geometrical specifications and operating parameters are given in table 6.1. The temperatures of the loop fluid (T_1 to T_4), external fluid (T_5 and T_6) and heater wall surface (T_7 to T_{10}) were measured by using RTDs as shown in fig. 6.1. These RTDs were connected to a computer integrated data acquisition system (Agilent-34972A) to log the temperature data at regular intervals. Pressure drop between different sections in the NCL was measured using U-tube manometers. Both heater and cold heat exchangers were operated at constant pressure condition. Therefore, manometer tubes were connected at the entrance and exit of the riser and downcomer sections respectively, as shown in fig. 6.1. To measure cold fluid mass flow rate, a rotameter was connected between CHE inlet and thermostatic bath outlet. Classic scientific made thermostatic bath was used to control the cold fluid temperature sent to CHE.

Table 6.1. Geometrical specifications and operating parameters of NCL with heater

Parameter	Value
Loop pipe diameter	0.012 m
Inner diameter of the annulus at CHE	0.0215 m
Loop width	1.22 m
Loop height	1.64 m
Total length of the loop	10.4 m
Length of heater	1 m
Length of cold heat exchanger	5 m
Power input to heater	500 W – 2500 W
Cold water inlet temperature	5 °C to 20 °C
Cold fluid mass flow rate	0.05 kg/s
Particle volume concentration *(Ø)*	0.5 % , 1.0 % and 1.5 %
Working/loop fluids	SiO_2-water, Al_2O_3-water and CuO-water nanofluids

6.1.2 Experimental procedure

An experimental study on single phase rectangular natural circulation loop was initially conducted with distilled water, and soon after was conducted with three different nanofluids (SiO_2-water, Al_2O_3-water and CuO-water) at 0.5%, 1.0% and 1.5% concentrations. During the experiment, the combined effects of power input, particle concentration and cooling water inlet temperatures were analysed. The experimentation was carried out with the following procedure:

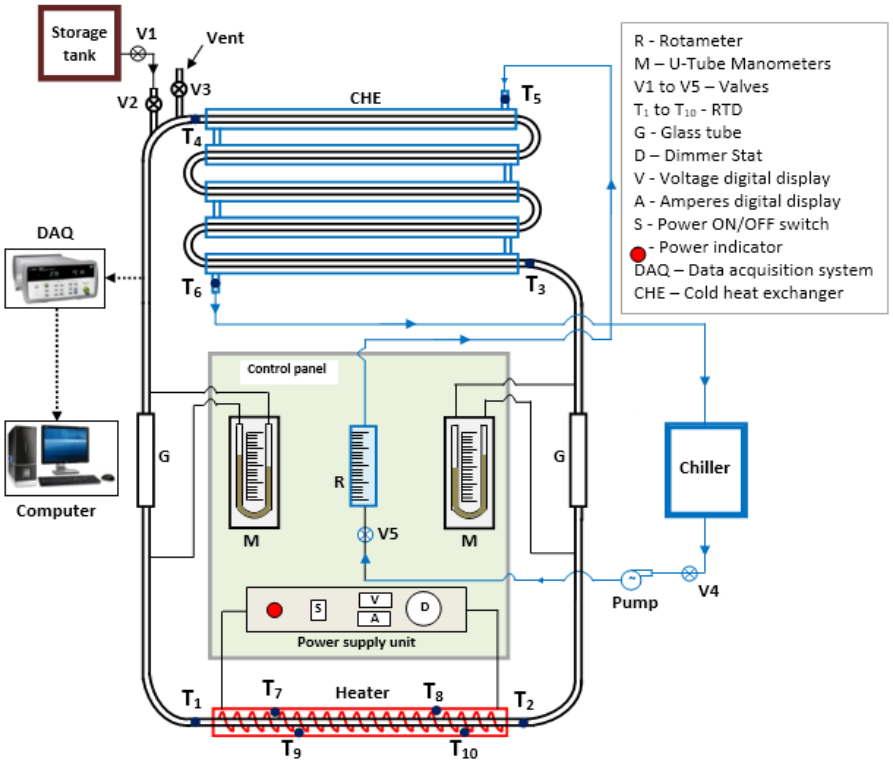

Fig.6.1. Schematic diagram of the experimental setup

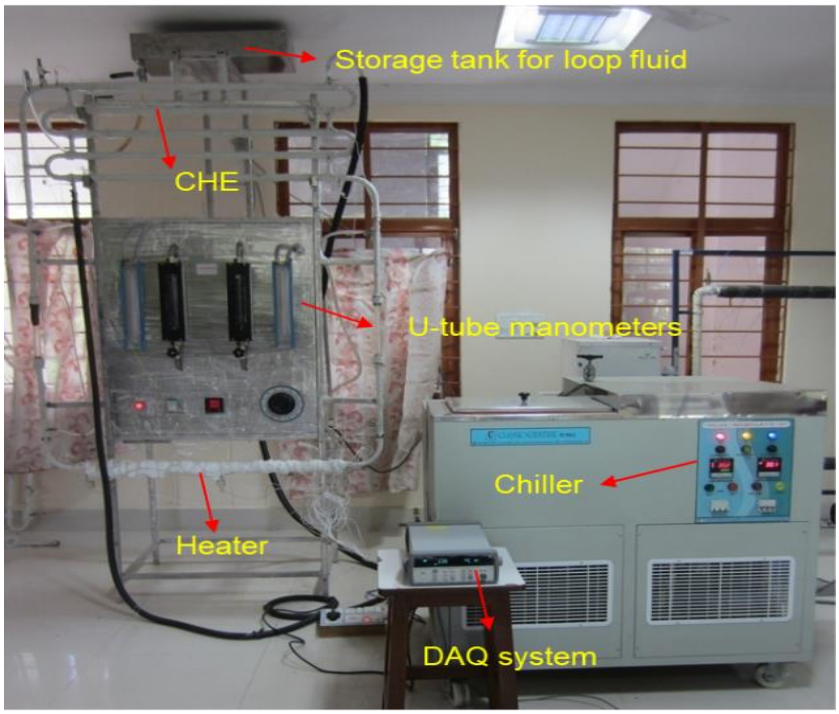

Fig.6.2. Photographic view of the Experimental test rig

- The NCL was filled with working fluid.
- Air bubbles were drained out by giving continuous pulses while filling the loop.

- Sufficient time was given to the loop fluid to obtain thermal equilibrium with room temperature without heating.
- The cold fluid temperature at CHE was set at a required value.
- The DAQ system was switched on and the initial readings were taken.
- After ensuring the thermal equilibrium from the data acquisition (DAQ) system, the thermostatic bath and heater are started simultaneously.
- Repeatability of the test rig was ensured.
- The same procedure was repeated for all the experiments.

6.1.3 Data reduction

For NCL, the steady - state condition was attained, when the buoyancy and frictional forces were balanced. The steady state mass flow rate ($\dot{m}$) and Reynolds number of working fluid can be calculated using following relation:

$$\text{Power input} = \mathrm{Q_{heater}} = \dot{m}_{lf} \cdot \mathrm{C_{p,}}_{lf} \cdot (\mathrm{T_2} - \mathrm{T_1}) \quad (6.1)$$

The Reynold number is estimated by:

$$Re_{lf} = \frac{4\,\dot{m}_{lf}}{\pi\, d\, \mu_{lf}} \quad (6.2)$$

The average heat transfer coefficient and average Nusselt numbers are calculated by:

$$h_{lf} = \frac{\mathrm{Q_{heater}}}{A_s\,(\bar{T}_{wall,in} - \mathrm{T_{b,}}_{lf})} \quad (6.3)$$

$$\mathrm{Nu} = \frac{h_{lf}\, D}{k_{lf}} \quad (6.4)$$

Where $\bar{T}_{wall,in}$ is the inside average wall surface temperature which can be estimated by using heat conduction equation which is given as follows [203].

$$\bar{T}_{wall,in} = \bar{T}_{wall,out} - \left(\frac{2r_{in}q'' + r_{in}^2\varphi}{2k}\right) \ln\left(\frac{r_{out}}{r_{in}}\right) - \frac{\varphi}{4k}\left(r_{in}^2 - r_{out}^2\right) \quad (6.5)$$

Where, $\bar{T}_{wall,out}$ is the outside average wall surface temperature which can be estimated by using following relation:

$$\bar{T}_{wall,out} = \frac{\mathrm{T_{7,out}} + \mathrm{T_{8,out}} + \mathrm{T_{9,out}} + \mathrm{T_{10,out}}}{4} \quad (6.6)$$

Where, $\mathrm{T_{7,out}}$, $\mathrm{T_{8,out}}$, $\mathrm{T_{9,out}}$, and $\mathrm{T_{10,out}}$ are the temperatures at outer surface of the heater wall.

$\mathrm{T_{b,}}_{lf}$ is the bulk fluid temperature and is estimated by:

$$T_{b,lf} = \frac{T_1 + T_2}{2} \quad (6.6)$$

The Rayleigh number can be estimated by:

$$Ra_{lf} = \frac{\left(g\,\beta_{lf}\,q''\,d^4\,\rho_{lf}^2\,C_{p,lf}\right)}{\left(\mu_{lf} \times k_{lf}^2\right)} \quad (6.7)$$

6.1.4 Results and discussion

In the present study, the effect of the type of working fluid, particle concentration, power input and inlet temperature of cold fluid on thermal performance of the NCL were experimentally investigated. Different nanofluids such as CuO-water, SiO_2-water, and Al_2O_3-water were used at different particle concentrations (0.5%, 1.0% and 1.5%) and results were compared with water. The power input at heater was varied from 500 W to 2500 W with an increment of 500 W. The inlet temperature of cold fluid was varied from 5 °C to 20 °C with a step size of 5 °C.

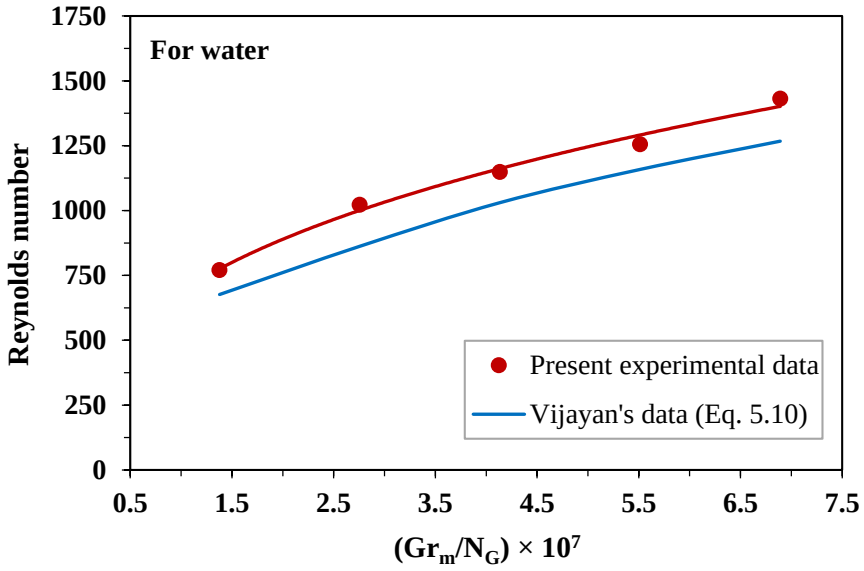

Fig. 6.3. Comparison of experimental results with published data

Comparison of experimental results with analytical results:

Figure 6.3 illustrates that the comparison of experimental outcomes with the analytical results of Vijayan's correlation (eq. 5.10) [75]. The experimental outcomes of the current study were compared with the analytical approach of Vijayan's correlation and it was noticed that the analytical approach did not come close to Reynolds number; the deviation however was within manageable limits - lower than 15 %.

Transient response of the NCL for different working fluids:

Figure 6.4 shows the temperature gradient across the heater at 2000 W power input, and 20 °C cooling water inlet temperature with water and different nanofluids at 1% particle concentration. It is observed from fig. 6.4 that the transient response of NCL with water and nanofluids was similar. As seen in fig.6.4 the steady state reaching time for water, SiO_2-water, Al_2O_3-water, and CuO-water nanofluids was 25.33, 22.17, 20.41 and 18.40 minutes respectively. In particular, NCL operated with CuO-water nanofluid reached a steady state condition quickly when compared with other working fluids, due to its higher thermal conductivity than other fluids. From fig. 6.4 it is concluded that the steady state reaching time can be reduced by 12% to 27% with different nanofluids compared to water.

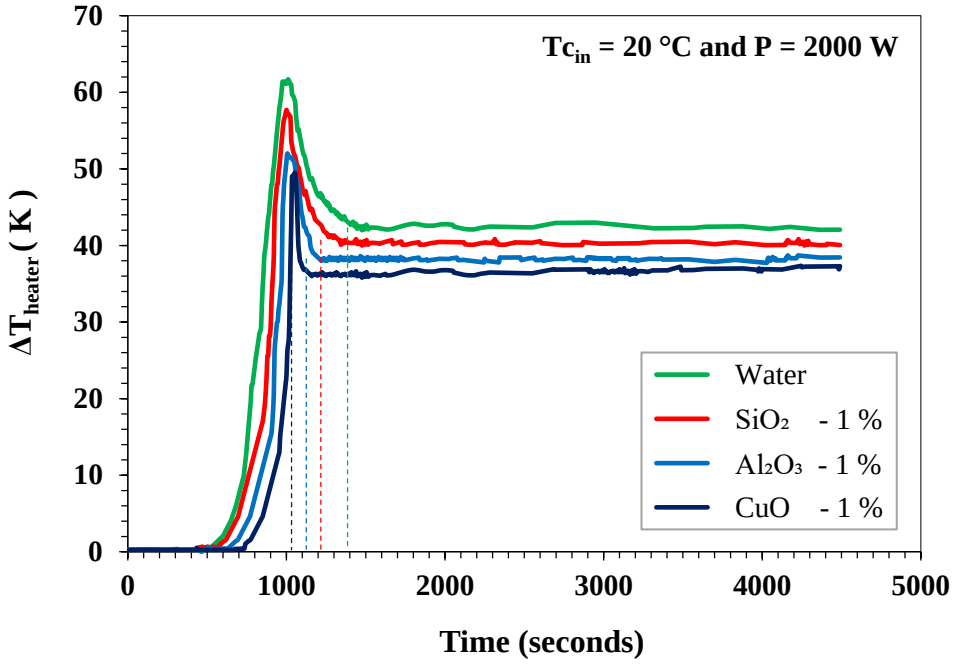

Fig. 6.4. Transient response of NCL with different working fluids

Effect of power input and particle concentration on mass flow rate:

The variation of steady state mass flow rate of loop fluid in NCL at different power inputs and for different working fluids is described in fig. 6.5. It is well known that the mass flow rate of the loop fluid increases with power input. By increasing the power input, the density gradient developed across the heater and cold heat exchanger sections was high, which causes buoyancy forces, that subsequently increases the mass flow rate. For a given power input, the mass flow rate of any nanofluid is higher than that of water. By suspending the nanoparticles in the base fluid at 1 % concentration, the net specific heat of SiO_2-water, Al_2O_3-water and

CuO-water nanofluids was reduced by 1.80%, 3.09% and 5.29%, respectively, when compared with water. This decrement in specific heat gives larger rise in temperature in the fluid for a given power input. The temperature rise gives a large increase in density gradient between the heater and cold heat exchanger sections which increases the steady state mass flow rate in the loop. In addition to this, the thermal expansion coefficient of the nanofluid is another important parameter for mass flow rate enhancement. By dispersing nano-sized particles in water, the thermal expansion coefficient was enhanced and this enhancement, improved the driving force [29]. At a given power input the CuO-water nanofluid has a higher mass flow rate than SiO_2-water and Al_2O_3-water nanofluids due to its lower specific heat and higher thermal expansion coefficient. It is observed from Fig. 6.5 that the mass flow rate of the loop fluid was enhanced by 4.05%, 7.51% and 10.95% for SiO_2-water, Al_2O_3-water, and CuO-water nanofluids, respectively, when compared with water at high power input.

Figure 6.6 shows the variation of steady state mass flow rate with particle concentration. The steady state mass flow rate was gradually increased with the particle concentration. The ameliorated thermophysical properties of nanofluids were responsible for improving the mass flow rate in NCL. It is observed from fig. 6.6 that the steady state mass flow rate increased by 4.02%, 4.17% and 3.92% for SiO_2-water, Al_2O_3-water, and CuO-water nanofluids, respectively, by varying particle concentration from 0.5% to 1.5% at 2000 W power input.

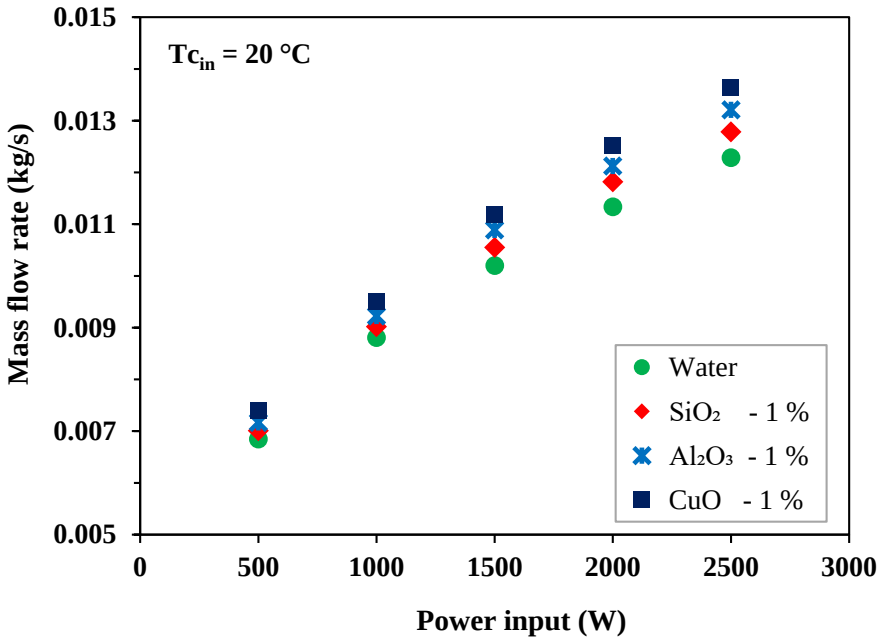

Fig. 6.5. Variation of mass flow rate with power input

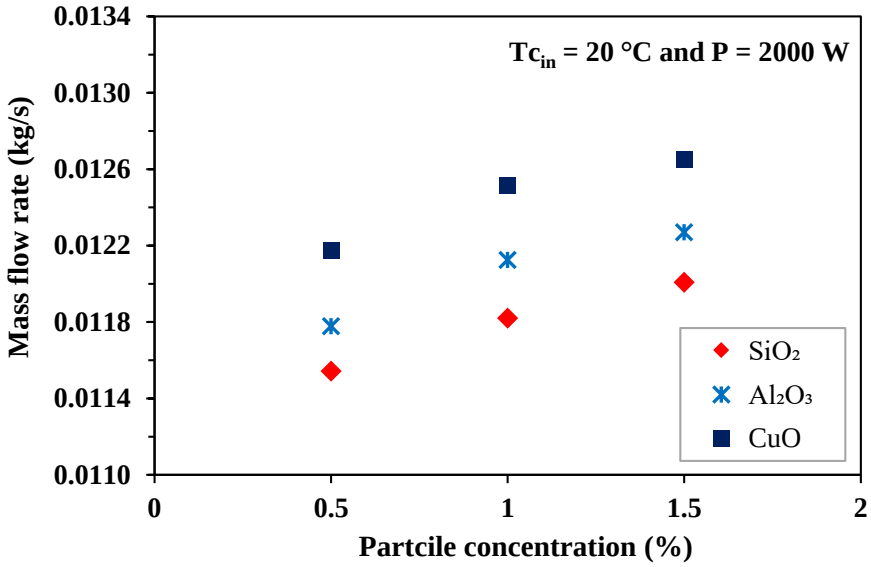

Fig. 6.6. Variation of mass flow rate with particle concentration

Effect of power input and particle concentration on temperature difference at heater:

The analysis was carried out to study the temperature difference of the loop fluid across the heater for different power inputs and particle concentrations. Figure 6.7 shows the temperature gradient at the heater for different power inputs, at 1% particle concentration of nanofluids and 20 °C cooling water inlet temperature. It is noticed from fig. 6.7 that the temperature gradient of the loop fluid increases with power input. The enhanced thermal and transport properties of nanofluids facilitate a reduction in temperature gradient at the heater by 5.55%, 9.81% and 14.46% for SiO_2-water, Al_2O_3-water and CuO-water nanofluids, respectively, when compared with water at the maximum power input.

Figure 6.8 shows the influence of particle concentration on the temperature gradient at the heater section for a given power input of 2000 W. Figure 6.8 demonstrates that temperature difference was decreasing with particle concentration for all nanofluids. One possible reason is, as the particle concentration increases, specific heat reduces, which leads to an increase in mass flow rate. The higher mass flow rate of loop fluid causes reduction in the temperature gradient at the heater section for a given power input. From fig. 6.8 it is observed that the temperature gradient is decreased by 7.94%, 7.74% and 6.26% for SiO_2-water, Al_2O_3-water, and CuO-water nanofluids, respectively, by varying particle concentration from 0.5% to 1.5% at 2000 W power input.

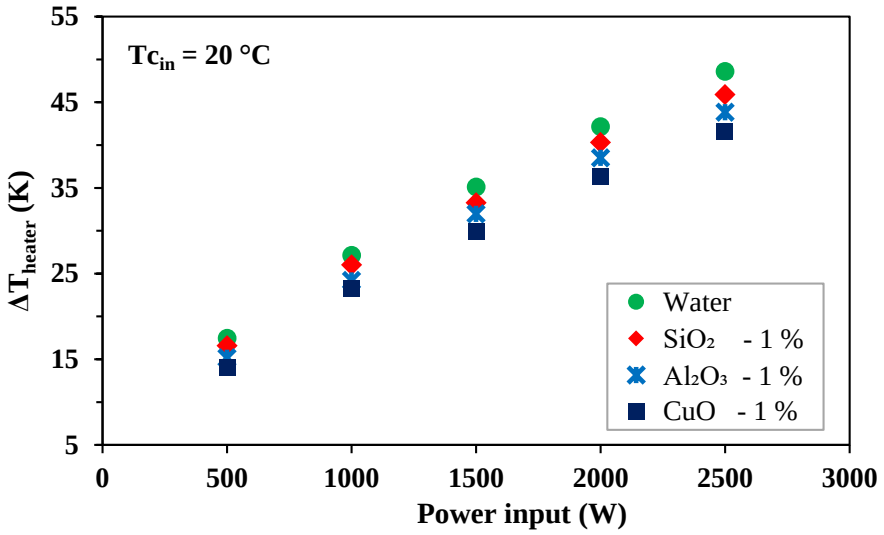

Fig. 6.7. Variation of temperature difference at heater with power input

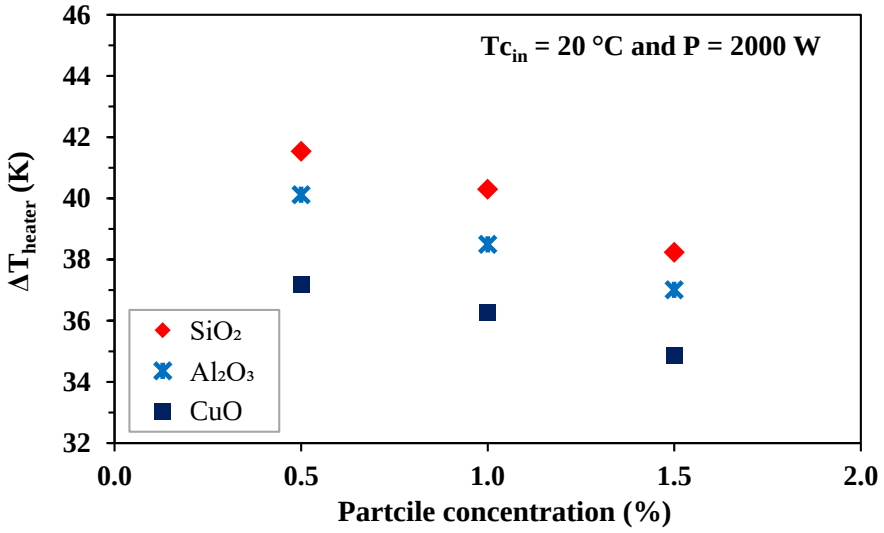

Fig. 6.8. Variation of temperature difference at heater with particle concentration

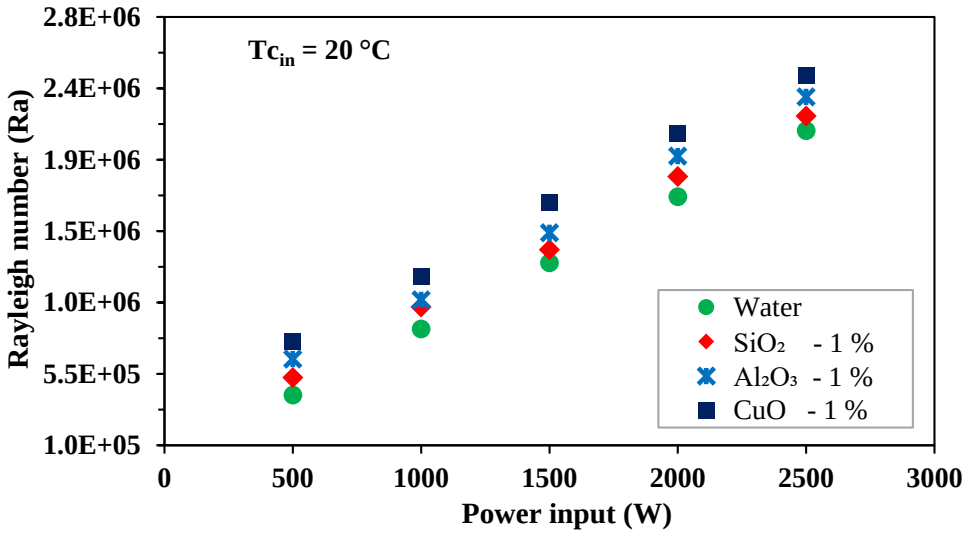

Fig. 6.9. Variation of Rayleigh number with power input

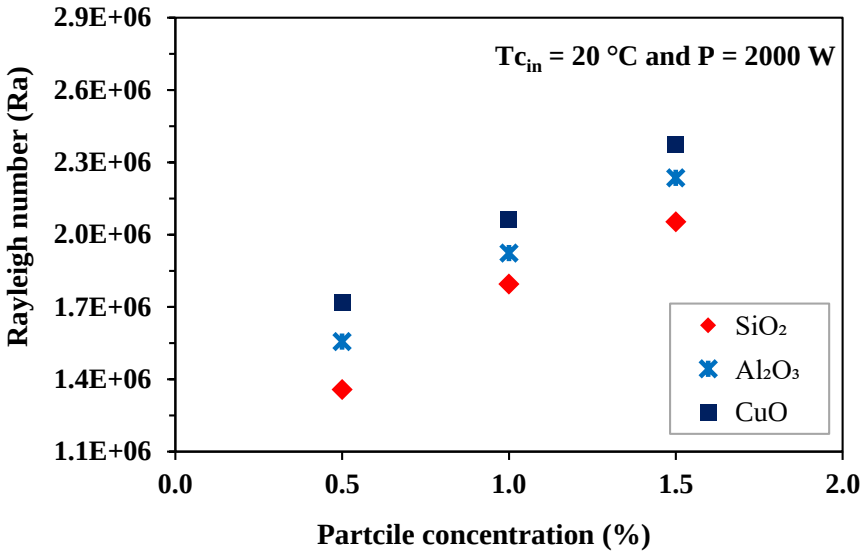

Fig. 6.10. Variation of Rayleigh number with particle concentration

Effect of power input and particle concentration on Rayleigh number:

Rayleigh number is an important dimensionless parameter which is helpful to study the buoyancy effect of natural circulation flows. The Rayleigh number of a working fluid can be estimated using eq. (6.7). It can be noticed from this equation that for a given geometry, the Rayleigh number depends purely on thermo-physical properties of the working fluid. Figure 6.9 demonstrates the variation of the Rayleigh number with power input for water and different nanofluids. As seen from fig. 6.9, the Rayleigh number of the working fluid is increasing with power input. The resultant high buoyancy force could be the reason for the higher Rayleigh number for nanofluids compared to water. It is observed from fig. 6.9 that the Rayleigh number is enhanced by 4.41%, 10.20% and 16.64% for SiO_2-water, Al_2O_3-water, and CuO-water nanofluids, respectively, when compared with water at highest power input.

The influence of particle concentration on Rayleigh number is presented in fig. 6.10. It is observed from fig. 6.10 that by increasing particle concentration from 0.5% to 1.5%, the Rayleigh number is increased by 51.29%, 43.63% and 38.20% for SiO_2-water, Al_2O_3-water, and CuO-water nanofluids, respectively, at 2000 W power input. At fixed concentration, CuO-water nanofluid has a higher Rayleigh number than SiO_2-water or Al_2O_3-water. The improved thermo-rheological properties of CuO-water nanofluid leads to a higher Rayleigh number.

Effect of power input and particle concentration on average Nusselt number:

Figure 6.11 shows the variation of average Nusselt number with power input and different working fluids at 20 °C cooling water inlet temperature. The average Nusselt number

of the working fluid at the heater section is estimated using eq. (6.4). As illustrated in fig. 6.11, for a given working fluid, the average Nusselt number increases with power input due to increased average heat transfer coefficient. At a given power input to the heater, the flow rate of the nanofluid is higher than that of water, which causes an increase in convection at the heater; this in turn result in an increase in the average Nusselt number. It is noticed from fig. 6.11 that the average Nusselt number is enhanced by 2.20%, 4.53% and 8.10% for SiO_2-water, Al_2O_3-water, and CuO-water nanofluids, respectively, when compared with water at high power input. At a fixed power input, the CuO-water nanofluid has a higher average Nusselt number than SiO_2-water, Al_2O_3-water nanofluids, as it has a higher average heat transfer coefficient.

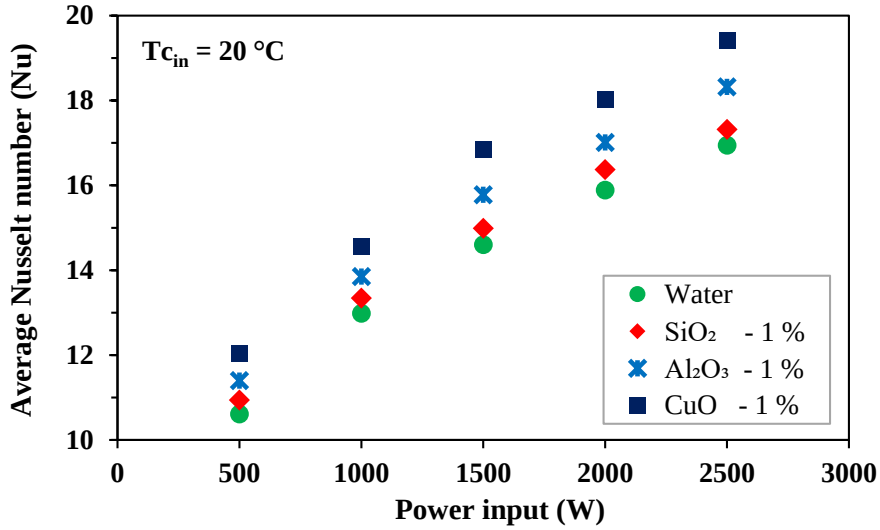

Fig. 6.11. Variation of average Nusselt number at heater with power input

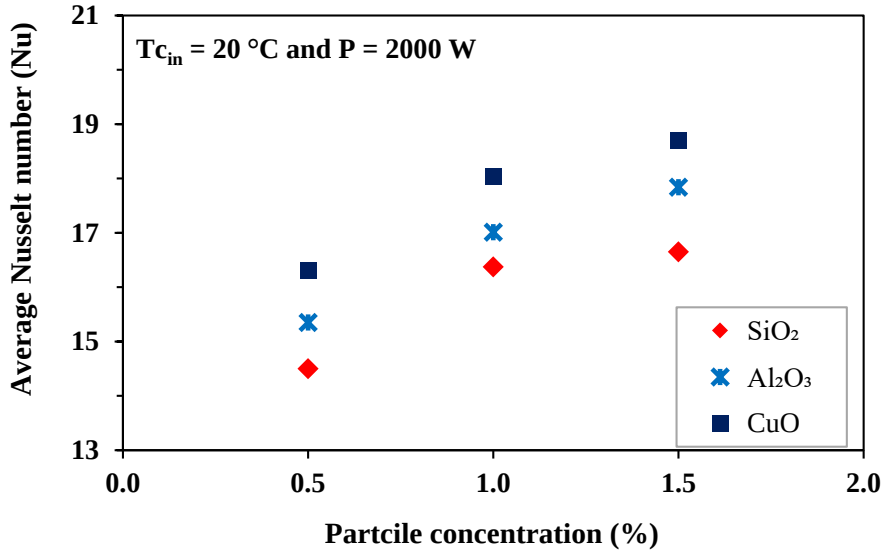

Fig. 6.12. Variation of average Nusselt number at the heater with particle concentration

The influence of particle concentration on average Nusselt number at the heater section is illustrated in fig. 6.12. The average Nusselt number is increasing with particle concentration. When the concentration of nanoparticles increased, the thermal conductivity of the nanofluid also increased. This enhancement of thermal conductivity of the nanofluid has a positive effect on the average heat transfer coefficient and consequently on the average Nusselt number. Another cause for the enhanced average Nusselt number is attributed to the enhanced average heat transfer coefficient at a higher mass flow rate. It is noticed from fig. 6.12 that the average Nusselt number is enhanced by 14.82%, 16.22% and 14.61% for SiO_2-water, Al_2O_3-water, and CuO-water nanofluids, respectively, by varying particle concentration from 0.5% to 1.5%.

Effect of power input and particle concentration on pressure drop in NCL:

Figure 6.13 shows the pressure drop as a function of the power input for pure water and different nanofluids. As expected, irrespective of working fluid, the pressure drop increases with power input. As can be seen from fig. 6.13 all the nanofluids show higher pressure drop than pure water due to the high viscosity and high density. At low power input, the pressure drop difference is small among all nanofluids when compared to water and it is increasing with power input. The pressure drop is increased by 6.90%, 12.44% and 19.08% for SiO_2-water, Al_2O_3-water, and CuO-water nanofluids, respectively, when compared with water at high power input. The CuO-water nanofluid has more pressure drop than other working fluids due to its higher viscosity and density.

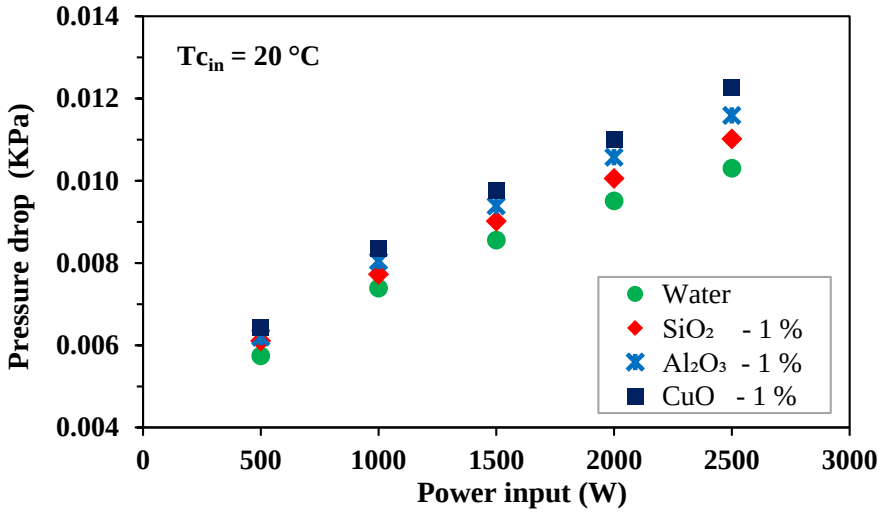

Fig. 6.13. Variation of pressure drop with power input

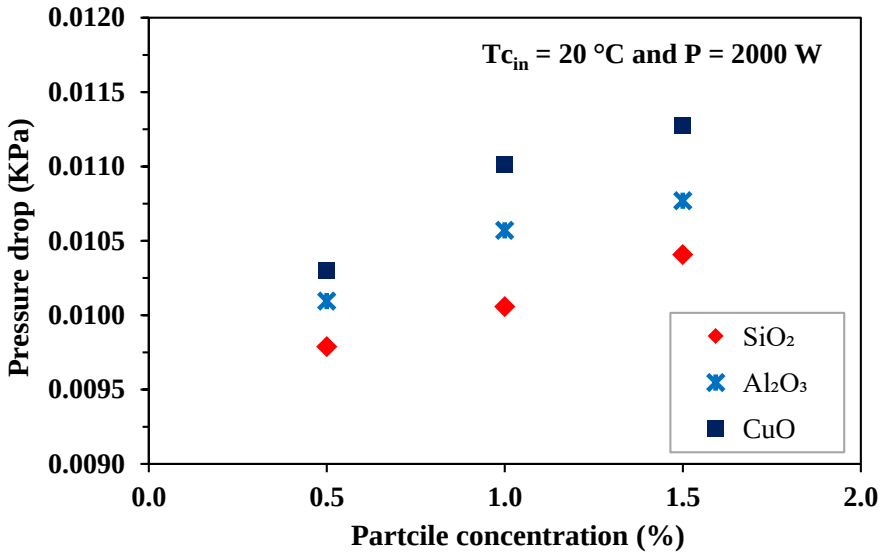

Fig. 6.14. Variation of pressure drop with particle concentration

Figure 6.14 shows the pressure drop with particle concentration at 2000 W power input. The pressure drop increases with particle concentration. It is observed from fig. 6.14 that by varying particle concentration from 0.5% to 1.5% the pressure drop is increased by 6.32%, 6.68% and 9.48% for SiO_2-water, Al_2O_3-water, and CuO-water nanofluids, respectively.

Effect of cooling water inlet temperature on mass flow rate and average Nusselt number:

The variation of mass flow rate with inlet temperature of cooling water is described in fig. 6.15. By reducing the inlet temperature of cold fluid at CHE, high temperature gradient across the heater and CHE is developed in the loop fluid. That leads to an increase in the buoyancy and mass flow rate.

Figure 6.16 shows the effect of cooling water inlet temperature on an average Nusselt number of different working fluids at 2000 W power input. It is seen that the inlet temperature of cold water has a much stronger effect on average Nusselt number. When the power input to the heater is kept constant, and when the inlet temperature of the cooling water is decreased, mass flow rate of the working fluid increases, which causes an increase in the convective heat transfer rate as well as average Nusselt number.

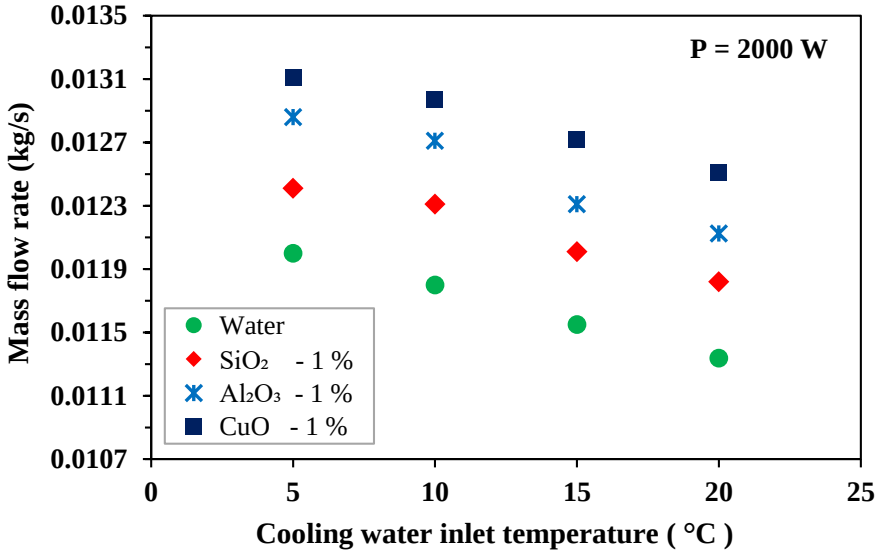

Fig. 6.15. Variation of mass flow rate with cooling water inlet temperature

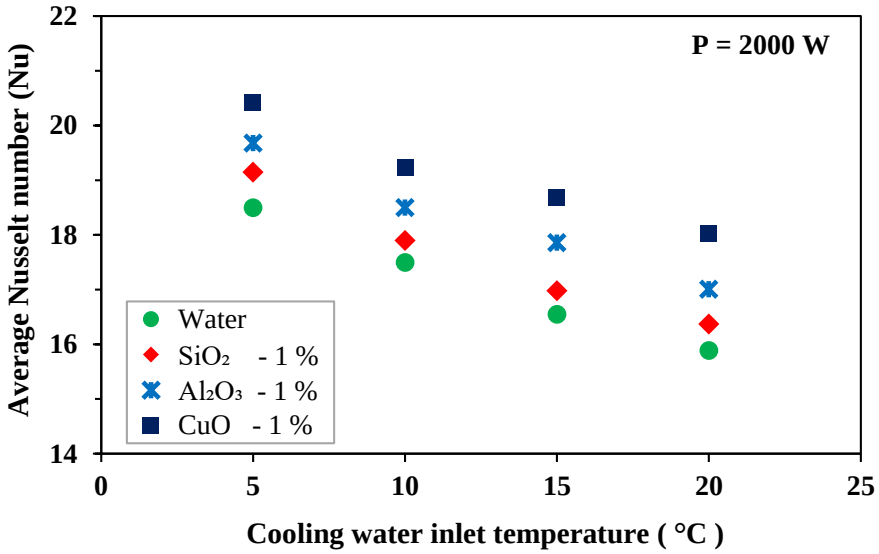

Fig. 6.16. Variation of average Nusselt number with inlet temperature of the cooling water

6.1.5 Transient analysis of nanofluid based NCL with heater as heat source

Figure 6.17 shows the variation of temperature difference of the loop fluid across the heater under increasing power input to the heater. After the loop fluid attains steady state and runs for one hour in this condition, the power input is increased step wise (500 W step) up to 2500 W. With the stepwise increase in power input, heat transfer also increases step wise. Initially, when power was 500 W, the system took 28.5 min, 26.67 min, 24. 17 min and 20.83 min, respectively, to reach steady state from the rest (25 °C) for pure water, SiO_2-water

nanofluid, Al_2O_3-water nanofluid and CuO-water nanofluids respectively. After the system was run for about 1 hour at this steady state condition, the power input increased to 1000 W. Now it took 26.2 min, 25.33 min, 22.83 min and 18.51 min to reach steady state for pure water, SiO_2-water nanofluid, Al_2O_3-water nanofluid and CuO-water nanofluids respectively. In the next step when the power input was increased to 1500 W and later 2000 W similar trend was observed. Finally, after increasing the power input to 2500 W, the system took 20.5 min, 18.32 min, 15.33 min and 13.45 min to reach steady state for pure water, SiO_2-water nanofluid, Al_2O_3-water nanofluid and CuO-water nanofluids respectively. Therefore, from fig. 6.17 it can be concluded that the steady state time is reduced by increasing the power input. In particular, CuO-water nanofluid quickly reaches the steady state condition than other nanofluids. The present experimental results with heater as a heat source and with no oscillations or pulsating flow is observed within the range of study for any type of nanofluid. In the next experimental work, power input was decreased step wise (500 W) from 2500 W to 500 W. The results are shown in fig. 6.18. It is observed that the system returns to the original condition when the power input change is reversed.

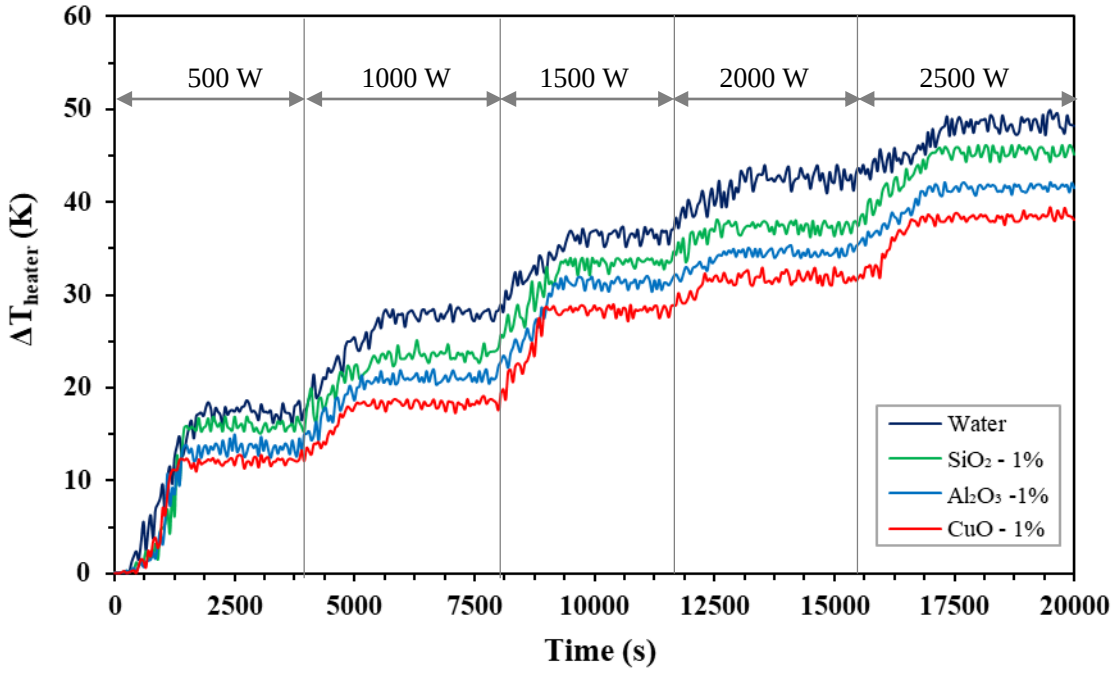

Fig. 6.17. Temperature difference of the loop fluid across heater under increasing the power input

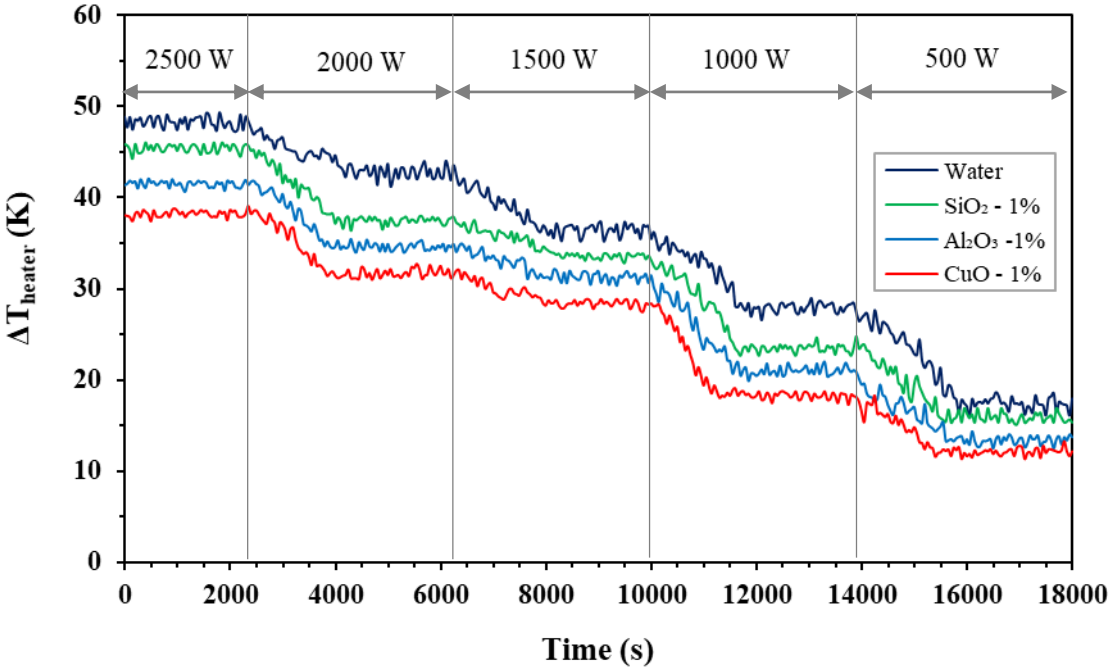

Fig. 6.18. Temperature difference of the loop fluid across heater under decreasing the power input

6.2 Experimental studies on nanofluid based NCL with end heat exchangers

6.2.1 Experimental facility

A detailed schematic diagram of the experimental facility used for this study is shown in fig. 6.19. The photographic view of the experimental test rig is presented in fig. 6.20. The system consists of a tube-in-tube hot heat exchanger at the bottom and tube-in-tube cold heat exchanger at the top. These two were connected by two parallel vertical legs called riser and downcomer. The present 1-D numerical results show that frictional resistance was almost negligible beyond 15mm tube diameter, a smooth stainless steel tube of 12.7mm inner diameter with 1.6mm wall thickness was selected for the inner tube. To prevent heat leak from or to ambient surroundings, the entire loop was insulated with 4 mm thick asbestos rope. On the water side (outer tube), 1mm thick copper tube of 22 mm outer diameter was chosen. The total tube length of each heat exchanger was 5 m with 5 parallel segments of 1m each, as shown in fig. 6.20. The geometrical specifications and operating parameters are given in table 6.20. The temperatures of the loop fluid (T_1 to T_4), external hot water (T_5 and T_6) and external cold water (T_7 to T_8) were measured using RTDs, as shown in fig. 6.19. These RTDs were connected to a computer integrated data acquisition system (Agilent-34972A) to log the temperature data at

regular intervals. Pressure drop between different sections in the NCL was measured using U-tube manometers. Both hot heat exchanger and cold heat exchangers were operated at constant pressure condition. Therefore, the manometer tubes were connected at the entrance and exit of the riser and downcomer sections, respectively, as shown in fig. 6.19. To measure hot water and cold water mass flow rates rotameters were connected between cold heat exchanger inlet and chiller outlet and hot heat exchanger inlet and thermostatic bath outlet, respectively. A classic scientific made thermostatic bath was used to control the hot water temperature sent to HHE. To control temperature of the cold water, Aditya scientific made chiller was used.

6.2.2 Experimental procedure

The experimental study on a single phase rectangular natural circulation loop was initially conducted with distilled water, and then after conducted with three different nanofluids (SiO_2-water, Al_2O_3-water and CuO-water) at 0.5%, 1.0% and 1.5% concentrations. During the experiment, the combined effect of power input, particle concentration and cooling water inlet temperatures were analysed. The experiment was carried out with the following procedure:

- The NCL was filled with the working fluid.
- Air bubbles were drained out by giving continuous pulses while filling the loop.
- Sufficient time was given to the loop fluid to obtain thermal equilibrium with room temperature without heating.
- The secondary cooling water and hot water flow rates were set at the required value.
- The DAQ system was switched on and the initial readings were taken.
- 10 min after the DAQ system began, the chiller and thermostatic bath were started simultaneously.
- At steady-state condition, which can observe from the trend of the temperature variation in the graphical display mode on the DAQ system, all the temperature data are collected.
- The same procedure is repeated for all the experiments.
- Repeatability of the test results is also checked.

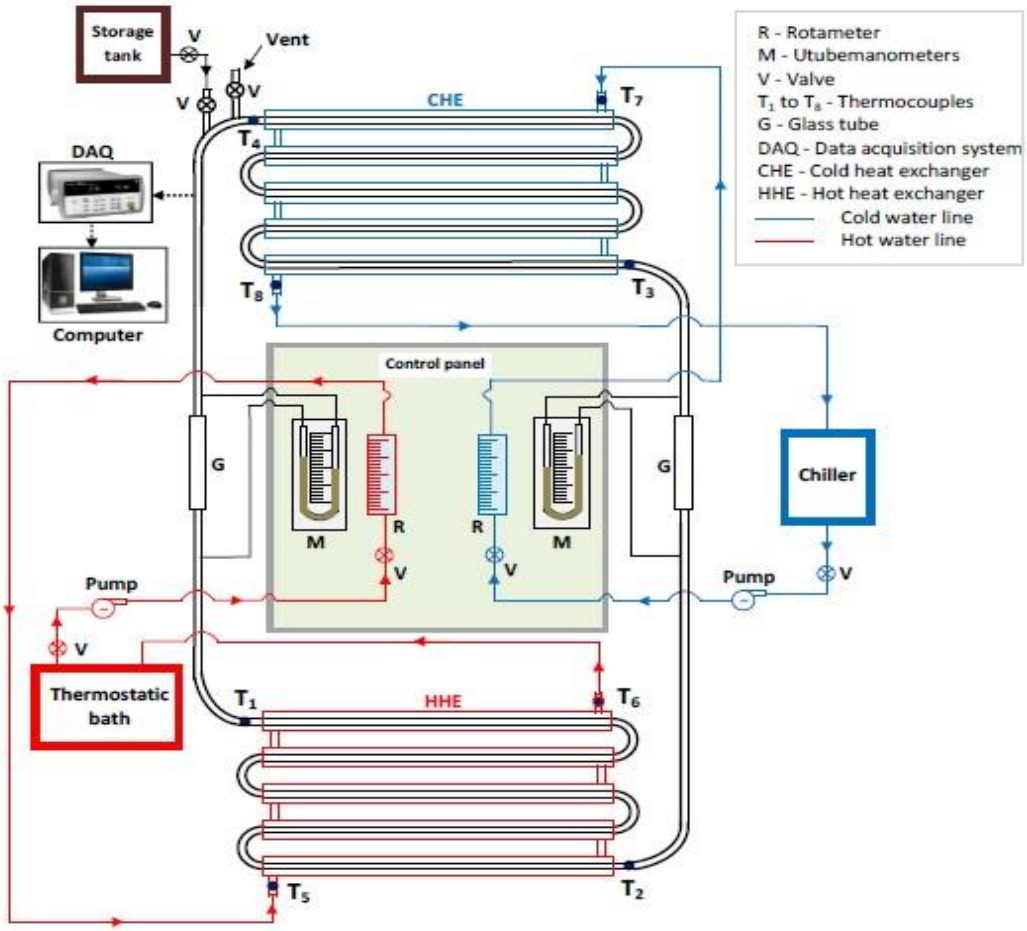

Fig.6.19. Schematic diagram of the experimental setup

Fig.6.20. Photographic view of the experimental test rig

Table 6.2. Geometrical specifications and operating parameters of NCL with end heat exchangers

Parameter	Value
Loop pipe diameter	0.012 m
Inner diameter of the annulus at CHE	0.0215 m
Loop width	1.22 m
Loop height	2.5 m
Total length of the loop	15.5 m
Length of heater	1 m
Length of CHE and HHE	5 m each
Hot water inlet temperature	30 °C to 70 °C
Cold water inlet temperature	05 °C to 20 °C
Pipe wall thickness	0.0016 m
Hot and cold fluid mass flow rate	0.05 kg/s
Particle volume concentration (ϕ)	0.5 % , 1.0 % and 1.5 %
External fluid to CHE and HHE	Water

6.2.3 Data reduction

For NCL, the steady-state condition was attained, when the buoyancy and frictional forces were balanced. The heat transfer rate (Q_{HHE}) can be calculated using the following relations:

$$Q_{HHE} = m_{w,HHE} \cdot C_{p,w,HHE} \cdot \left(T_{h,i} - T_{h,o}\right) \quad (6.8)$$

$$Q_{HHE} = (UA)_{HHE} \cdot MTD_{HHE} \quad (6.9)$$

MTD_{HHE} is mean temperature difference at HHE and calculated as:

$$MTD_{HHE} = \frac{\left(T_{h,i} - T_{lf,o}\right) - \left(T_{h,i} - T_{lf,in}\right)}{\ln\left(\frac{T_{h,i} - T_{lf,o}}{T_{h,o} - T_{lf,in}}\right)} \quad (6.10)$$

Overall thermal conductance of the loop was calculated in terms of entropic average temperatures of the external fluid by using the following equation:

$$(UA)_{loop} = \frac{Q}{\left(T_{h,avg} - T_{c,avg}\right)} \quad (6.11)$$

$T_{h,avg}$ and $T_{c,avg}$ are entropic average temperatures (defines as ratio of heat transfer rate to entropy change) of the external hot and cold fluids and these can be calculated as follows:

$$T_{h,avg} = \frac{(T_{h,i} - T_{h,o})}{\ln\left(\frac{T_{h,i}}{T_{h,o}}\right)} \quad (6.12)$$

$$T_{c,avg} = \frac{(T_{c,o} - T_{c,i})}{\ln\left(\frac{T_{c,o}}{T_{c,i}}\right)} \quad (6.13)$$

From the energy balance relation, the steady state mass flow rate of loop fluid was calculated using eq. (6.14).

$$Q_{HHE} = m_{w,HHE} \cdot C_{p,w,HHE} \cdot (T_{h,i} - T_{h,o}) = m_{lf} \cdot C_{p,lf} \cdot (T_2 - T_1) \quad (6.14)$$

6.2.4 Results and discussion

In the present study, the effects of type of particle concentration, hot fluid inlet temperature and cold fluid inlet temperatures on thermal performance of the NCL were experimentally investigated. Different nanofluids such as CuO-water, SiO_2-water, and Al_2O_3-water were used at different particle concentrations (0.5%, 1.0% and 1.5%) and the results were compared with that of water. The power input at heater was varied from 500 W to 2500 W with increment of 500 W. The inlet temperature of cold fluid was varied from 5 °C to 20 °C with a step size of 5 °C.

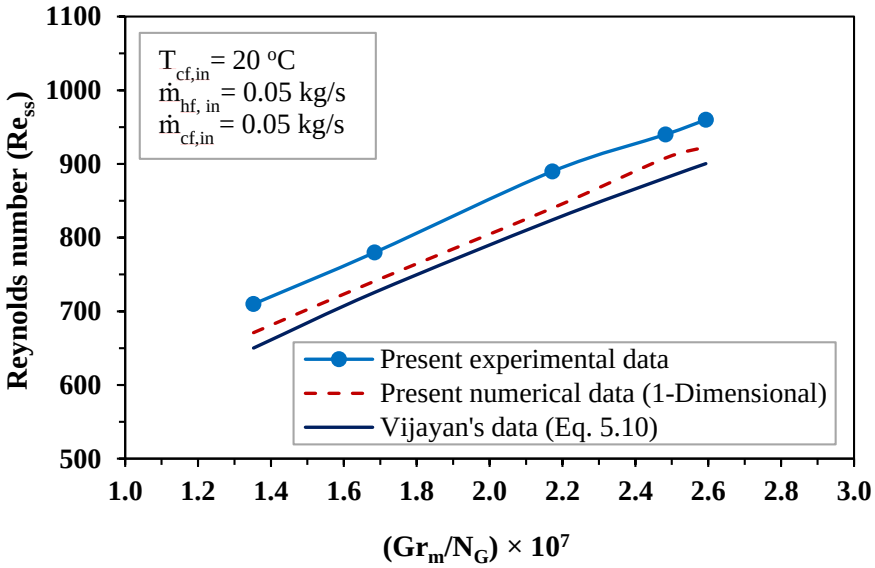

Fig. 6.21. Comparison of experimental results with numerical and published data

Comparison of experimental results with analytical and numerical results:

The experimental outcomes were compared with the analytical results of Vijayan's correlation [75] which is given in eq. (5.10). Figure 6.21 illustrates that the experimental outcomes follow the same trend with the results of Vijayan's correlation. The experimental outcomes of the current study were compared with the analytical approach of Vijayan's correlation and it was noticed that the analytical approach was not coming close to Reynolds number, though this was lower than 13%, which is acceptable.

Temperature of the loop fluid at various locations:

The variance of the loop fluid temperature with time at different locations of the loop is presented in fig. 6.22. Even though the system was insulated, a temperature difference of 2 °C was observed between the inlet and outlet of the riser. This temperature difference may be attributed to the pressure drop of nanofluid as well as heat loss to ambient surroundings. A similar temperature difference was observed between the downcomer inlet and outlet. From fig. 6.22 it was observed that the time taken to reach the steady state was around 40 min.

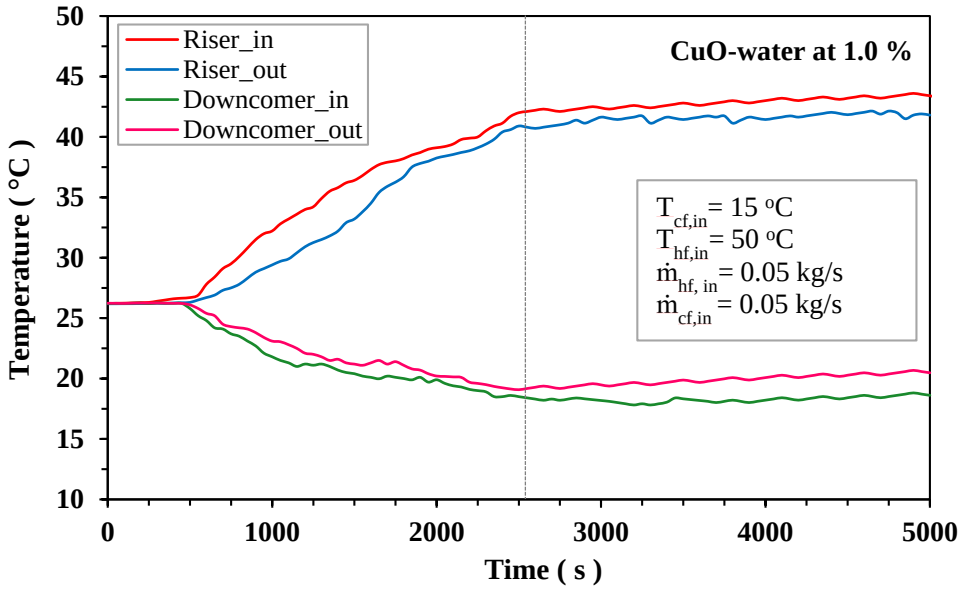

Fig. 6.22. Variation of loop fluid temperature at various locations of the loop

Repeatability tests:

Figure 6.23 shows steady state mass flow rate with hot water inlet temperature. With an increase in hot water inlet temperature the loop fluid mass flow rate also increases as discussed in the theoretical background to the experiment. The cold fluid temperature was maintained at

a constant temperature of 20 °C. External fluid flow rates were the same and equal to 0.05 kg/s in both heat exchangers. Repeatability tests were conducted for this range of parametric variation. All data points are found to lie within the uncertainty range (± 6%). A reasonably good agreement is found between the experimental results and the numerical values.

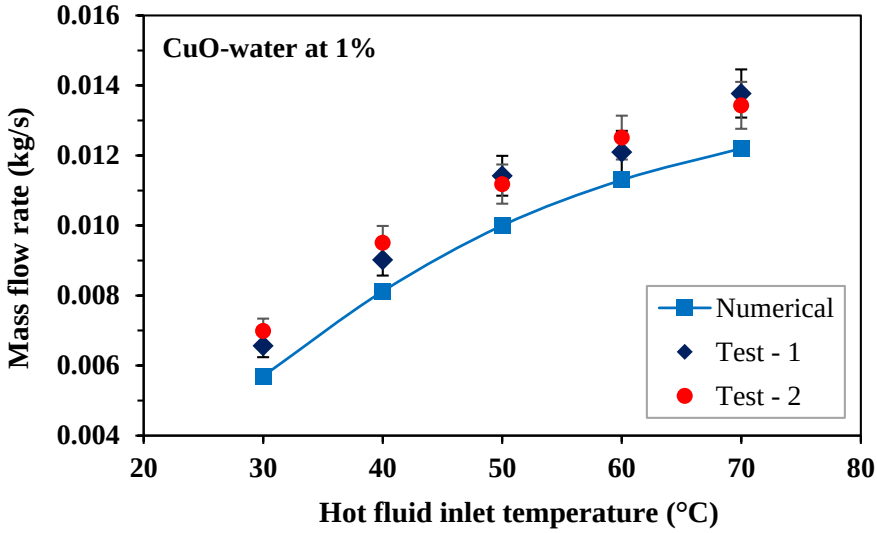

Fig. 6.23. Repeatability tests of mass flow rate with CuO-water as loop fluid

Effect of hot fluid inlet temperature and particle concentration on mass flow rate:

The variation of steady state mass flow rate of the loop fluid in NCL with hot water inlet temperature for different working fluids is described in fig. 6.24. It is well known that the mass flow rate of the loop fluid increases with hot water inlet temperature. By increasing the inlet temperature of the hot water, the density gradient developed across HHE and CHE sections is high, which creates buoyancy forces, that subsequently increases the mass flow rate. For a given hot water inlet temperature, the mass flow rate of any nanofluid is higher than that of water. By suspending the nanoparticles in the base fluid the net specific heat of the nanofluids reduces. This decrement in specific heat gives a large temperature rise in the loop fluid for a given hot water inlet temperature. The temperature rise leads to a large increase in the density gradient between HHE and CHE sections which causes an increase in the steady state mass flow rate in the loop. At a given hot water inlet temperature, the CuO-water nanofluid has a higher mass flow rate than SiO_2-water and Al_2O_3-water nanofluids due to its lower specific heat and higher thermal expansion coefficient. It is observed from fig. 6.5 that the mass flow rate of loop fluid is enhanced by 9.11%, 16.75% and 22.43% for SiO_2-water, Al_2O_3-water, and CuO-water nanofluids, respectively, when compared with pure water at 70 °C of the hot water inlet temperature.

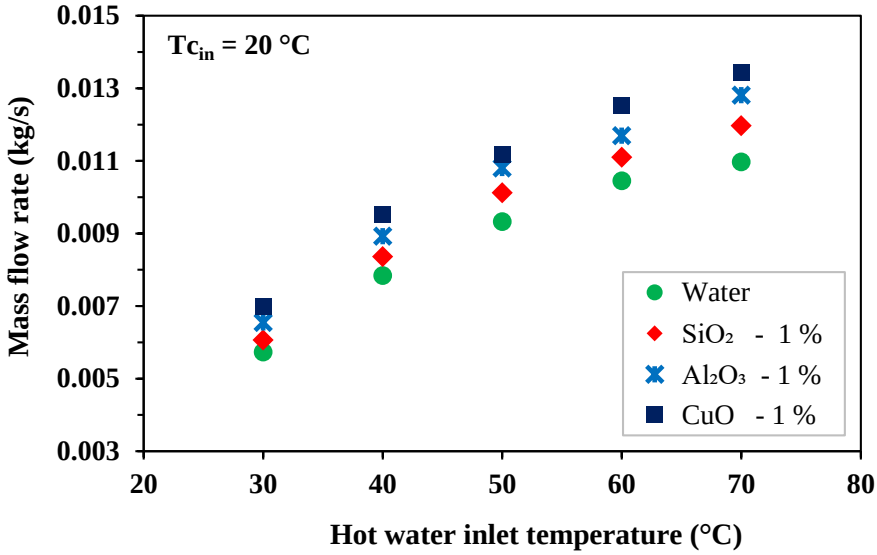

Fig. 6.24. Variation of mass flow rate with hot water inlet temperature

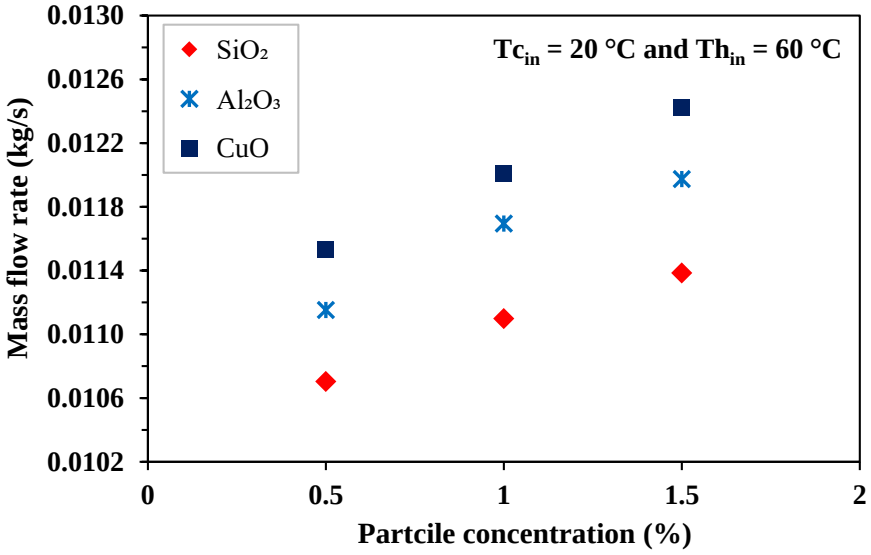

Fig. 6.25. Variation of mass flow rate with particle concentration

Figure 6.25 shows the variation of steady state mass flow rate with particle concentration. The steady state mass flow rate is gradually increasing with particle concentration. The ameliorated thermophysical properties of nanofluids are responsible for improving the mass flow rate in NCL. It is observed from fig. 6.25 that the steady state mass flow rate is increased by 6.36%, 7.37% and 7.73% for SiO_2-water, Al_2O_3-water, and CuO-water nanofluids, respectively, by varying particle concentration from 0.5% to 1.5% at 70 °C of the hot water inlet temperature.

Effect of hot fluid inlet temperature and particle concentration on heat transfer rate:

The analysis was carried out to study the heat transfer rate of the loop fluid for different hot water inlet temperatures and particle concentrations. Figure 6.26 shows the variation of heat transfer rate with hot water inlet temperature, at 1% particle concentration and 20 °C cooling water inlet temperature. As expected, it is observed that with an increase in hot fluid inlet temperature, heat transfer rate increases due to an increase in the temperature gradient between the loop fluid and external fluid (water) in HHE. It is noticed from fig. 6.26 that the heat transfer rate is increased by 14.7%, 26.95% and 36.58% for SiO_2-water, Al_2O_3-water and CuO-water nanofluids, respectively, when compared with water at the maximum hot water inlet temperature.

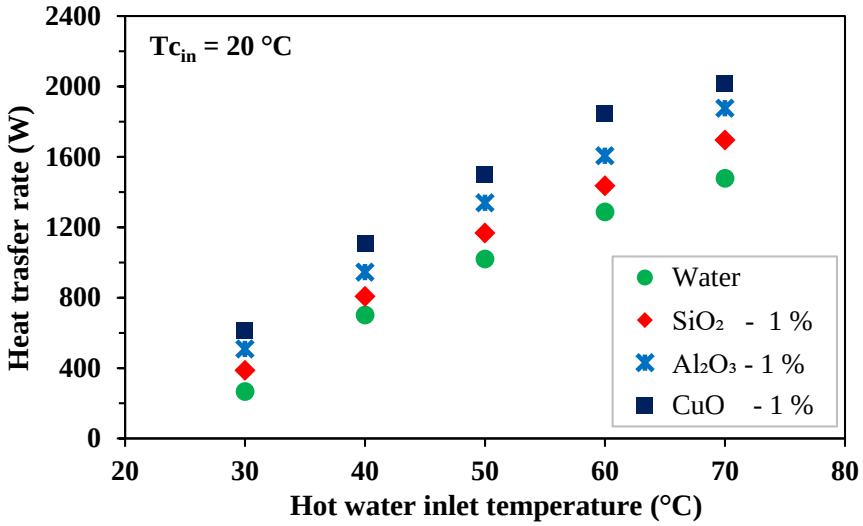

Fig. 6.26. Variation of heat transfer rate with hot water inlet temperature

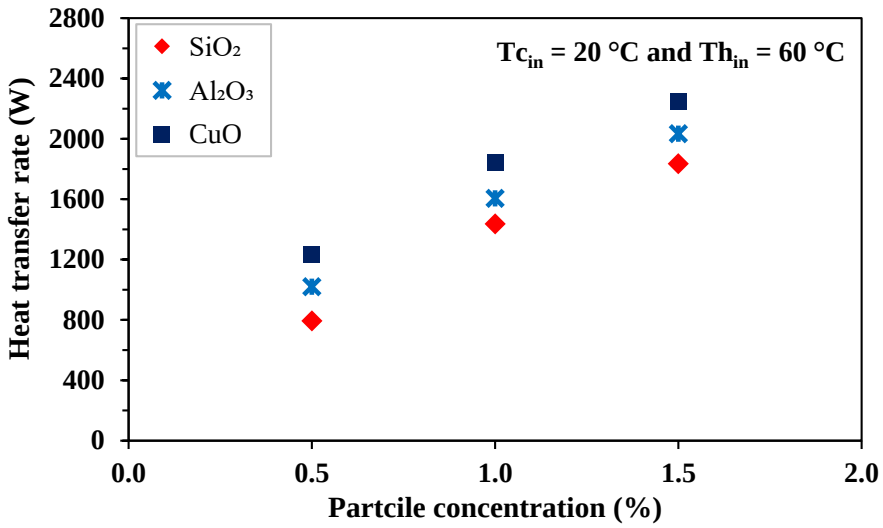

Fig. 6.27. Variation of heat transfer rate with particle concentration

Figure 6.27 shows the influence of particle concentration on the heat transfer rate for a given hot water inlet temperature of 60 °C. Figure 6.27 points that the heat transfer rate increases with particle concentration for all nanofluids. The possible reason is, as discussed in the previous section, the mass flow rate increases with particle concentration which leads to increase heat transfer rate.

Effect of hot fluid inlet temperature and particle concentration on thermal conductance:

Figure 6.28 shows the variation of thermal conductance (UA) with hot water inlet temperature for water and different nanofluids. As seen from fig. 6.28, the thermal conductance of the working fluid is increasing with hot water inlet temperature. As seen in the previous section, the heat transfer rate increases with hot water inlet temperature, which causes an increase in thermal conductance. It is observed from fig. 6.28 that thermal conductance enhanced by 13.55%, 40.67% and 67.79% for SiO_2-water, Al_2O_3-water, and CuO-water nanofluids, respectively, when compared with water at 70 °C of the hot water inlet temperature.

The influence of particle concentration on thermal conductance is presented in fig. 6.29. It is observed from fig. 6.29 that by increasing particle concentration from 0.5% to 1.5%, thermal conductance increased by 64.92%, 55.62% and 50.60% for SiO_2-water, Al_2O_3-water, and CuO-water nanofluids, respectively, at 60 °C of the hot water inlet temperature. At fixed concentration, CuO-water nanofluid has a higher thermal conductance than SiO_2-water, Al_2O_3-water due to higher thermal conductivity.

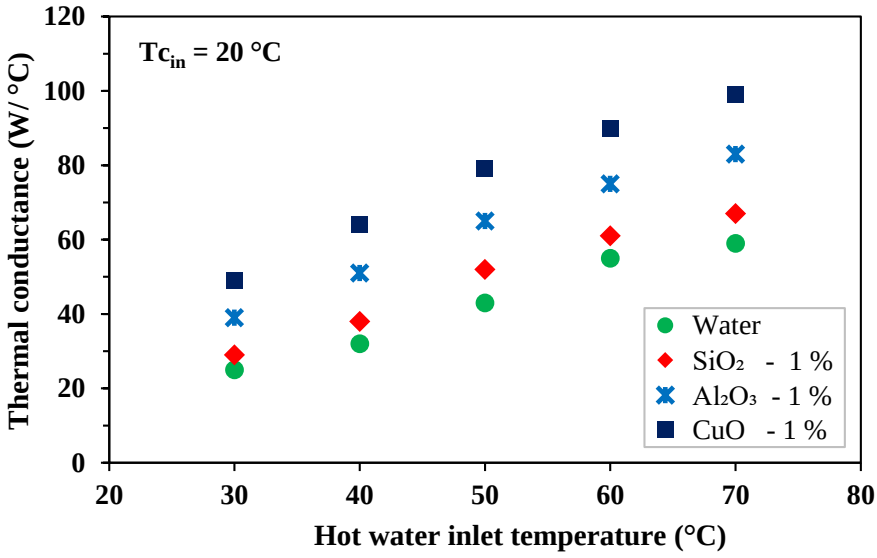

Fig. 6.28. Variation of thermal conductance with hot water inlet temperature

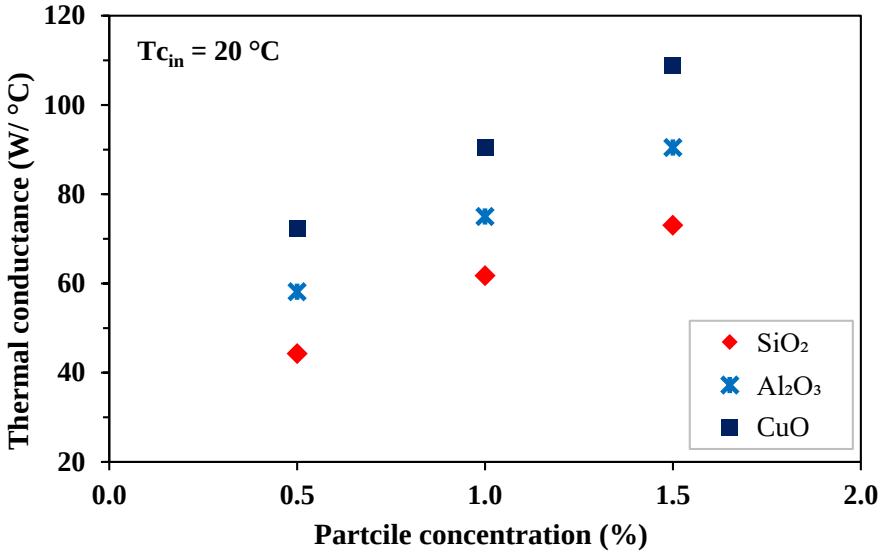

Fig. 6.29. Variation of thermal conductance with particle concentration

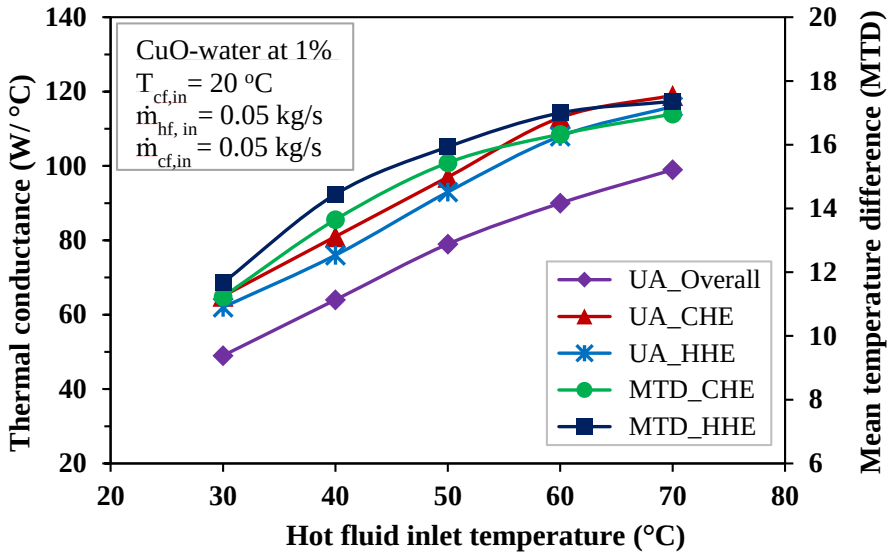

Fig. 6.30. Variation of thermal conductance and MTD of Cuo-water nanofluid

The variation of thermal conductance (UA) of HHE, CHE and total loop is shown in fig. 6.30. Mean temperature difference of external fluid and loop fluid (CuO-water nanofluid) in CHE and HHE are also shown in the secondary axis. It can be observed that thermal conductance increases with hot fluid inlet temperature. Thermal conductance of HHE and CHE is found to be almost the same. This may be attributed to an equal flow rate through both heat exchangers.

Effect of cooling water inlet temperature on mass flow rate and heat transfer rate:

The variation of mass flow rate with inlet temperature of cooling water is described in fig. 6.31. By reducing the inlet temperature of cold fluid at CHE, high temperature gradient across the heater and CHE is developed in the loop fluid. That leads to an increase in the buoyancy and mass flow rate. Figure 6.32 shows the effect of cooling water inlet temperature on the heat transfer rate for different working fluids at 60 °C hot water inlet temperature. It is seen that the inlet temperature of cold water has a much stronger effect on the heat transfer rate. With the hot water inlet temperature is kept constant, and by decreasing the inlet temperature of the cooling water, mass flow rate of the working fluid increases, which causes an increase in the convective heat transfer rate.

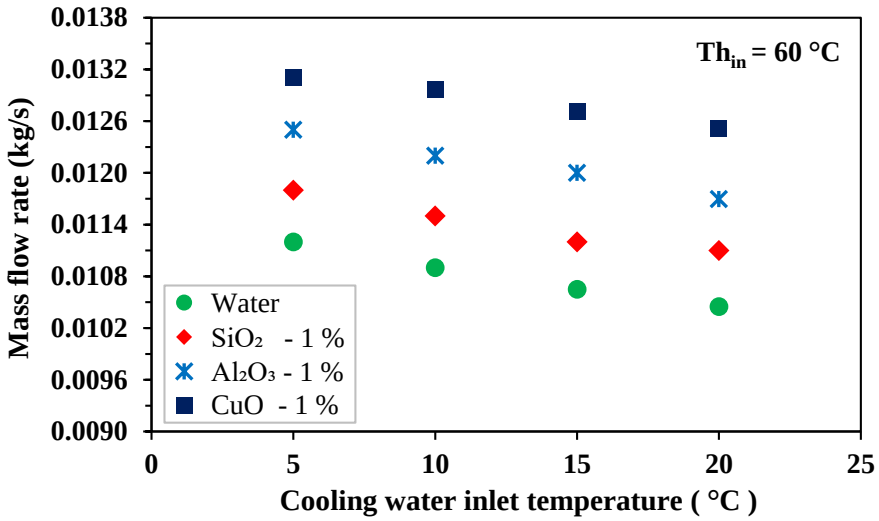

Fig. 6.31. Variation of mass flow rate with cooling water inlet temperature

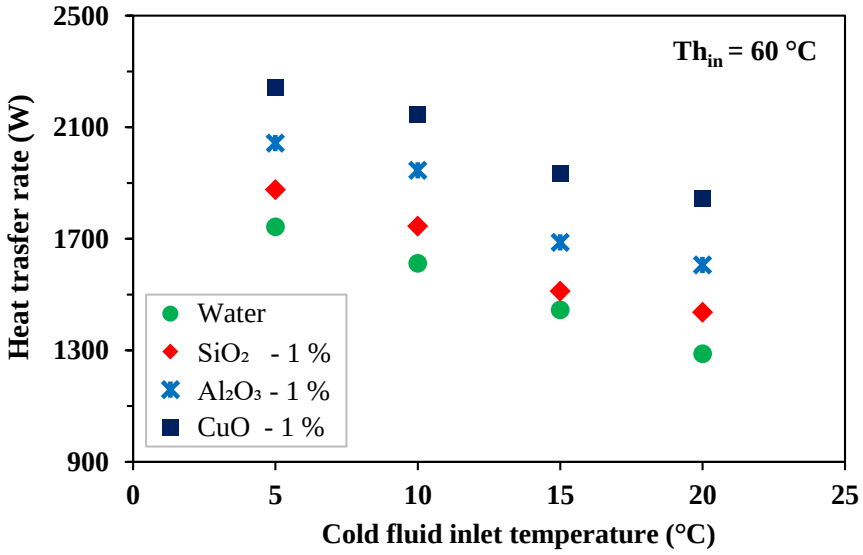

Fig. 6.32. Variation of heat transfer rate with inlet temperature of the cooling water

6.3 Uncertainty analysis

To find the errors associated with the experiment uncertainty analysis was carried out by Kline and McClintock [204]. The maximum uncertainties of mass flow rate, average heat transfer coefficient and average Nusselt number were estimated and presented in table 6.3.

Table 6.3. Uncertainties of various variables.

S.No.	Variable	Uncertainty
1.	Steady state mass flow rate	0.3934 %
2	Average heat transfer coefficient	0.3631 %
3.	Average Nusselt number	0.4718 %

(1) Power input, Q_{heater}

$$Q_{heater} = V \times I \ , \qquad \frac{U_{Q_{heater}}}{Q_{heater}} = \sqrt{\left(\frac{U_V}{V}\right)^2 + \left(\frac{U_I}{I}\right)^2}$$

$$= \sqrt{(0.28)^2 + (0.15)^2}$$

$$= 0.3176\ \%$$

(2) Steady state mass flow rate, $\dot{m}$

$$\dot{m}_{ss} = \frac{Q_{heater}}{C_p \times (T_2 - T_1)} \ , \quad \frac{U_{\dot{m}_{ss}}}{\dot{m}_{ss}} = \sqrt{\left(\frac{U_{Q_{heater}}}{Q_{heater}}\right)^2 + \left(\frac{U_{(T_2-T_1)}}{T_2-T_1}\right)^2}$$

$$= \sqrt{(0.3176)^2 + (-0.232)^2}$$

$$= 0.3934\ \%$$

(3) Average heat transfer coefficient, h_{avg}

$$h_{avg} = \frac{\mathrm{Q_{heater}}}{A_s\,(\bar{T}_{wall} - \mathrm{T_b})} \ , \quad \frac{U_{h_{avg}}}{h_{avg}} = \sqrt{\left(\frac{U_Q}{Q}\right)^2 + \left(\frac{U_{(\bar{T}_{wall}-\mathrm{T_b})}}{(\bar{T}_{wall}-\mathrm{T_b})}\right)^2}$$

$$= \sqrt{(0.3176)^2 + (-0.176)^2}$$

$$= 0.3631\ \%$$

(4) Average Nusselt number, Nu_{avg}

$$Nu_{avg} = \frac{h_{avg}\, d}{k} \ , \qquad \frac{U_{Nu_{avg}}}{Nu_{avg}} = \sqrt{\left(\frac{U_{h_{avg}}}{h_{avg}}\right)^2 + \left(\frac{U_k}{k}\right)^2}$$

$$= \sqrt{(0.3631)^2 + (0.3)^2}$$

$$= 0.4718\ \%$$

6.4 Conclusion

The single phase natural circulation of water and different nanofluids in NCL was experimentally investigated and the results are presented in this chapter. The conclusions from experimental results can be summarized as follows:

1. A reasonably good agreement is found between theoretical and experimental results, thereby validating the mathematical models developed for the study.
2. Natural circulation loop operated with nanofluid quickly reaches a steady state condition compared to water. The steady state reaching time can be reduced by 12 to 27% by using nanofluids. In particular, the NCL operated with CuO-water nanofluid quickly reaches the steady state condition when compared with other nanofluids.
3. The average Nusselt number increases with power input and particle concentration.
4. As expected, with a decrease in cooling water inlet temperature, the mass flow rate and average Nusselt number increases for any working fluid.
5. Overall thermal conductance increases with particle volume concentration.
6. As expected, with an increase in external hot fluid temperature, mass flow rate and heat transfer rates also increase.
7. Within the range of study, the loop was found to be stable.

Chapter - 7

General conclusions and scope of future work

7.1 General conclusions

In the present work a detailed literature survey on natural circulation loops and their applications was carried out. Following the survey, theoretical studies (one dimensional and three dimensional) on the steady state performance of the nanofluid based natural circulation loops were carried out. Based on the theoretical studies, an instrumented nanofluid based natural circulation loop with heater as a heat source and heat exchanger as heat source was designed, fabricated and tested. The following are the important conclusions based on this study.

7.1.1 Based on the literature review

1. A large number of theoretical and experimental studies on natural circulation loops that use water as loop fluid is available for heat transfer applications, such as in nuclear power plants, solar collectors etc. However, studies on nanofluid based NCLs are very limited.
2. Most of the studies on NCL consider constant heat flux condition at the heat source. Studies on NCLs with heat exchangers at heat source and heat sink are relatively few.

7.1.2 Comparison between different working fluids in NCL

1. Since the same temperature difference across the heat exchanger, both for laminar and turbulent single-phase liquid flows, the required pipe diameters are smaller when nanofluids (SiO_2-water, Al_2O_3-water and CuO-water) are used in place of water. Of the fluids considered here, CuO-water nanofluid require a least pipe diameter at fixed temperature and concentration.
2. For the same geometry and heat input, the temperature difference across heat exchangers is least for the systems using nanofluids, both for laminar and turbulent flows.
3. Since nanofluids have enhanced thermo-physical properties, they may be considered as a suitable fluid in natural convection loops for solar and nuclear heat transfer applications.

7.1.3 Based on theoretical studies using 1-D numerical modelling

1. For a given set of operating parameters, an optimum heat exchanger length is found to be around 9 m, 11 m, 13 m and 13 m for CuO-water, Al_2O_3-water, SiO_2-water nanofluids and pure water, respectively.
2. For a given set of operating parameters, an optimum diameter of the loop pipe is found to be around 0.015 m for any working fluid.
3. The mass flow rate of the external fluids does not influence much the heat transfer rate of the loop significantly. However, the loop heat transfer rate is strongly influenced by the temperatures of external fluids.

7.1.4 Based on theoretical studies using 3-D numerical modelling

1. The steady state mass flow rate of the NCL increases with the heat input and it decreases with the loop inclination angle.
2. If the particle volume concentration increased from 0% to 5%, then the mass flow rate of the loop fluid increased by 26%, but with further increase in particle concentration, the mass flow rate decreased due to viscous forces that dominate the buoyancy forces. Therefore, for this kind of NCL model, 5% particle concentration can be considered an optimum value.
3. Effectiveness increases with particle concentration and inclination angle. Therefore, the effectiveness of a nanofluid-based NCL is more than a water based NCL.

4. At a given power input and fixed inclination angle, the average heat transfer coefficient of the nanofluid is enhanced with the particle concentration. Moreover, the average heat transfer coefficient is not influenced much by the loop inclination angle.
5. Rayleigh number is reduced with the inclination angle; however, the effect of inclination angle is relatively low for up to 15°. Therefore, lower inclination angles of up to 15° will be preferable without any noticeable effect on Rayleigh number.
6. The performance of the NCL with multiple channels (DRDD) was enhanced by 2.5% when compared with single channel (SRSD) in terms of the mass flow rate.

7.1.5 Based on experimental studies on nanofluid based NCL

1. A reasonably good agreement is found between theoretical and experimental results, thus validating the mathematical models developed.
2. Natural circulation loop operated with nanofluid quickly reaches a steady state condition compared to water. The steady state reaching time can be reduced by 12 to 27% by using nanofluids. In particular, an NCL operated with CuO-water nanofluid quickly reaches the steady state condition when compared with other nanofluids.
3. The average Nusselt number increases with power input and particle concentration.
4. As expected, with a decrease in cooling water inlet temperature, the mass flow rate and average Nusselt number increase for any working fluid.
5. Overall thermal conductance increases with particle volume concentration.
6. Predictably, with an increase in external hot fluid temperature, mass flow rate and heat transfer rates increase too.
7. Within the range of the study, a loop was found to be stable.

7.2 Scope of future work

In the present work, a nanofluid based natural circulation loop suitable for high temperature applications was successfully analysed, designed, fabricated and tested. However, to make these systems commercially viable, the following aspects need to be considered:

1. Since stability is always an issue with NCL systems, stability analysis of nanofluid based NCLs with end heat exchangers should be carried out before using them.
2. Commercialization of these systems require reduction in the overall size of the system. This may call for efficient heat exchangers compared to the tube-in-tube type heat exchangers used in the present study. Theoretical and experimental studies on other

types of heat exchangers specially designed for nanofluid based NCLs are very necessary.

3. Performance enhancing techniques, such as use of hybrid nanofluid (mixing of the two types of nano particles in the base fluid) as loop fluid can be explored in greater detail for industrial use.

7.3 Closure

This chapter consolidates the important findings based on various cases studied in the thesis. The prominent conclusions and recommendations for future work have been presented in this chapter.

Publications

International Journals

S.No.	Title of the paper	Name of the Journal and Publisher	Volume and Year
1.	Numerical investigation to study the effect of loop inclination angle on thermal performance of nanofluid based natural circulation loop.	International Journal of Ambient Energy, Taylor and Francis.	March 2018
2.	Numerical study on heat transfer characteristics of nanofluid based natural circulation loop.	Thermal Science, Vinca publication.	Vol. 22, No. 2, 2018.
3.	On the suitability of nanofluid as working fluid in natural circulation loops.	International Journal of Applied Engineering Research, Research India Publication.	Vol. 10, No. 8, 2015.
4.	Numerical investigation of nanofluid based thermosyphon system.	International Journal of Mechanical, Aerospace, Industrial and Mechatronics Engineering, Waset publication.	Vol. 10, No. 12, 2014.
5.	Experimental studies on nanofluid based natural circulation loop with heater as heat source.	International Journal of Heat and Fluid flow. Elsevier.	Communicated
6.	Experimental studies on nanofluid based natural circulation loop with end heat exchangers.	Applied Thermal engineering, Elsevier.	Communicated

International/ National Conferences

S.No.	Title of the paper	Name of the Conference and Place	Date
1.	Steady state analysis of nanofluid based thermosyphon system.	5th International and 41st National Conference on Fluid Mechanics and Fluid Power (FMFP), IIT Kanpur, UP, India.	12th-14th December, 2014.
2.	Review on single phase thermosyphon loop	National Symposium of Mechanical Engineering Research Scholars (NSMERS), NIT Warangal, Telangana, India.	7th Oct, 2016.
3.	Numerical study on heat transfer and fluid flow behaviour in nanofluid based natural circulation loop.	International Conference on Recent Trends in Engineering, Science and Technology (ICRTEST), St. Peters Engineering college, Hyderabad, Telangana, India.	27th-28th October, 2016.
4	Numerical investigation on heat transfer and fluid flow characteristics of natural circulation loop with multiple channels.	International Conference on Numerical Heat Transfer & Fluid Flow (NHTFF18), NIT Warangal, Telangana, India,	19th-21th, January. 2018.

References

[1] B. Gebhart, “Natural Convection Flows and Stability,” *Adv. Heat Transf.*, vol. 9, no. C, pp. 273–348, 1973.

[2] “https://hubpages.com/education/The-anatomy-and-physiology-of-the-heart.” .

[3] “https://www.cleanwaterstore.com/blog/top-10-states-affected-drought-u-s/.” .

[4] Lord Rayleigh, “On convection currents in a horizontal layer of fluid , when the higher temperature is on the under side,” *Philos. Mag. J. Sci. Ser. 6.*, vol. 32, no. 192, pp. 529–546, 1916.

[5] I. Budihardjo, G. L. Morrison and M. Behnia, “Natural circulation flow through water-in-glass evacuated tube solar collectors,” *Sol. Energy*, vol. 81, no. 12, pp. 1460–1472, 2007.

[6] D. Japikse, “Advances in Thermosyphon Technology,” *Adv. Heat Transf. Acad. Press. New York*, vol. 9, pp. 1–111, 1973.

[7] P. K. Vijayan and A. K. Nayak, “Natural Circulation Systems: Advantages and Challenges,” *Proc. NUTHOS-6*, no. May, pp. 1–12, 2004.

[8] N. M. Rao, M. Mishra, B. Maiti and P. K. Das, “Effect of end heat exchanger parameters on the performance of a natural circulation loop,” *Int. Commun. Heat Mass Transf.*, vol. 29, no. 4, pp. 509–518, 2002.

[9] S. Khandekar, M. Groll, P. Charoensawan, S. Rittidech and P. Terdtoon, “Closed and Open Loop Pulsating Heat Pipes,” *Proc. 13th Int. Heat Pipe Conf*, vol. 26, p. 38, 2004.

[10] S. Khandekar and A. Gupta, “Embedded Pulsating Heat Pipe Radiators,” *14th Int. Heat Pipe Conf. Florianopolis, Brazil*, vol. 1, no. 1, pp. 258–263, 2007.

[11] B. Tong, T. Wong and K. Ooi, “Closed-loop pulsating heat pipe,” *Appl. Therm. Eng.*, vol. 21, no. 18, pp. 1845–1862, 2001.

[12] B. H. Cohen, P. D. A. Member and F. J. Bayley “Heat- transfer Problems of Liquid-cooled Gas- turbine Blades,” in *Proceedings of Institution of Mechanical Engineers*, 1955, vol. 169, pp. 1063–1080.

[13] D. J. Close, “The performance of solar water heaters with natural circulation,” *Sol. Energy*, vol. 6, no. 1, pp. 33–40, 1962.

[14] A. Mertol, W. Place, T. Webster and R. Greif, “Detailed Loop Model (DLM) analysis of liquid solar thermosiphons with heat exchangers,” *Sol. Energy*, vol. 27, no. 5, pp. 367–386, 1981.

[15] K. S. Ong, “A finite-difference method to evaluate the thermal performance of a solar water heater,” *Sol. Energy*, vol. 16, no. 3–4, pp. 137–147, 1974.

[16] A. Shitzer, D. Kalmanoviz, Y. Zvirin and G. Grossman, “Experiments with a flat plate solar water heating system in thermosyphonic flow,” *Sol. Energy*, vol. 22, no. 1, pp. 27–35, 1979.

[17] Y. Zvirin, A. Shitzer and G. Grossman, “The natural circulation solar heater-models with linear and nonlinear temperature distributions,” *Int. J. Heat Mass Transf.*, vol. 20, no. 9, pp. 997–999, 1977.

[18] H. D. Koca, S. Doganay and A. Turgut, “Thermal characteristics and performance of Ag-water nanofluid: Application to natural circulation loops,” *Energy Convers. Manag.*, vol. 135, pp. 9–20, 2017.

[19] H. R. McKee, “Thermosiphon Reboilers-A Review,” *Ind. Eng. Chem.*, vol. 62, no. 12, pp. 76–82, 1970.

[20] N. V. L. S. Sarma, P. J. Reddy and P. S. Murti, “A Computer Design Method for Vertical Thermosyphon Reboilers,” *Ind. Eng. Chem. Process Des. Dev.*, vol. 12, no. 3, pp. 278–290, 1973.

[21] D. B. Kreitlow and G. M. Reistad, “Themosyphon models for downhole heat exchanger application in shallow geothermal systems,” *J. Heat Transf.*, vol. 100, no. November 1978, pp. 713–719, 1978.

[22] H. R. Tuma and P. E. Mortazavi, “Indirect Thermosyphons for Cooling Electronic Devices,” *Electron. Cool.*, vol. 12, no. 1, pp. 26–32, 2006.

[23] J. B. Joshi, “Computational flow modelling and design of bubble column reactors,” *Chem. Eng. Sci.*, vol. 56, no. 21–22, pp. 5893–5933, 2001.

[24] J. H. Choi, J. Cleveland and N. Aksan, “Improvement in understanding of natural circulation phenomena in water cooled nuclear power plants,” *Nucl. Eng. Des.*, vol. 241, no. 11, pp. 4504–4514, 2011.

[25] K. E. Torrance, “Open-Loop Thermosyphons with Geological Applications,” *J. Heat Transfer*, vol. 101, no. 4, p. 677, 1979.

[26] J. Madejski, W. S. Iniynierska and J. Mikielewicz, “Liquid fin- A New Device for Heat-Transfer Equipment,” *Int. J. Heat Mass Transf.*, vol. 14, pp. 357–363, 1971.

[27] Y. Wang, J. Singer and H. H. Bau, “Controlling chaos in a thermal convection loop,” *J. Fluid Mech.*, vol. 237, no. 479, pp. 479–498, 1992.

[28] K. Kiran Kumar and M. Ram Gopal, “Carbon dioxide as a secondary fluid in natural circulation loops,” *Proc. Inst. Mech. Eng. Part E J. Process Mech. Eng.*, vol. 223, no. 3, pp. 189–194, 2009.

[29] S. Gumus, H. Ozcan, M. Ozbey and B. Topaloglu, “Aluminum oxide and copper oxide nanodiesel fuel properties and usage in a compression ignition engine,” *Fuel*, vol. 163, pp. 80–87, 2016.

[30] J. C. A. Maxwell, *Treatise on Electricity and Magnetism*. 1881.

[31] Hamilton R. L. and Crosser O. K., “Thermal conductivity of heterogeneous two-component systems,” *Ind. Eng. Chem. Fundam.*, vol. 1, no. 3, pp. 187–191, 1962.

[32] X. Wang, X. Xu and S. U. S. Choi, “Thermal Conductivity of Nanoparticle - Fluid Mixture,” *J. Thermophys. Heat Transf.*, vol. 13, no. 4, pp. 474–480, 1999.

[33] Alpaslan Turgut, Ziya Haktan Karadeniz and Serkan Doganay, “Numerical study on nanofluid based single phase natural circulation mini loops: A steady 3D approach.” pp. 321–335, 2016.

[34] A. K. Nayak, P. P. Kulkarni and P. K. Vijayan, “Study on the transient and stability behaviour of a boiling two-phase natural circulation loop with Al_2O_3 nanofluids,” *Appl. Therm. Eng.*, vol. 31, no. 10, pp. 1673–1681, 2011.

[35] S. Doganay and A. Turgut, “Enhanced effectiveness of nanofluid based natural circulation mini loop,” *Appl. Therm. Eng.*, vol. 75, pp. 669–676, 2015.

[36] S. A. Angayarkanni and J. Philip, “Review on thermal properties of nanofluids: Recent developments,” *Adv. Colloid Interface Sci.*, vol. 225, pp. 146–176, 2015.

[37] A. A. Hussien, M. Z. Abdullah and M. A. Al-Nimr, “Single-phase heat transfer enhancement in micro/minichannels using nanofluids: Theory and applications,” *Appl. Energy*, vol. 164, pp. 733–755, 2016.

[38] Babita, S. K. Sharma and S. M. Gupta, “Preparation and evaluation of stable nanofluids for heat transfer application: A review,” *Exp. Therm. Fluid Sci.*, vol. 79, pp. 202–212, 2016.

[39] J. M. Wu and J. Zhao, “A review of nanofluid heat transfer and critical heat flux enhancement - Research gap to engineering application,” *Prog. Nucl. Energy*, vol. 66, pp. 13–24, 2013.

[40] G. Huminic and A. Huminic, “Application of nanofluids in heat exchangers: A review,” *Renew. Sustain. Energy Rev.*, vol. 16, no. 8, pp. 5625–5638, 2012.

[41] S. Ebrahimi, a Gavili, M. Lajevardi and T. Isfahani, “New Class of Coolants: Nanofluids,” *Cdn.Intechopen.Com*, pp. 251–279, 1995.

[42] K. S. Suganthi, V. Leela Vinodhan and K. S. Rajan, “Heat transfer performance and transport properties of ZnO-ethylene glycol and ZnO-ethylene glycol-water nanofluid coolants,” *Appl. Energy*, vol. 135, pp. 548–559, 2014.

[43] B. C. Pak and Y. I. Cho, “Hydrodynamic and heat transfer study of dispersed fluids with submicron metallic oxide particles,” *Exp. Heat Transf.*, vol. 11, no. 2, pp. 151–170, 1998.

[44] K. K. and K. V. S. Adnan M. Hussein and R.A. Bakar, “Experimental Measurement of nanofluids thermal properties,” *Int. J. Automot. Mech. Eng.*, vol. 7, no. 2, pp. 850–863, 2013.

[45] A. R. Sajadi and M. H. Kazemi, “Investigation of turbulent convective heat transfer and pressure drop of TiO_2/water nanofluid in circular tube,” *Int. Commun. Heat Mass Transf.*, vol. 38, no. 10, pp. 1474–1478, 2011.

[46] H. Zhu, C. Zhang, S. Liu, Y. Tang and Y. Yin, “Effects of nanoparticle clustering and alignment on thermal conductivities of Fe_3O_4 aqueous nanofluids,” *Appl. Phys. Lett.*, vol. 89, no. 2, pp. 4–7, 2006.

[47] S. W. Lee, S. D. Park, S. Kang, I. C. Bang and J. H. Kim, “Investigation of viscosity and thermal conductivity of SiC nanofluids for heat transfer applications,” *Int. J. Heat Mass Transf.*, vol. 54, no. 1–3, pp. 433–438, 2011.

[48] Y. Ding, H. Alias, D. Wen and R. A. Williams, “Heat transfer of aqueous suspensions of carbon nanotubes (CNT nanofluids),” *Int. J. Heat Mass Transf.*, vol. 49, no. 1–2, pp. 240–250, 2006.

[49] W. Duangthongsuk and S. Wongwises, “An experimental study on the heat transfer performance and pressure drop of TiO_2-water nanofluids flowing under a turbulent flow regime,” *Int. J. Heat Mass Transf.*, vol. 53, no. 1–3, pp. 334–344, 2010.

[50] A. M. Hussein, R. A. Bakar and K. Kadirgama, “Study of forced convection nanofluid heat transfer in the automotive cooling system,” *Case Stud. Therm. Eng.*, vol. 2, pp. 50–61, 2014.

[51] S. E. Ghasemi, A. A. Ranjbar and M. J. Hosseini, “Experimental evaluation of cooling performance of circular heat sinks for heat dissipation from electronic chips using nanofluid,” *Mech. Res. Commun.*, vol. 84, pp. 85–89, 2017.

[52] C. T. Nguyen, G. Roy, C. Gauthier and N. Galanis, “Heat transfer enhancement using Al2O3-water nanofluid for an electronic liquid cooling system,” *Appl. Therm. Eng.*, vol. 27, no. 8–9, pp. 1501–1506, 2007.

[53] T. Yousefi, F. Veysi, E. Shojaeizadeh and S. Zinadini, “An experimental investigation on the effect of Al_2O_3-H_2O nanofluid on the efficiency of flat-plate solar collectors,” *Renew. Energy*, vol. 39, no. 1, pp. 293–298, 2012.

[54] Visa I, Duta A, Comsit M, Moldovan M, Ciobanu D, Saulescu R and Burduhos B, “Design and experimental optimisation of a novel flat plate solar thermal collector with trapezoidal shape for facades integration,” *Appl. Therm. Eng.*, vol. 90, pp. 432–443, 2015.

[55] A. J. Moghadam, M. Farzane-Gord, M. Sajadi and M. Hoseyn-Zadeh, “Effects of CuO/water nanofluid on the efficiency of a flat-plate solar collector,” *Exp. Therm. Fluid Sci.*, vol. 58, pp. 9–14, 2014.

[56] Zvirin Y, “A review of natural circulation loops in pressurized water reactore and other

systems," *Nucl. Eng. Des. 67*, vol. 67, pp. 203–225, 1981.

[57] R. Greif, "Natural Circulation Loops," *J. Heat Transfer*, vol. 110, pp. 1243–1258, 1988.

[58] S. Ostrach, "Natural convection in enclosures, Adv," *Heat Transf.*, vol. 110, no. November 1988, 1972.

[59] B. Norton and S. D. Probert, "Chapter 2 Thermosyphon Solar Energy Water Heaters," *Adv. Sol. Energy*, pp. 125–170, 1986.

[60] M. K. S. Sarkar, A. K. Tilak and D. N. Basu, "A state-of-the-art review of recent advances in supercritical natural circulation loops for nuclear applications," *Ann. Nucl. Energy*, vol. 73, pp. 250–263, 2014.

[61] B. J. B. Keller, "Periodic oscillations in a model of thermal convection," *J. Fluid Mech.*, vol. 26, no. 3, pp. 599–606, 1966.

[62] P. Welander, "On the oscillatory instability of a differentially heated fluid loop," *J. Fluid Mech.*, vol. 29, no. 1, pp. 17–30, 1967.

[63] P. S. Damerell and R. J. Schoenhals, "Flow in a Toroidal Thermosyphon with Angular Displacement of Heated and Cooled Sections," *Trans. ASME*, vol. 101, no. 1979, pp. 672–676, 1979.

[64] H. F. Creveling, J. F. de Paz, J. Y. Baladi and R. J. Schoenhals, "Stability characteristics of a single-phase free convection loop," *J. Fluid Mech.*, vol. 67, no. 1, pp. 65–84, 1975.

[65] A. R. Greif, Y. Zvirin and Mertol, "The Transient and Stability Behafior of a Natural Convection Loop," *Trans. ASME*, vol. 101, pp. 684–688, 1979.

[66] A. Mertol, R. Greif and Y. Zvirin, "Two-Dimensional Study of Heat Transfer and Fluid Flow in a Natural Convection Loop," *Trans. ASME*, vol. 104, pp. 508–514, 1982.

[67] Y. Zvirin and R. Greif, "Transient behavior of natural circulation loops: Two vertical branches with point heat source and sink," *Int. J. Heat Mass Transf.*, vol. 22, no. 4, pp. 499–504, 1979.

[68] Y. Zvirin, "The effect of dissipation on free convection loops," *Int. J. Heat Mass Transf.*, vol. 22, no. 11, pp. 1539–1546, 1979.

[69] K. Chen, “On the oscillatory instability of closed-loop thermosyphons,” *J. Heat Transfer*, vol. 107, no. 4, pp. 826–832, 2016.

[70] K. Chen, “The optimum configuration of natural convection loops,” *Sol. Energy*, vol. 34, no. 4–5, pp. 407–416, 1985.

[71] P. K. Vijayan, S. K. Mehta and A. W. Date, “On the steady-state performance of natural circulation loops,” *Int. J. Heat Mass Transf.*, vol. 34, no. 9, pp. 2219–2230, 1991.

[72] W. Ambrosini and J. C. Ferreri, “Stability analysis of single-phase thermosyphon loops by finite-difference numerical methods,” *Nucl. Eng. Des.*, vol. 201, no. 1, pp. 11–23, 2000.

[73] N. M. Rao, B. Maiti and P. K. Das, “Comparison of dynamic performance for direct and fluid coupled indirect heat exchange systems,” *Int. J. Heat Mass Transf.*, vol. 48, no. 15, pp. 3244–3252, 2005.

[74] P. K Vijayan, V. K. Bhojwani, M H. Bade, M. Sharma, A. K. Nayak, D. Saha and R. K. Sinha, “Investigations on the Effect of Heater and Cooler Orientation on the Stear State Transient and Stability Behaviour of Single Phase Natiral Circulation in a Rectangular Loop,” *ExternalReportNo. BARC/2001/E/034, BhabhaAtomic Res. Centre, Mumbai, India.*, pp. 1–128, 2001.

[75] P. K. Vijayan, “Experimental observations on the general trends of the steady state and stability behaviour of single-phase natural circulation loops,” *Nucl. Eng. Des.*, vol. 215, no. 1–2, pp. 139–152, 2002.

[76] S. K. Mousavian, M. Misale, F. D’Auria and M. A. Salehi, “Transient and stability analysis in single-phase natural circulation,” *Ann. Nucl. Energy*, vol. 31, no. 10, pp. 1177–1198, 2004.

[77] D. N. Basu, S. Bhattacharyya and P. K. Das, “Effect of heat loss to ambient on steady-state behaviour of a single-phase natural circulation loop,” *Appl. Therm. Eng.*, vol. 27, no. 8–9, pp. 1432–1444, 2007.

[78] D. N. Basu, S. Bhattacharyya and P. K. Das, “Effect of geometric parameters on steady-state performance of single-phase NCL with heat loss to ambient,” *Int. J. Therm. Sci.*, vol. 47, no. 10, pp. 1359–1373, 2008.

[79] D. N. Basu, S. Bhattacharyya and P. K. Das, “Performance comparison of rectangular and toroidal natural circulation loops under steady and transient conditions,” *Int. J. Therm. Sci.*, vol. 57, pp. 142–151, 2012.

[80] D. N. Basu, S. Bhattacharyya and P. K. Das, “Development of a unified model for the steady-state operation of single-phase natural circulation loops,” *Int. J. Heat Mass Transf.*, vol. 62, no. 1, pp. 452–462, 2013.

[81] J. C. F. D. S. Pilkhwal, W. Ambrosini, N. Forgione, P. K. Vijayan and D. Saha, “Analysis of the unstable behaviour of a single-phase natural circulation loop with one-dimensional and computational fluid-dynamics models.” pp. 339–355, 2007.

[82] J. F. Lin, S. Y. Chiu and C. J. Ho, “Conjugate heat transfer simulation of a rectangular natural circulation loop,” *Heat Mass Transf. und Stoffuebertragung*, vol. 45, no. 2, pp. 167–175, 2008.

[83] D. N. Basu, S. Bhattacharyya and P. K. Das, “Influence of geometry and operating parameters on the stability response of single-phase natural circulation loop,” *Int. J. Heat Mass Transf.*, vol. 58, no. 1–2, pp. 322–334, 2013.

[84] K. Kiran Kumar and M. Ram Gopal, “Steady-state analysis of CO_2based natural circulation loops with end heat exchangers,” *Appl. Therm. Eng.*, vol. 29, no. 10, pp. 1893–1903, 2009.

[85] L. Chen, X. R. Zhang, B. L. Deng and B. Jiang, “Effects of inclination angle and operation parameters on supercritical CO_2natural circulation loop,” *Nucl. Eng. Des.*, vol. 265, pp. 895–908, 2013.

[86] J. Y. Wang, T. J. Chuang and Y. M. Ferng, “CFD investigating flow and heat transfer characteristics in a natural circulation loop,” *Ann. Nucl. Energy*, vol. 58, pp. 65–71, 2013.

[87] A. K. Yadav, M. Ram Gopal and S. Bhattacharyya, “CO_2based natural circulation loops: New correlations for friction and heat transfer,” *Int. J. Heat Mass Transf.*, vol. 55, no. 17–18, pp. 4621–4630, 2012.

[88] A. K. Yadav, M. Ram Gopal and S. Bhattacharyya, “Transient analysis of subcritical/supercritical carbon dioxide based natural circulation loops with end heat exchangers: Numerical studies,” *Int. J. Heat Mass Transf.*, vol. 79, pp. 24–33, 2014.

[89] D. Lu, X. Zhang and C. Guo, “Stability analysis for single-phase liquid metal rectangular natural circulation loops,” *Ann. Nucl. Energy*, vol. 73, pp. 189–199, 2014.

[90] N. Goudarzi and S. Talebi, “An approach to stability analysis and entropy generation minimization in the single-phase natural circulation loops,” *Energy*, vol. 80, pp. 213–226, 2015.

[91] A. K. Srivastava, J. Y. Kudariyawar, A. Borgohain, S. S. Jana, N. K. Maheshwari and P. K. Vijayan, “Experimental and theoretical studies on the natural circulation behavior of molten salt loop,” *Appl. Therm. Eng.*, vol. 98, pp. 513–521, 2016.

[92] J. Y. Kudariyawar, A. K. Srivastava, A. M. Vaidya, N. K. Maheshwari and P. Satyamurthy, “Computational and experimental investigation of steady state and transient characteristics of molten salt natural circulation loop,” *Appl. Therm. Eng.*, vol. 99, pp. 560–571, 2016.

[93] A. C. L. Luzzi, M. Misale, F. Devia, A. Pini, M.T. Cauzzi and F. Fanale, “Assessment of analytical and numerical models on experimental data for the study of single-phase natural circulation dynamics in a vertical loop.” pp. 262–283, 2017.

[94] M. Krishnani and D. N. Basu, “Computational stability appraisal of rectangular natural circulation loop: Effect of loop inclination,” *Ann. Nucl. Energy*, vol. 107, pp. 17–30, 2017.

[95] S. T. N. Goudarzi, “Heat removal ability for different orientations of single-phase natural circulation loops using entransy method,” *Ann. Nucl. Energy*, vol. 111, pp. 509–522, 2018.

[96] M. Misale and M. Frogheri, “Stabilization of a single-phase natural circulation loop by pressure drops,” *Exp. Therm. Fluid Sci.*, vol. 25, no. 5, pp. 277–282, 2001.

[97] M. Misale, P. Garibaldi, J. C. Passos and G. G. de Bitencourt, “Experiments in a single-phase natural circulation mini-loop,” *Exp. Therm. Fluid Sci.*, vol. 31, no. 8, pp. 1111–1120, 2007.

[98] P. K. Vijayan, M. Sharma and D. Saha, “Steady state and stability characteristics of single-phase natural circulation in a rectangular loop with different heater and cooler orientations,” *Exp. Therm. Fluid Sci.*, vol. 31, no. 8, pp. 925–945, 2007.

[99] A. K. Nayak, M. R. Gartia and P. K. Vijayan, “An experimental investigation of single-phase natural circulation behavior in a rectangular loop with Al_2O_3nanofluids,” *Exp. Therm. Fluid Sci.*, vol. 33, no. 1, pp. 184–189, 2008.

[100] P. Garibaldi and M. Misale, “Experiments in Single-Phase Natural Circulation Miniloops With Different Working Fluids and Geometries,” *J. Heat Transfer*, vol. 130, no. 10, pp. 104506-1–5, 2008.

[101] M. Misale, P. Garibaldi, L. Tarozzi and G. S. Barozzi, “Influence of thermal boundary conditions on the dynamic behaviour of a rectangular single-phase natural circulation loop,” *Int. J. Heat Fluid Flow*, vol. 32, no. 2, pp. 413–423, 2011.

[102] M. Misale, F. Devia and P. Garibaldi, “Experiments with Al2O3nanofluid in a single-phase natural circulation mini-loop: Preliminary results,” *Appl. Therm. Eng.*, vol. 40, pp. 64–70, 2012.

[103] M. Misale, “Experimental study on the influence of power steps on the thermohydraulic behavior of a natural circulation loop,” *Int. J. Heat Mass Transf.*, vol. 99, pp. 782–791, 2016.

[104] S. Sadhu, M. Ramgopal and S. Bhattacharyya, “Experimental studies on an air-cooled natural circulation loop based on supercritical carbon dioxide - Part A: Steady state operation,” *Appl. Therm. Eng.*, vol. 133, pp. 809–818, 2017.

[105] S. U. S.Choi and J. A. Eastman, “Enhancing Thermal Conductivity of Fluids With nanoparticles,” *American Society of Mechanical Engineers*. pp. 99–105, 1995.

[106] D. Wen and Y. Ding, “Experimental investigation into convective heat transfer of nanofluids at the entrance region under laminar flow conditions,” *Int. J. Heat Mass Transf.*, vol. 47, no. 24, pp. 5181–5188, 2004.

[107] S. M. Fotukian and M. Nasr Esfahany, “Experimental investigation of turbulent convective heat transfer of dilute γ-Al_2O_3/water nanofluid inside a circular tube,” *Int. J. Heat Fluid Flow*, vol. 31, no. 4, pp. 606–612, 2010.

[108] M. Kao, H. Chang and Y. Wu, “Producing aluminum-oxide brake nanofluids using plasma charging system,” *J. Chinese …*, vol. 28, no. 2, pp. 123–131, 2007.

[109] M. J. Kao, C. H. Lo, T. T. Tsung, Y. Y. Wu, C. S. Jwo and H. M. Lin, “Copper-oxide

brake nanofluid manufactured using arc-submerged nanoparticle synthesis system," *J. Alloys Compd.*, vol. 434–435, no. SPEC. ISS., pp. 672–674, 2007.

[110] N. Ahammed, L. G. Asirvatham and S. Wongwises, "Effect of volume concentration and temperature on viscosity and surface tension of graphene-water nanofluid for heat transfer applications," *J. Therm. Anal. Calorim.*, vol. 123, no. 2, pp. 1399–1409, 2016.

[111] A. Ghadimi, R. Saidur and H. S. C. Metselaar, "A review of nanofluid stability properties and characterization in stationary conditions," *Int. J. Heat Mass Transf.*, vol. 54, no. 17–18, pp. 4051–4068, 2011.

[112] Y. Xuan and Q. Li, "Heat transfer enhancement of nanofluids," *Int. J. Heat Fluid Flow*, vol. 21, pp. 58–64, 2000.

[113] R. Lenin and P. A. Joy, "Role of base fluid on the thermal conductivity of oleic acid coated magnetite nanofluids," *Colloids Surfaces A Physicochem. Eng. Asp.*, vol. 529, pp. 922–929, 2017.

[114] S. U. Ilyas, R. Pendyala and M. Narahari, "Stability and thermal analysis of MWCNT-thermal oil-based nanofluids," *Colloids Surfaces A Physicochem. Eng. Asp.*, vol. 527, pp. 11–22, 2017.

[115] Y. Ueki, T. Aoki, K. Ueda and M. Shibahara, "Thermophysical properties of carbon-based material nanofluid," *Int. J. Heat Mass Transf.*, vol. 113, pp. 1130–1134, 2017.

[116] K. V. Wong and O. De Leon, "Applications of nanofluids: Current and future," *Adv. Mech. Eng.*, vol. 2010, pp. 1–11, 2010.

[117] S. J. Kim, I. C. Bang, J. Buongiorno and L. W. Hu, "Study of pool boiling and critical heat flux enhancement in nanofluids," *Bull. Polish Acad. Sci.*, vol. 55, no. 2, pp. 211–216, 2007.

[118] S. J. Kim, I. C. Bang, J. Buongiorno and L. W. Hu, "Surface wettability change during pool boiling of nanofluids and its effect on critical heat flux," *Int. J. Heat Mass Transf.*, vol. 50, no. 19–20, pp. 4105–4116, 2007.

[119] J. Buongiorno, L. W. Hu, S. J. Kim, R. Hannink, B. Truong and E. Forrest, "Nanofluids for Enhanced Economics and Safety of Nuclear Reactors: An Evaluation of the Potential Features, Issues, and Research Gaps," *Nucl. Technol.*, vol. 162, no. 1, pp. 80–91, 2008.

[120] S. C. Tzeng, C. W. Lin and K. D. Huang, “Heat transfer enhancement of nanofluids in rotary blade coupling of four-wheel-drive vehicles,” *Acta Mech.*, vol. 179, no. 1–2, pp. 11–23, 2005.

[121] Y. H. Lin, S. W. Kang and H. L. Chen, “Effect of silver nano-fluid on pulsating heat pipe thermal performance,” *Appl. Therm. Eng.*, vol. 28, no. 11–12, pp. 1312–1317, 2008.

[122] J. F. Yan and J. Liu, “Nanocryosurgery and its mechanisms for enhancing freezing efficiency of tumor tissues,” *Nanomedicine Nanotechnology, Biol. Med.*, vol. 4, no. 1, pp. 79–87, 2008.

[123] S. K. Das, S. U. S. Choi, W. Yu and T. Pradeep, *Nanofluids: Science and Technology*. 2007.

[124] Jari Vartiainen, Tiina Pohler, Kristiina Sirola, Lea Pylkkanen, Harri Alenius, Jouni Hokkinen, Unto Tapper, Panu Lahtinen, Anu Kapanen, Kaisa Putkisto, Panu Hiekkataipale, Paula Eronen, Janne Ruokolainen and Antti Laukkanen, “Health and environmental safety aspects of friction grinding and spray drying of microfibrillated cellulose,” *Cellulose*, vol. 18, no. 3, pp. 775–786, 2011.

[125] S. Sakthivel, V. V. Krishnan and B. Pitchumani, “Influence of suspension stability on wet grinding for production of mineral nanoparticles,” *Particuology*, vol. 6, no. 2, pp. 120–124, 2008.

[126] S. Palaniandy, K. Azizi Mohd Azizli, H. Hussin and S. Fuad Saiyid Hashim, “Mechanochemistry of silica on jet milling,” *J. Mater. Process. Technol.*, vol. 205, no. 1–3, pp. 119–127, 2008.

[127] R. Rajkhowa, L. Wang, J. Kanwar and X. Wang, “Fabrication of ultrafine powder from eri silk through attritor and jet milling,” *Powder Technol.*, vol. 191, no. 1–2, pp. 155–163, 2009.

[128] M. J. Nine, B. Munkhbayar, M. S. Rahman, H. Chung and H. Jeong, “Highly productive synthesis process of well dispersed CuO and Cu/CuO nanoparticles and its thermal characterization,” *Mater. Chem. Phys.*, vol. 141, no. 2–3, pp. 636–642, 2013.

[129] R. Dvorsky, A. Slíva and N. A. C. Ek, “Preparation of Silicon Nanoparticles By Means of Disintegration in a Cavitation Water Jet,” 2010.

[130] Catherine J. Murphy, Tapan K. Sau, Anand M. Gole, Christopher J. Orendorff, Jinxin Gao, Linfeng Gou, Simona E. Hunyadi and Tan Li, "Anisotropic Metal Nanoparticles: Synthesis, Assembly, and Optical Applications," *J. Phys. Chem. B*, vol. 109, pp. 13857–13870, 2005.

[131] H. K. Chan and P. C. L. Kwok, "Production methods for nanodrug particles using the bottom-up approach," *Adv. Drug Deliv. Rev.*, vol. 63, no. 6, pp. 406–416, 2011.

[132] C. Keck, S. Kobierski, R. Mauludin and R. H. Müller, "Second Generation of Drug Nanocrystals for Delivery of Poorly Soluble Drugs: Smartcrystals Technology," *Dosis*, vol. 24, no. 2, pp. 124–128, 2008.

[133] T. T. Baby and S. Ramaprabhu, "Experimental investigation of the thermal transport properties of a carbon nanohybrid dispersed nanofluid.," *Nanoscale*, vol. 3, no. 5, pp. 2208–14, 2011.

[134] R. Shende and R. Sundara, "Nitrogen doped hybrid carbon based composite dispersed nanofluids as working fluid for low-temperature direct absorption solar collectors," *Sol. Energy Mater. Sol. Cells*, vol. 140, pp. 9–16, 2015.

[135] S. C. Lyu, Y. Zhang, C. J. Lee, H. Ruh and H. J. Lee, "Low-temperature growth of ZnO nanowire array by a simple physical vapor-deposition method," *Chem. Mater.*, vol. 15, no. 17, pp. 3294–3299, 2003.

[136] R. B. Galindo, P. Y. R. Rodriguez, B. A. P. Urbina, C. A. A. Orta, O. S. R. Fernandez, G. C. Pliego, R. H. L. Saldivar and L. A. G. Cerde, "Synthesis of Copper Nanoparticles by Thermal Decomposition and Their Antimicrobial Properties," *J. Nanomater.*, vol. 2014, pp. 1–5, 2014.

[137] J. Pérez-Juste, I. Pastoriza-Santos, L. M. Liz-Marzán and P. Mulvaney, "Gold nanorods: Synthesis, characterization and applications," *Coord. Chem. Rev.*, vol. 249, no. 17–18 SPEC. ISS., pp. 1870–1901, 2005.

[138] M. B. Mohamed, Z. L. Wang and M. a El-Sayed, "Temperature-Dependent Size-Controlled Nucleation and Growth of Gold Nanoclusters," *J. Phys. Chem. A*, vol. 103, no. 49, pp. 10255–10259, 1999.

[139] L. Rodríguez-Sánchez, M. C. Blanco and M. A. López-Quintela, "Electrochemical

Synthesis of Silver Nanoparticles," *J. Phys. Chem. B*, vol. 104, pp. 9683–9688, 2000.

[140] S. M. Abbasi, A. Rashidi, A. Nemati and K. Arzani, "The effect of functionalisation method on the stability and the thermal conductivity of nanofluid hybrids of carbon nanotubes/gamma alumina," *Ceram. Int.*, vol. 39, no. 4, pp. 3885–3891, 2013.

[141] Y. J. Noh, S. I. Na and S. S. Kim, "Inverted polymer solar cells including ZnO electron transport layer fabricated by facile spray pyrolysis," *Sol. Energy Mater. Sol. Cells*, vol. 117, pp. 139–144, 2013.

[142] S. Harikoshi and N. Serpone, *Microwaves in Nanoparticle Synthesis Fundamentals and Applications*, First edit. Tokyp: Willey, 2013.

[143] H. Chang, C. S. Jwo, P. S. Fan and S. H. Pai, "Process optimization and material properties for nanofluid manufacturing," *Int. J. Adv. Manuf. Technol.*, vol. 34, no. 3–4, pp. 300–306, 2007.

[144] M.-S. Liu, M. Ching-Cheng Lin, I.-T. Huang and C.-C. Wang, "Enhancement of thermal conductivity with carbon nanotube for nanofluids," *Int. Commun. Heat Mass Transf.*, vol. 32, no. 9, pp. 1202–1210, 2005.

[145] S. U. S. Choi, Z. G. Zhang, W. Yu, F. E. Lockwood and E. A. Grulke, "Anomalous thermal conductivity enhancement in nanotube suspensions," *Appl. Phys. Lett.*, vol. 79, no. 14, pp. 2252–2254, 2001.

[146] T. P. Teng, Y. H. Hung, T. C. Teng, H. E. Mo and H. G. Hsu, "The effect of alumina/water nanofluid particle size on thermal conductivity," *Appl. Therm. Eng.*, vol. 30, no. 14–15, pp. 2213–2218, 2010.

[147] Bin-Juine Huang, Wei-Zhe Ton, Chen-Chun Wu, Hua-Wei Ko, Hsien-Shun Chang, Rue-Her Yen and Jiunn-Cherng Wang, "Maximum-power-point tracking control of solar heating system," *Sol. Energy*, vol. 86, no. 11, pp. 3278–3287, 2012.

[148] Y. Hwang, J.K. Lee, C.H. Lee, Y.M. Jung, S.I. Cheong, C.G. Lee, B.C. Ku and S.P. Jang, "Stability and thermal conductivity characteristics of nanofluids," *Thermochim. Acta*, vol. 455, no. 1–2, pp. 70–74, 2007.

[149] J. Huang, X. Wang, Q. Long and L. Liming, "Influence of pH on the Stability Characteristics of Nanofluids," *Symp. Photonics Optoelectron.*, vol. 1, pp. 1–4, 2009.

[150] F. X. Li, D. S. Zhu, X. J. Wang, N. Wang, J. W. Gao and H. Li, "Thermal conductivity enhancement dependent pH and chemical surfactant for Cu–H_2O nanofluids," *Thermochim. Acta*, vol. 469, no. 1, pp. 98–103, 2008.

[151] D. Zhu, X. Li, N. Wang, X. J. Wang, J. W. Gao and H. Li, "Dispersion behaviour and thermal conductivity characteristics of Al_2O_3–H_2O nanofluids," *Curr. Appl. Phys.*, vol. 9, no. 1, pp. 131–139, 2009.

[152] Jiango L, Gao L and Sun J, "Production of aqueous colloidal dispersions of carbon nanotubes," *J. Colloid Interface Sci.*, vol. 1, pp. 89–94, 2003.

[153] S. H. Kim, S. R. Choi and D. Kim, "Thermal conductivity of metal-oxide nanofluids: particle size dependence and effect of laser irradiation," *J. Heat Transfer*, vol. 129, pp. 298–307, 2007.

[154] M. J. Assael, I. N. Metaxa, J. Arvanitidis, D. Christofilos and C. Lioutas, "Thermal conductivity enhancement in aqueous suspensions of carbon multi-walled and double-walled nanotubes in the presence of two different dispersants," *Int. J. Thermophys.*, vol. 26, no. 3, pp. 647–664, 2005.

[155] I. Madni, C. Y. Hwang, S. D. Park, Y. H. Choa and H. T. Kim, "Mixed surfactant system for stable suspension of multiwalled carbon nanotubes," *Colloids Surfaces A Physicochem. Eng. Asp.*, vol. 358, no. 1–3, pp. 101–107, 2010.

[156] Y. H. Wang, J. K. Lee, Y. M. Jeong, S. I. Cheong, Y. C. Ahn and S. H. Kim, "Production and dispersion stability of nanoparticles in nanofluids," *Powder Technol.*, vol. 186, no. 2, pp. 145–153, 2008.

[157] C. Choi, H. S. Yoo and J. M. Oh, "Preparation and heat transfer properties of nanoparticle-in-transformer oil dispersions as advanced energy-efficient coolants," *Curr. Appl. Phys.*, vol. 8, no. 6, pp. 710–712, 2008.

[158] M. Sato, Y. Abe, Y. Urita, R. D. Paola, A. Cecere and R. Savino, "Thermal performance of self-rewetting fluid heat pipe containing dilute solutions of polymer capped silver nanoparticles synthesized by microwave-polyol process," in *Proceeding ITP*, 2009.

[159] C. Walleck, "Development of Steady-State, Parallel-Plate Thermal Conductivity Apparatus for Poly-Nanofluids and Comparative Measurements with Transient HWTC

Apparatus," Northern Illinois University United States, 2009.

[160] C. Cao, L. Zhang, X. X. Zhang and F. P. Du, "Effect of gum arabic on the surface tension and surface dilational rheology of trisiloxane surfactant," *Food Hydrocoll.*, vol. 30, no. 1, pp. 456–462, 2013.

[161] A. T. Utomo, H. Poth, T. Philip, Robbins and W. P. Pacek, "Experimental and theoretical studies of thermal conductivity, viscosity and heat transfer coefficient of titania and alumina nanofluids," *Int. J. Heat Mass Transf.*, vol. 55, pp. 7772–7781, 2012.

[162] P. C. Hiemenz and M. Decker, *Principles of colloid and surface chemistry*, Second Edi. New York: Dekker, 1986.

[163] P.C. Hiemenz and R. Rajagopalan, *Principles of colloids and surface chemistry*, 3rd Editio. Newyork: Madison Avenue, New york, 1997.

[164] S. Suresh, K. P. Venkitaraj, P. Selvakumar and M. Chandrasekar, "Synthesis of Al_2O_3-Cu/water hybrid nanofluids using two step method and its thermo physical properties," *Colloids Surfaces A Physicochem. Eng. Asp.*, vol. 388, no. 1–3, pp. 41–48, 2011.

[165] R. S. Vajjha and D. K. Das, "A review and analysis on influence of temperature and concentration of nanofluids on thermophysical properties, heat transfer and pumping power," *Int. J. Heat Mass Transf.*, vol. 55, no. 15–16, pp. 4063–4078, 2012.

[166] Yarmand Hooman, Gharehkhani Samira, Ahmadi Goodarz, Shirazi Seyed Farid Seyed, Baradaran Saeid, Montazer Elham, Zubir Mohd Nashrul Mohd, Alehashem Maryam Sadat, Kazi S. N. and Dahari Mahidzal, "Graphene nanoplatelets-silver hybrid nanofluids for enhanced heat transfer," *Energy Convers. Manag.*, vol. 100, pp. 419–428, 2015.

[167] C. J. Ho, J. B. Huang, P. S. Tsai and Y. M. Yang, "Preparation and properties of hybrid water-based suspension of Al_2O_3 nanoparticles and MEPCM particles as functional forced convection fluid," *Int. Commun. Heat Mass Transf.*, vol. 37, no. 5, pp. 490–494, 2010.

[168] M. L. Khalil Khanafer and Kambiz Vafai, "Buoyancy-driven heat transfer enhancement in a two-dimensional enclosure utilizing nanofluids," *Int. J. Heat Mass Transf.*, vol. 46, pp. 3639–3653, 2003.

[169] K. S. Hwang, J. H. Lee and S. P. Jang, “Buoyancy-driven heat transfer of water-based Al_2O_3 nanofluids in a rectangular cavity,” *Int. J. Heat Mass Transf.*, vol. 50, no. 19–20, pp. 4003–4010, 2007.

[170] A. K. Nayak, R. K. Singh and P. P. Kulkarni, “Experimental measurement of volumetric thermal expansion coefficient of various nanofluids,” *Tech. Phys. Lett.*, vol. 36, no. 8, pp. 696–698, 2010.

[171] K. Khanafer and K. Vafai, “A critical synthesis of thermophysical characteristics of nanofluids,” *Int. J. Heat Mass Transf.*, vol. 54, no. 19–20, pp. 4410–4428, 2011.

[172] C. J. Ho, W. K. Liu, Y. S. Chang and C. C. Lin, “Natural convection heat transfer of alumina-water nanofluid in vertical square enclosures: An experimental study,” *Int. J. Therm. Sci.*, vol. 49, no. 8, pp. 1345–1353, 2010.

[173] A. Einstein, “Eine neue Bestimmung der molekul dimensionen,” Ann. of Physics, vol. 14, pp. 229–247, 1906.

[174] H. C. Brinkman, “The Viscosity of Concentrated Suspensions and Solutions,” vol. 571, pp. 1–2, 1952.

[175] G. K. Batchelor, “Effect of Brownian-motion on bulk stress in a suspension of spherical-particles,” *J. Fluid Mech.*, vol. 83, no. NOV, pp. 97–117, 1977.

[176] C.T. Nguyen, F. Desgranges, G. Roy, N. Galanis, T. Mare, S. Boucher and H. Angue Mints, “Temperature and particle-size dependent viscosity data for water-based nanofluids - Hysteresis phenomenon,” *Int. J. Heat Fluid Flow*, vol. 28, no. 6, pp. 1492–1506, 2007.

[177] S. M. S. Murshed and P. Estellé, “A state of the art review on viscosity of nanofluids,” *Renew. Sustain. Energy Rev.*, vol. 76, no. August 2016, pp. 1134–1152, 2017.

[178] D. A. G. Bruggeman, “Berechnung verschiedener physikalischer Konstanten von heterogenen Substanzen. I. Die elastischen Konstanten der quasiisotropen Mischkorper aus isotropen Substanzen,” *Ann. Phys.*, vol. 24, no. 5, pp. 636–664, 1935.

[179] J. Koo and C. Kleinstreuer, “A new thermal conductivity model for nanofluids,” *J. Nanoparticle Res.*, vol. 6, no. 6, pp. 577–588, 2004.

[180] X. Liu and Y. Chen, “Fluid flow and heat transfer in flat-plate oscillating heat pipe,” *Energy Build.*, vol. 75, pp. 29–42, 2014.

[181] J. Lee and I. Mudawar, “Assessment of the effectiveness of nanofluids for single-phase and two-phase heat transfer in micro-channels,” *Int. J. Heat Mass Transf.*, vol. 50, no. 3, pp. 452–463, 2007.

[182] Y. Feng, B. Yu, P. Xu and M. Zou, “The effective thermal conductivity of nanofluids based on the nanolayer and the aggregation of nanoparticles,” *J. Appl. Phys.*, vol. 40, no. 10, pp. 3164–3171, 2007.

[183] S M S Murshed, K C Long and C Yang, “Enhanced Thermal Conductivity of TiO_2-Water Based Nanofluids,” *Int. J. Therm. Sci.*, vol. 44, pp. 367–373, 2005.

[184] H. E. Patel, S. K. Das and T. Sundararajan, “Thermal Conductivities of Naked and Monolayer Protected Metal Nanoparticle Based Nanofluids: Manifestation of Anomalous Enhancement and Chemical Effects,” *Appl. Phys. Lett.*, vol. 83, no. 14, pp. 2931–2933, 2003.

[185] R. Prasher, I. Corporation, W. Chandler and V. Boule, “Effect of Aggregation Kinetics on the Thermal Conductivity of Nanoscale Colloidal Solutions (Nanofluid),” pp. 8–12, 2006.

[186] X. Ju Wang, D. Sheng Zhu and S. Yang, “Investigation of pH and SDBS on enhancement of thermal conductivity in nanofluids,” *Chem. Phys. Lett.*, vol. 470, no. 1–3, pp. 107–111, 2009.

[187] NIST, “Standard Reference Database-REFPROP, Version 9.1.” 2013.

[188] N. Putra, W. Roetzel and S. K. Das, “Natural convection of nano-fluids,” *Heat Mass Transf. und Stoffuebertragung*, vol. 39, no. 8–9, pp. 775–784, 2003.

[189] M. T. Zafarani-Moattar and R. Majdan-Cegincara, “Effect of temperature on volumetric and transport properties of nanofluids containing ZnO nanoparticles poly(ethylene glycol) and water,” *J. Chem. Thermodyn.*, vol. 54, pp. 55–67, 2012.

[190] A. Einstein, “On the Motion of Small Particles Suspended in a Stationary Liquid, as Required by the Molecular Kinetic Theory of Heat,” *Ann. Phys.*, vol. 322, pp. 549–560, 1905.

[191] B. G. K. Batchelor, “The effect of Brownian motion on the bulk stress in a suspension of spherical particles,” vol. 83, 1977.

[192] P. M. Kumar, J. Kumar, R. Tamilarasan, S. Sendhilnathan and S. Suresh, “Review on nanofluids theoretical thermal conductivity models,” *Eng. J.*, vol. 19, no. 1, pp. 67–83, 2015.

[193] T. T. Baby and R. Sundara, “Synthesis and transport properties of metal oxide decorated graphene dispersed nanofluids,” *J. Phys. Chem. C*, vol. 115, no. 17, pp. 8527–8533, 2011.

[194] W. und D. bei nichtausgebildeter Stephan K, “Laminar stomung in Rohren und ebenen spalten,” *Chem.Ing.Tech*, p. 773, 1959.

[195] Gnielinski V, “Equations for calculating heat transfer in single tube rows and banks of tubes,” *Int.Chem Eng*, vol. 19, no. 3, pp. 380–391, 1979.

[196] London A and Shah R K, *Laminar forced convective in ducts*. Academic press, 1978.

[197] Y. Xuan and Q. Li, “Investigation on Convective Heat Transfer and Flow Features of Nanofluids,” vol. 125, no. February 2003, pp. 151–155, 2013.

[198] P. K. Vijayan, A. K. Nayak, D. Saha and M. R. Gartia, “Effect of Loop Diameter on the Steady State and Stability Behaviour of Single-Phase and Two-Phase Natural Circulation Loops,” *Sci. Technol. Nucl. Install.*, vol. 2008, pp. 1–17, 2008.

[199] “ANSYS Fluent Theory Guide,” vol. 15317, November, pp. 724–746, 2013.

[200] F. M. M. Rashidi, A. Hosseini, I. Pop and S. Kumar, “Comparative numerical study of single and two-phase models of nanofluid heat trasnfer in wavy channel.” pp. 1–18, 2014.

[201] E. G. P. Stern, F. R. V. Wilson and H. W. Coleman, “Comprehensive Approach to Verification and Validation of CFD Simulations – Part 1: Methodology and Procedures,” *J. Fluids Eng.*, vol. 123, pp. 793–802, 2001.

[202] E. G. P. Wilson, F. R. V. Stern and H. W. Coleman, “Comprehensive Approach to Verification and Validation of CFD Simulations - Part 2: Methodology and Procedures,” *J. Fluids Eng.*, vol. 123, pp. 803–810, 2001.

[203] G. H. S. Y Wang, K H Deng, B Liu and J M Wu, “a correlation of nanofluid flow boiling heat transfer based on the experimental results of AIN/H_2O and Al_2O_3/H_2O nanofluid,” *Exp. Therm. Fluid Sci.*, vol. 80, pp. 376–383, 2017.

[204] J. P. Holman, *Experimental Methods for Engineers*, 8th Edition. The McGraw-Hill Publishing company, New York, 2011.